Interaction Notes

Note 341

June 1977

Electromagnetic Shielding by
Advanced Composite Materials

K. F. Casey*
Kansas State University
Manhattan, KS 66506

Abstract

The transmission of electromagnetic waves through planar sheets and
cylindrical shells of advanced composite laminates is considered in both
the frequency and time domains. Attention is concentrated on the frequency
range characteristic of the nuclear electromagnetic pulse. The composite
laminates are modeled for the purposes of this study by isotropic dielectric
or conducting materials.

A new "boundary connection operator" is developed to describe the connec-
tion between the tangential electric and magnetic fields on either side of a
general multilayer shield. An equivalent sheet impedance operator is developed
to describe the bonded wire-mesh screen which is often incorporated in boron-
epoxy composite laminates to improve their shielding effectiveness. These
analyses are used to study the transmission of EMP signals through planar
composite sheets and into cylindrical composite shells in the frequency and
time domains. Both graphite-epoxy and "screened" boron-epoxy laminates are
considered. Numerical results are presented to illustrate the analytical
formulas which are derived.

*presently with Dikewood Industries, Inc., Los Angeles, CA

Electromagnetic Shielding by
Advanced Composite Materials

K. F. Casey*
Kansas State University
Manhattan, KS 66506

Abstract

The transmission of electromagnetic waves through planar sheets and cylindrical shells of advanced composite laminates is considered in both the frequency and time domains. Attention is concentrated on the frequency range characteristic of the nuclear electromagnetic pulse. The composite laminates are modeled for the purposes of this study by isotropic dielectric or conducting materials.

A new "boundary connection operator" is developed to describe the connection between the tangential electric and magnetic fields on either side of a general multilayer shield. An equivalent sheet impedance operator is developed to describe the bonded wire-mesh screen which is often incorporated in boron-epoxy composite laminates to improve their shielding effectiveness. These analyses are used to study the transmission of EMP signals through planar composite sheets and into cylindrical composite shells in the frequency and time domains. Both graphite-epoxy and "screened" boron-epoxy laminates are considered. Numerical results are presented to illustrate the analytical formulas which are derived.

*presently with Dikewood Industries, Inc., Los Angeles, CA

It is found that the shielding effect of a screened boron-epoxy composite laminate is essentially that of the screen itself. The laminate only has an effect on the equivalent sheet impedance of the screen for parallel-polarized fields, and this effect is relatively minor over the EMP frequency spectrum.

The temporal behavior of the fields transmitted through a planar layer or penetrating a cylindrical shell of composite material is interpreted on the basis of the "low-pass" behavior of the graphite composite and the "high-pass" behavior of wire-mesh screens. Comparisons are made between the shielding effectiveness of the two types of composite materials which are discussed in the report, and it is noted that the screened boron-epoxy composites can be decidedly superior to graphite composites insofar as their shielding effectiveness with respect to EMP waveforms is concerned.

CONTENTS

TABLE OF CONTENTS (Continued)

4

ILLUSTRATIONS

SECTION I
GENERAL INTRODUCTION

1. COMPOSITE MATERIALS

Advanced composite materials have become increasingly important in recent years because of their great strength and relatively light weight. In fact, it is estimated that the F-18 aircraft will use advanced composites to the extent of nearly 40% by weight and 80% outer surface coverage [1].

Advanced composite materials are laminates, or multilayer "layups", of many individual laminae. A single lamina consists of a planar array of fibers (of boron/boron tungstate, graphite[+], etc.) in an epoxy matrix. Typical lamina thicknesses are around 0.2 mm, and a typical aircraft skin panel comprises seven layers. The arrangement of the layers can be varied to suit the strength requirements of the liminate in given directions. Typically, however, a $0°-90°$ or $0°-45°-90°$ layup will be used, so that the laminate is nearly isotropic in its mechanical characteristics in directions parallel to its surfaces.

A review of the literature has shown that the basic electrical parameters (e.g., permittivity and conductivity) of advanced composites are only now beginning to be studied [1,2]. However, it seems generally to be agreed that graphite composites behave as good conductors (in the sense that conduction currents dominate displacement currents in the material) with conductivity roughly one-fourth that of pure graphite (7.14×10^4 mho m^{-1}), and that boron-epoxy composites behave as mildly lossy dielectrics.

[+] i.e., a pyrolyzed organic fiber such as polyacrilonitrile.

In this Note we shall assume that these materials are isotropic. It is clear from consideration of the physical structure of composite laminates that they are probably anisotropic, but for simplicity we shall for the present ignore this aspect of these materials. In a related study [3] it has been shown that the anisotropic conductivity of graphite composites is not of prime importance in characterizing the material, the transverse conductivity (i.e., that in the directions parallel to the laminate surface) being the descriptive parameter of principal interest. Furthermore, the anisotropy of boron-epoxy laminates appears to be weak.

Since boron-epoxy composite is such a poor conductor, it provides negligible shielding against penetration by electromagnetic fields. To improve the shielding effectiveness of a boron-epoxy composite laminate, a conducting screen may be embedded in one of its surfaces. In this study we shall assume that the wires in the screen are bonded at the junctions and develop an extension of the now classic theory of Kontorovich [4] in order to take into account the effect of the presence of a dielectric layer on the behavior of the screen.

The advanced composite materials we shall consider, therefore, are of two types: graphite composites, which are modeled as homogeneous, isotropic, conducting materials; and screened boron-epoxy composites, modeled as dielectric layers with a bonded wire-mesh screen in one surface. The conductivity of the graphite composites will be taken to be around 1.5×10^4 mho m^{-1} (roughly one-fourth the conductivity of pure graphite) and the relative permittivity of the boron-epoxy composites will be assumed to be in the range 4-5 [3]. Typical laminate thicknesses are in the range 1-3 mm and typical wire-mesh screen parameters are:

10

mesh size:	20 × 20 to 200 × 200 (per inch)
wire radius:	0.05 to 0.15 mm
wire conductivity:	1.1×10^6 mho m^{-1} (stainless steel)
	to 3.7×10^7 mho m^{-1} (aluminum)

2. ELECTROMAGNETIC SHIELDING CONSIDERATIONS

We shall concentrate in this study on the nuclear electromagnetic pulse (EMP) shielding characteristics of graphite and screened boron-epoxy composites. This restricts the frequency range of interest to $f < 10^8$ Hz. It should be noted that characterizations of advanced composite materials which are valid in this frequency range may not be useful, say, for studying the interactions of advanced composites with radar signals. The inhomogeneity and anisotropy of the materials, which may be neglected for EMP studies, may become critically important in dealing with higher-frequency interactions.

The standard EMP waveform which we shall use in this study is [5]

$$E(t) = E_p A (e^{-\alpha t} - e^{-\beta t}) \tag{1.1}$$

in which E_p denotes the peak amplitude of the electric field, and

$$A = \left[e^{-\alpha t_o} - e^{-\beta t_o} \right]^{-1} = 1.1373 \ldots \tag{1.2a}$$

$$t_o = \frac{1}{\beta - \alpha} \ln \frac{\beta}{\alpha} = 2.104 \times 10^{-9} \text{ sec .} \tag{1.2b}$$

$$\alpha = 4.80 \times 10^7 \text{ sec}^{-1} \tag{1.2c}$$

$$\beta = 1.76 \times 10^9 \text{ sec}^{-1} \tag{1.2d}$$

A plot of $E(t)/E_p$ vs. t is shown in Fig. 1.1[†]. The magnitude and phase

---

[†]The logarithmic time plot will be used throughout this report, in order best to display the detailed time history of the transient signals considered.

11
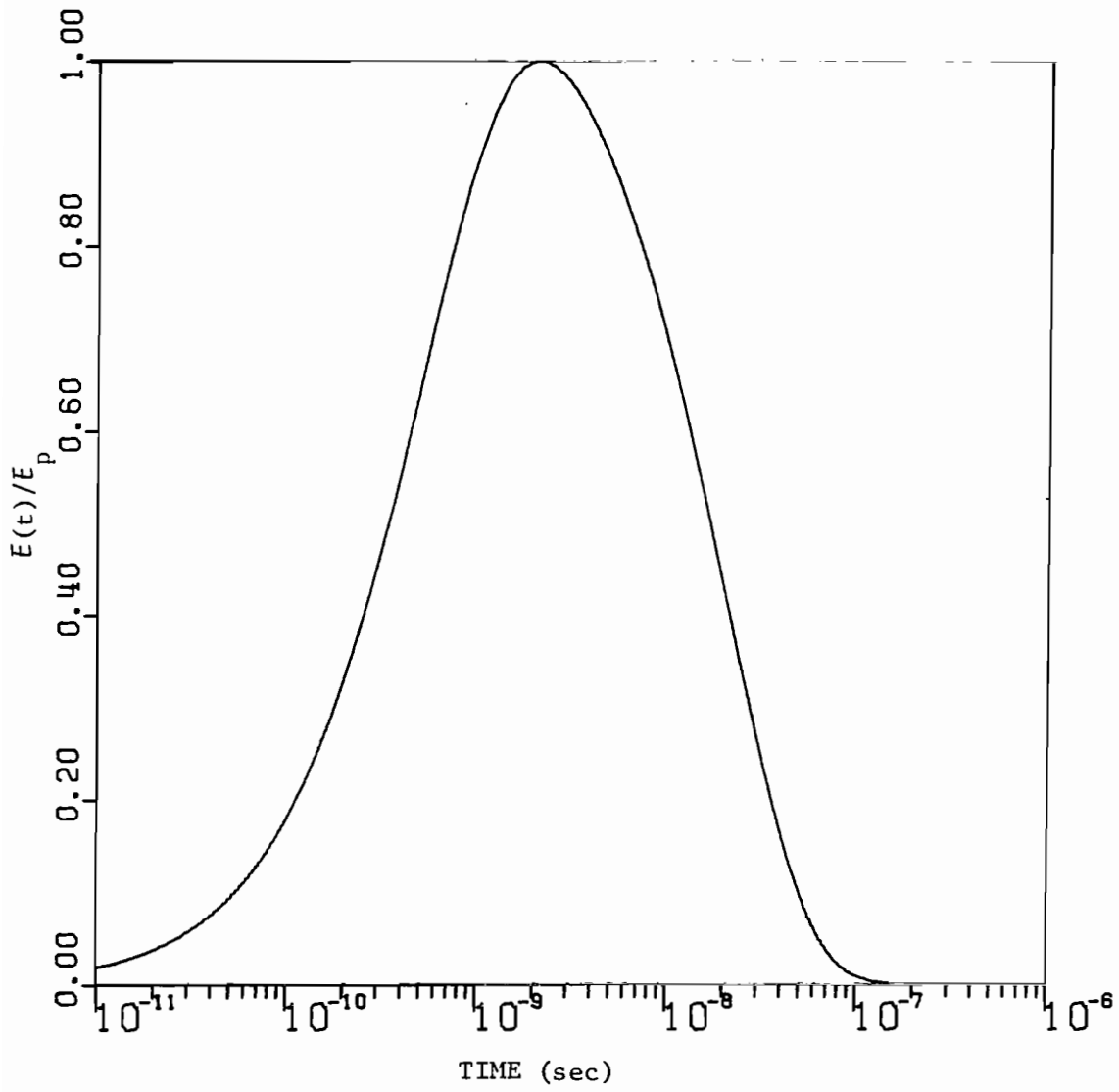
Figure 1.1.   Standard EMP waveform vs. t

12

spectra of this EMP signal are shown in Fig. 1.2. The function $E(t)$ describes the electric field time history of an incident electromagnetic wave, which is assumed to be plane. The associated magnetic field $H(t)$ = $E(t)/\eta_o$, in which η_o denotes the intrinsic impedance of free space.

Two geometrical forms, the infinite sheet and the infinitely long cylindrical shell, are of principal interest to us. We shall address the problems of electromagnetic wave transmission through an infinite sheet of advanced composite and of electromagnetic wave penetration into the interior of a cylindrical shell of advanced composite. Both types of composites (graphite and screened boron-epoxy) will be considered and both frequency and time-domain calculations of the transmitted or penetrated field will be made, under the assumption that the incident field is as given above in (1.1) and (1.2).

3. OVERVIEW OF THE WORK

In Section II we shall develop a "boundary connection supermatrix" which relates the electromagnetic fields on either side of a multilayer shield of more or less arbitrary shape. In addition to its utility in non-separable geometries, it simplifies the analysis of separable problems in that the number of regions to be explicitly considered is reduced. This supermatrix is used in the problem formulations in Sections III-VI.

The interaction of plane electromagnetic waves with planar graphite composite laminates is discussed in Section III and the interaction with cylindrical graphite composite shells in Section IV. Both the frequency and the time domains are investigated (the latter via inverse Laplace transformation).

13
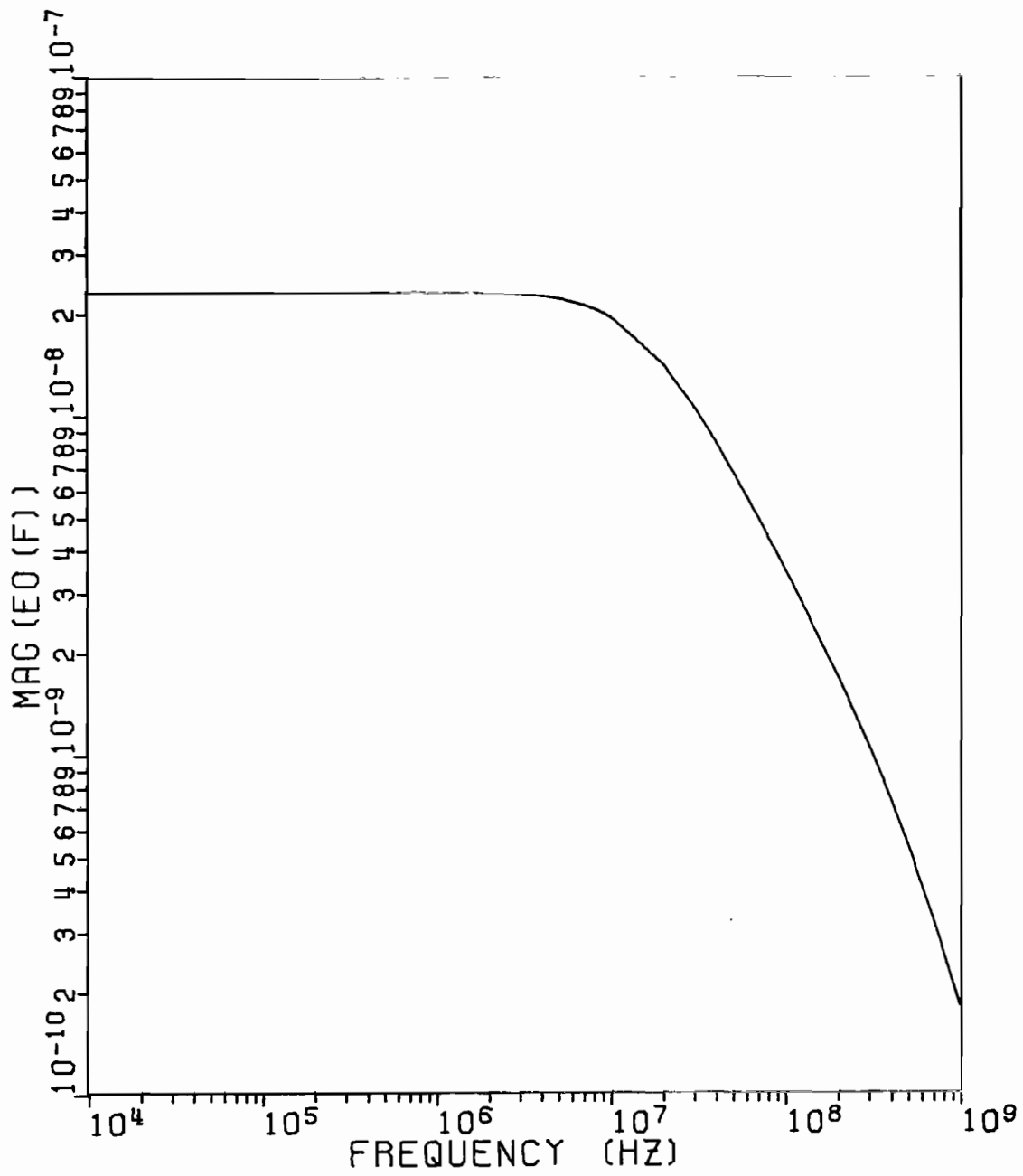
Figure 1.2a. Standard EMP spectrum: magnitude vs. frequency

14
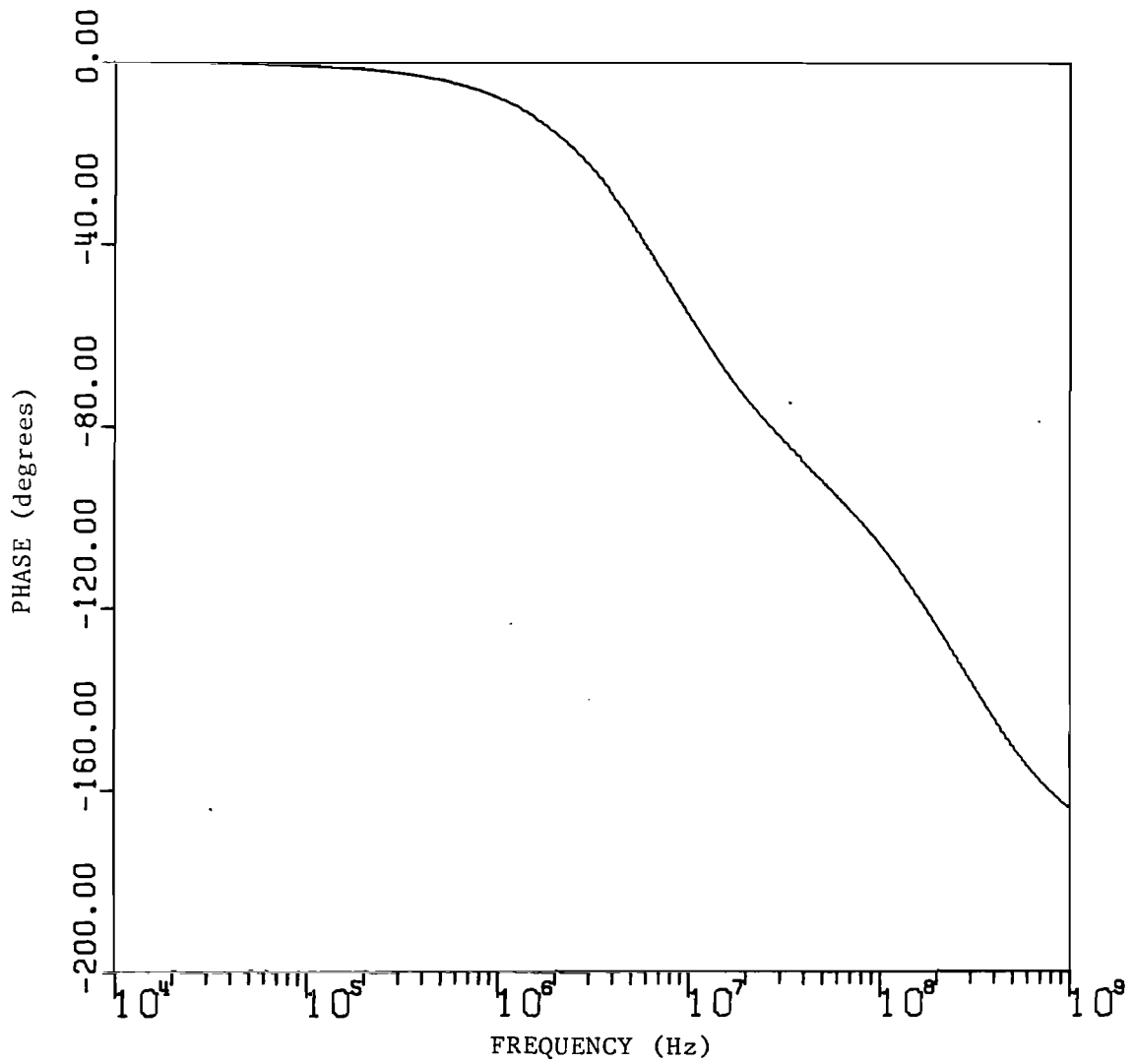
Figure 1.2b. Standard EMP spectrum: phase vs. frequency

Screened boron-epoxy laminates and their interactions with plane electromagnetic waves are considered in sections V and VI, the planar case in V and the cylindrical case in VI. Again, both frequency and time domains are discussed.

The work is summarized and the results are discussed in Section VII. We also suggest some extensions of the problems considered in this report, as well as some logical next steps to be taken in studies dealing with electromagnetic applications of advanced composite materials.

SECTION II

BOUNDARY CONNECTION SUPERMATRICES

1.   INTRODUCTION

In order to assess the degree of electromagnetic shielding provided by a layer of a given material of specified shape, one must determine the relationship between the electromagnetic field on one side of the layer and that on the other. This fundamental mathematical problem is often complicated by the fact that the geometry of the shielding layer does not correspond to one in which the vector wave equation is separable. Therefore, in order to determine the relation desired, one must either develop exact solutions of such complexity and generality as to be of little use for practical purposes, or take advantage of whatever special circumstances exist in order to develop useful, albeit approximate, solutions to the problem.

Fortunately, such special circumstances occur in the type of problem in which we are primarily interested. They are that

(a)   the thickness of the material layer is usually much smaller than either of its two principal radii of curvature,

(b)   the wavelength in the material is usually much smaller than the wavelength outside, and

(c)   the shield is usually made of a lossy material.

We conclude from the second and third conditions above that the electromagnetic behavior of a shield is largely a local phenomenon, in that the fields at points $(\xi_1,\xi_2,\xi_3)^+$ and $(\xi_1 + \Delta\xi_1,\xi_2 + \Delta\xi_2,\xi_3)$ are not closely

---

$^+\xi_1$, ξ_2, and ξ_3 are coordinates of a system whose origin lies in one surface of the layer, the other surface being at $\xi_3 = d$. ξ_1 and ξ_2 are therefore coordinates locally parallel to the shield surfaces.

coupled when $[(\Delta\xi_1)^2 + (\Delta\xi_2)^2]^{1/2} \gg d$, the thickness of the layer. Therefore, the development of the "transfer characteristic" of the shield layer requires consideration not of the whole shield, but only of local portions of it. By virtue of the first condition listed above, we may consider these portions to be planar and utilize a planar model to determine the shield transfer characteristic. Having developed this characteristic, we may then apply the results to geometrical configurations which are nonplanar and for which the shield characteristics may even change with position, provided that these changes are sufficiently gradual.

The planar geometry which we shall consider in this chapter is shown in Fig. 2.1. The region $0 \leq z \leq d_s$ contains the shield material. This material may be arranged in layers of different thicknesses and electrical properties, and the layers may be separated by admittance sheets. We shall assume that the individual layers and admittance sheets are homogeneous, linear, and isotropic. In the following paragraphs, we shall develop a matrix of dyadics $\overline{\overline{M}}$ (the Boundary Connection Supermatrix or BCS) which expresses the relation between the tangential components of the electromagnetic fields on either side of the layer[†]. The BCS's for single layers and admittance sheets are derived in section B, and simplified forms of these BCS's applicable in special circumstances are discussed in paragraph 3.

3. SINGLE LAYERS AND ADMITTANCE SHEETS

We consider first the derivation of the single-layer supermatrix $\overline{\overline{M}}_\ell$, which relates the tangential components of the electromagnetic field at $z = z_1 + d_\ell$ to those at $z = z_1$ in a homogeneous medium of permittivity

---

[†]The relations to be developed constitute an extension and modification of the ABCD matrix approach to the problem [6].
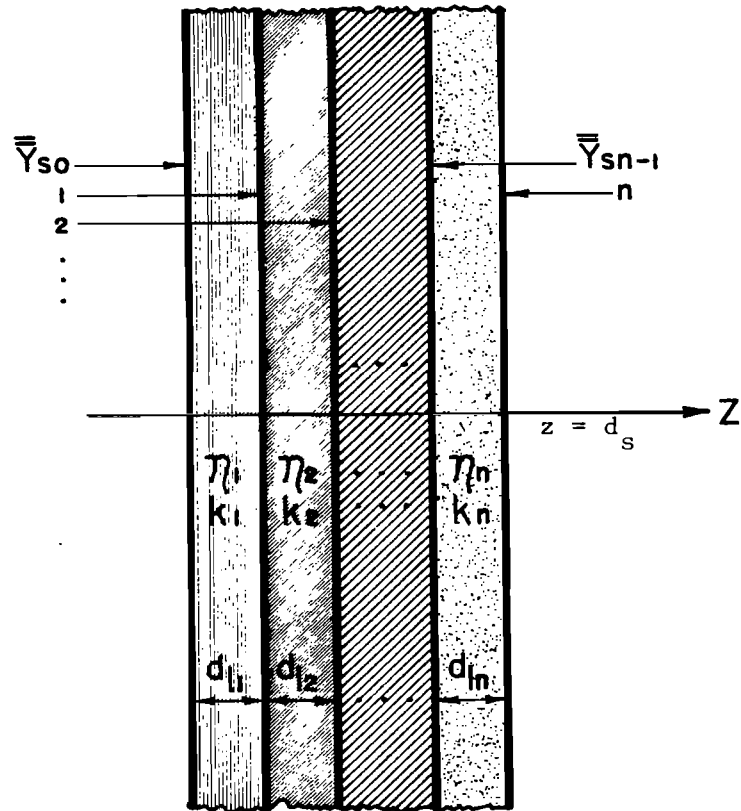
Figure 2.1. A general multilayer shield. η_i and k_i denote the intrinsic impedance and propagation constant of the $\underline{ith}$ layer. $\overline{\overline{Y}}_{si}$ denotes the sheet admittance operator on the right side of the $\underline{ith}$ layer.

$\varepsilon^{\dagger}$ and permeability μ_o. The time dependence $\exp(j\omega t)$ is assumed.

The relations which we seek are most conveniently developed in terms of the Fourier spectra of the electric and magnetic fields. Let us write the fields as follows:

$$
\begin{bmatrix} \bar{E}(x,y,z) \\ \\ \bar{H}(x,y,z) \end{bmatrix} = \int_{-\infty}^{\infty} \int_{-\infty}^{\infty} \begin{bmatrix} \tilde{\bar{E}}(\bar{k}_t,z) \\ \\ \tilde{\bar{H}}(\bar{k}_t,z) \end{bmatrix} e^{-j\bar{k}_t \cdot \bar{r}} \, d^2\bar{k}_t \tag{2.1}
$$

in which $\tilde{\bar{E}}$ and $\tilde{\bar{H}}$ denote the Fourier spectra of $\bar{E}$ and $\bar{H}$, $\bar{a}_z \cdot \bar{k}_t = 0$, and $\bar{r}$ is the position vector. $\tilde{\bar{E}}$ and $\tilde{\bar{H}}$ are expressible in terms of two functions $\tilde{\Phi}(z)$ and $\tilde{\Psi}(z)$ as

$$
\tilde{\bar{E}} = -j\bar{k}_t \times \bar{a}_z \tilde{\Phi} - \frac{\bar{k}_t}{\omega\varepsilon} \frac{d\tilde{\Psi}}{dz} + \frac{1}{j\omega\varepsilon}\left(k^2 + \frac{d^2}{dz^2}\right)\tilde{\Psi}\bar{a}_z \tag{2.2a}
$$

$$
\tilde{\bar{H}} = -j\bar{k}_t \times \bar{a}_z \tilde{\Psi} + \frac{\bar{k}_t}{\omega\mu_o} \frac{d\tilde{\Phi}}{dz} - \frac{1}{j\omega\mu_o}\left(k^2 + \frac{d^2}{dz^2}\right)\tilde{\Phi}\bar{a}_z \tag{2.2b}
$$

$k^2 \equiv \omega^2\mu_o\varepsilon$, and $\tilde{\Phi}$ and $\tilde{\Psi}$ satisfy the equation

$$
\frac{d^2f}{dz^2} + (k^2 - \bar{k}_t \cdot \bar{k}_t)f = 0 \tag{2.3}
$$

Solving eq. (2.3) for $\tilde{\Phi}$ and $\tilde{\Psi}$ and inserting the solutions in eq. (2.2) yields expressions for the tangential field components (denoted by subscript t) as functions of $z' = z - z_1$:

$$
\tilde{\bar{E}}_t(z') = -j\bar{k}_t \times \bar{a}_z(A_\phi \sin k_z z' + B_\phi \cos k_z z')
$$

$$
- \frac{k_z}{\omega\varepsilon} \bar{k}_t(A_\psi \cos k_z z' - B_\psi \sin k_z z') \tag{2.4a}
$$

---

†If the medium has finite conductivity σ, ε should be replaced by $\varepsilon + j\omega/\sigma$.

$$\tilde{\bar{H}}_t(z') = -j\bar{k}_t \times \bar{a}_z(A_\psi \sin k_z z' + B_\psi \cos k_z z')$$

$$+ \frac{k_z}{\omega\mu_o} \bar{k}_t(A_\phi \cos k_z z' - B_\phi \sin k_z z') \qquad (2.4b)$$

The constants A_ϕ, B_ϕ, A_ψ, and B_ψ, which are the arbitrary constants associated with the solutions of eq. (2.3), are to be evaluated in terms of the tangential field components at $z' = 0$, and

$$k_z^2 = k^2 - \bar{k}_t \cdot \bar{k}_t \qquad (2.5)$$

We have, setting $z' = 0$ in eq. (2.4),

$$\tilde{\bar{E}}_t(0) = -j\bar{k}_t \times \bar{a}_z B_\phi - \frac{k_z}{\omega\epsilon} \bar{k}_t A_\psi \qquad (2.6a)$$

$$\tilde{\bar{H}}_t(0) = -j\bar{k}_t \times \bar{a}_z B_\psi + \frac{k_z}{\omega\mu_o} \bar{k}_t A_\phi \qquad (2.6b)$$

from which we obtain

$$A_\psi = \frac{-\omega\epsilon}{k_z k_t^2} \bar{k}_t \cdot \tilde{\bar{E}}_t(0) \qquad (2.7a)$$

$$A_\phi = \frac{\omega\mu_o}{k_z k_t^2} \bar{k}_t \cdot \tilde{\bar{H}}_t(0) \qquad (2.7b)$$

$$B_\psi = \frac{1}{jk_t^2} \bar{a}_z \cdot [\bar{k}_t \times \tilde{\bar{H}}_t(0)] \qquad (2.7c)$$

$$B_\phi = \frac{1}{jk_t^2} \bar{a}_z \cdot [\bar{k}_t \times \tilde{\bar{E}}_t(0)] \qquad (2.7d)$$

where $k_t^2 \equiv \bar{k}_t \cdot \bar{k}_t$.

21

Now substitute eq. (2.7) into eq. (2.4) and set $z' = d_\ell$ ($z = z_1 + d_\ell$). We find, after some simple manipulations, the compact relation

$$\begin{bmatrix} \bar{\bar{\tilde{E}}}_t(d_\ell) \\[2mm] \eta\bar{\bar{\tilde{H}}}_t(d_\ell) \end{bmatrix} = \begin{bmatrix} \bar{\bar{I}} \cos k_z d_\ell & \bar{\bar{U}} \sin k_z d_\ell \\[2mm] -\bar{\bar{U}} \sin k_z d_\ell & \bar{\bar{I}} \cos k_z d_\ell \end{bmatrix} \begin{bmatrix} \bar{\bar{\tilde{E}}}_t(0) \\[2mm] \eta\bar{\bar{\tilde{H}}}_t(0) \end{bmatrix}. \tag{2.8}$$

where $\eta = \sqrt{\mu_o/\varepsilon}$ denotes the characteristic impedance of the medium, $\bar{\bar{I}}$ is the identity operator, and

$$\bar{\bar{U}} = -\frac{1}{jkk_z}\, \bar{a}_z \times (\bar{k}_t\bar{k}_t + k_z^2\bar{\bar{I}}) \tag{2.9}$$

Eq. (2.8) is the relation which has been sought. We define the single-layer connection supermatrix $\bar{\bar{M}}_\ell$ as follows;

$$\bar{\bar{M}}_\ell(z_1;k;z_2) = \begin{bmatrix} \bar{\bar{I}} \cos k_z(z_1 - z_2) & \bar{\bar{U}} \sin k_z(z_1 - z_2) \\[3mm] -\bar{\bar{U}} \sin k_z(z_1 - z_2) & \bar{\bar{I}} \cos k_z(z_1 - z_2) \end{bmatrix} \tag{2.10}$$

so that in general,

$$\begin{bmatrix} \bar{\bar{\tilde{E}}}_t(z_1) \\[2mm] \eta\bar{\bar{\tilde{H}}}_t(z_1) \end{bmatrix} = \bar{\bar{M}}_\ell(z_1;k;z_2) \cdot \begin{bmatrix} \bar{\bar{\tilde{E}}}_t(z_2) \\[2mm] \eta\bar{\bar{\tilde{H}}}_t(z_2) \end{bmatrix} \tag{2.11}$$

The notation chosen for the arguments of $\bar{\bar{M}}_\ell$ makes equations of the form of (2.11) read naturally from left to right. Note also that $\bar{\bar{M}}_\ell^{-1}(z_1;k;z_2) = \bar{\bar{M}}_\ell(z_2;k;z_1)$.

We now consider the connection between tangential field components across an interface. Such an interface may consist of a boundary between two different media, or of a sheet impedance, or both. We shall construct

the connection supermatrix for the general case; then, if the media on either

side of the boundary are identical or if the admittance sheet is absent,

the connection supermatrix will reduce to a simpler form.

Let the boundary be located at $z = z_s$. Then we require that

$$\tilde{\bar{E}}_t(z = z_s+) = \tilde{\bar{E}}_t(z = z_s-) = \tilde{\bar{E}}_t(z = z_s) \qquad (2.12a)$$

$$\bar{a}_z \times [\tilde{\bar{H}}_t(z = z_s +) - \tilde{\bar{H}}_t(z = z_s-)] = \bar{\bar{Y}}_s \cdot \tilde{\bar{E}}_t(z = z_s) \qquad (2.12b)$$

$\bar{\bar{Y}}_s$ is an admittance operator which relates the surface current density

$\tilde{\bar{J}}_s$ at $z = z_s$ to the tangential electric field there:

$$\tilde{\bar{J}}_s = \bar{\bar{Y}}_s \cdot \tilde{\bar{E}}_t(z_s) \qquad (2.13)$$

It follows immediately from eq. (2.12) that if the characteristic impedance

of the medium on the "z_s+" side of the sheet is η_+ and that on the "z_s-"

side is η_-, then

$$\begin{bmatrix} \tilde{\bar{E}}_t(z_s-) \\[2ex] \eta_- \, \tilde{\bar{H}}_t(z_s-) \end{bmatrix} = \begin{bmatrix} \bar{\bar{I}} & \bar{\bar{0}} \\[2ex] \bar{a}_z \times \eta_- \bar{\bar{Y}}_s & \dfrac{\eta_-}{\eta_+} \bar{\bar{I}} \end{bmatrix} \begin{bmatrix} \tilde{\bar{E}}_t(z_s+) \\[2ex] \eta_+ \tilde{\bar{H}}_t(z_s+) \end{bmatrix} \qquad (2.14)$$

Eq. (2.14) is the relation which has been sought. We define the 2×2

matrix in eq. (2.14) to be the admittance-sheet connection supermatrix

$\bar{\bar{M}}_s$ and write

$$\bar{\bar{M}}_s(\eta_-;\bar{\bar{Y}}_s;\eta_+) = \begin{bmatrix} \bar{\bar{I}} & \bar{\bar{0}} \\[2ex] \bar{a}_z \times \eta_- \bar{\bar{Y}}_s & \dfrac{\eta_-}{\eta_+} \bar{\bar{I}} \end{bmatrix} \qquad (2.15)$$

so that

$$
\begin{bmatrix} \tilde{\bar{E}}_t(z_s-) \\ \\ \eta_-\tilde{\bar{H}}_t(z_s-) \end{bmatrix} = \bar{\bar{M}}_s(\eta_-;\bar{\bar{Y}}_s;\eta_+) \cdot \begin{bmatrix} \tilde{\bar{E}}_t(z_s+) \\ \\ \eta_+\tilde{\bar{H}}_t(z_s+) \end{bmatrix} \tag{2.16}
$$

The notation chosen for the arguments of $\bar{\bar{M}}_s$ makes equations of the form of (2.16) read naturally from left to right. Note also that $\bar{\bar{M}}_s^{-1}(\eta_-;\bar{\bar{Y}}_s;\eta_+) = \bar{\bar{M}}_s(\eta_+;-\bar{\bar{Y}}_s;\eta_-)$.

Now as an illustrative example, let us construct the boundary connection supermatrix for the configuration shown in Fig. (2.2). This is a material layer of parameters η and k in the region $0 \leq z \leq d_\ell$, having an admittance sheet on the surface $z = 0$. The medium outside the structure is free space, and we wish to connect the free-space fields at $z = 0-$ to the free-space fields at $z = d_\ell+$. We have the following relations:

$$
\begin{bmatrix} \tilde{\bar{E}}_t(0-) \\ \\ \eta_o\tilde{\bar{H}}_t(0-) \end{bmatrix} = \bar{\bar{M}}_s(\eta_o;\bar{\bar{Y}}_s,\eta) \cdot \begin{bmatrix} \tilde{\bar{E}}_t(0+) \\ \\ \eta\,\tilde{\bar{H}}_t(0+) \end{bmatrix} \tag{2.17a}
$$

$$
\begin{bmatrix} \tilde{\bar{E}}_t(0+) \\ \\ \eta\tilde{\bar{H}}_t(0+) \end{bmatrix} = \bar{\bar{M}}_\ell(0;k;d_\ell) \cdot \begin{bmatrix} \tilde{\bar{E}}_t(d_\ell-) \\ \\ \eta\tilde{\bar{H}}_t(d_\ell-) \end{bmatrix} \tag{2.17b}
$$

$$
\begin{bmatrix} \tilde{\bar{E}}_t(d_\ell-) \\ \\ \eta\tilde{\bar{H}}_t(d_\ell-) \end{bmatrix} = \bar{\bar{M}}_s(\eta;\bar{\bar{0}};\eta_o) \cdot \begin{bmatrix} \tilde{\bar{E}}_t(d_\ell+) \\ \\ \eta_o\tilde{\bar{H}}_t(d_\ell+) \end{bmatrix} \tag{2.17c}
$$

from which it is apparent that

$$\begin{bmatrix} \tilde{\bar{E}}_t(0-) \\ \\ \eta_o \tilde{\bar{H}}_t(0-) \end{bmatrix} = \bar{\bar{M}}_t \cdot \begin{bmatrix} \tilde{\bar{E}}_t(d_\ell+) \\ \\ \eta_o \tilde{\bar{H}}_t(d_\ell+) \end{bmatrix} \qquad (2.18)$$

in which

$$\bar{\bar{M}}_t = \bar{\bar{M}}_s(\eta_o;\bar{\bar{Y}}_s;\eta) \cdot \bar{\bar{M}}_\ell(0;k;d_\ell) \cdot \bar{\bar{M}}_s(\eta;\bar{\bar{0}};\eta_o) \qquad (2.19)$$

One will note that the arguments in eq. (2.19) read naturally from left to right, and correspond to the physical features of the shield structure, as is shown in Fig. 2.2. Furthermore, note that

$$\bar{\bar{M}}_t^{-1} = \bar{\bar{M}}_s(\eta_o;\bar{\bar{0}};\eta) \cdot \bar{\bar{M}}_\ell(d_\ell;k;0) \cdot \bar{\bar{M}}_s(\eta;-\bar{\bar{Y}}_s;\eta_o) \qquad (2.20)$$

Generalizations to arbitrarily complicated shield structures are obvious.

In many practical problems, the connection supermatrices which have been developed in this section can be simplified under certain conditions. We consider this problem in the next section.

3. SPECIAL-CASE FORMS

In this section we consider the forms taken by the connection supermatrices when

(a) the electromagnetic field is either parallel-polarized or perpendicular-polarized

(b) the (effective) permittivity of the shield material is large compared to that of the surrounding medium (usually free space)

We also consider the conditions which must hold for an electrically thin layer to be modeled as an equivalent admittance sheet.
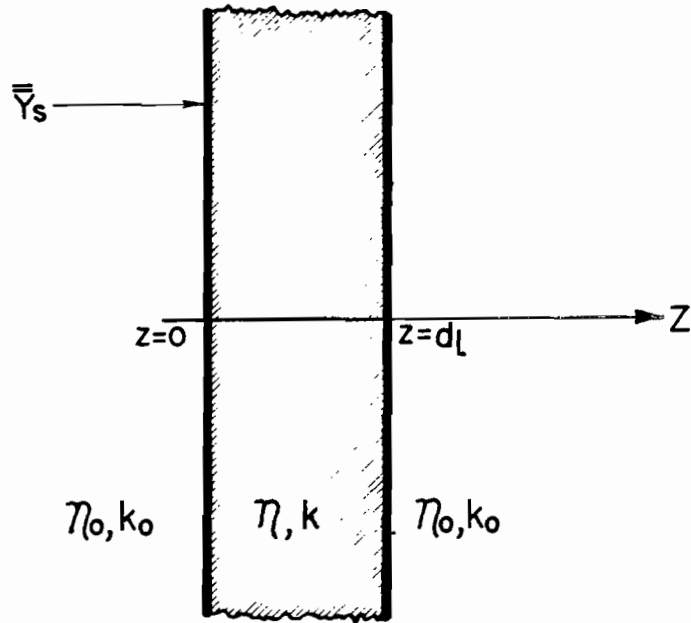
Figure 2.2. A single-layer shield in free space with a sheet admittance in one surface

The tangential fields $\tilde{\bar{E}}_t$ and $\tilde{\bar{H}}_t$ can be resolved into components parallel and perpendicular to $\bar{k}_t$ as follows: denoting either $\tilde{\bar{E}}_t$ or $\tilde{\bar{H}}_t$ by $\tilde{\bar{F}}_t$, we have

$$\tilde{\bar{F}}_t = \tilde{\bar{F}}_t' + \tilde{\bar{F}}_t'' \tag{2.21a}$$

$$\tilde{\bar{F}}_t' = \left(\bar{\bar{I}} - \frac{\bar{k}_t \bar{k}_t}{k_t^2}\right) \cdot \tilde{\bar{F}}_t \tag{2.21b}$$

$$\tilde{\bar{F}}_t'' = \frac{1}{k_t^2} \bar{k}_t \bar{k}_t \cdot \tilde{\bar{F}}_t \tag{2.21c}$$

in which $\tilde{\bar{F}}_t'$ denotes the perpendicularly polarized part of $\tilde{\bar{F}}_t$ and $\tilde{\bar{F}}_t''$ denotes the parallel polarized part. Substituting representations for $\tilde{\bar{E}}_t$ and $\tilde{\bar{H}}_t$ of this form into eq. (2.11), we find that the resulting equations decouple into two sets:

$$\begin{bmatrix} \tilde{\bar{E}}_t'(z_1) \\[2mm] n\tilde{\bar{H}}_t''(z_1) \end{bmatrix} = \bar{\bar{M}}_\ell'(z_1;k;z_2) \cdot \begin{bmatrix} \tilde{\bar{E}}_t'(z_2) \\[2mm] n\tilde{\bar{H}}_t''(z_2) \end{bmatrix} \tag{2.22a}$$

$$\begin{bmatrix} \tilde{\bar{E}}_t''(z_1) \\[2mm] n\tilde{\bar{H}}_t'(z_1) \end{bmatrix} = \bar{\bar{M}}_\ell''(z_1;k;z_2) \cdot \begin{bmatrix} \tilde{\bar{E}}_t''(z_2) \\[2mm] n\tilde{\bar{H}}_t'(z_2) \end{bmatrix} \tag{2.22b}$$

where

$$\bar{\bar{M}}_\ell'(z_1;k;z_2) = \begin{bmatrix} \bar{\bar{I}} \cos k_z(z_1 - z_2) & \dfrac{jk}{k_z} \bar{a}_z \times \bar{\bar{I}} \sin k_z(z_1 - z_2) \\[4mm] -\dfrac{jk_z}{k} \bar{a}_z \times \bar{\bar{I}} \sin k_z(z_1 - z_2) & \bar{\bar{I}} \cos k_z(z_1 - z_2) \end{bmatrix}$$

$$\tag{2.23a}$$

$$\overline{\overline{M}}''_\ell(z_1;k;z_2) = \begin{bmatrix} \overline{\overline{I}} \cos k_z(z_1 - z_2) & \dfrac{jk_z}{k} \, \overline{a}_z \times \overline{\overline{I}} \sin k_z(z_1 - z_2) \\[4mm] -\dfrac{jk}{k_z} \, \overline{a}_z \times \overline{\overline{I}} \sin k_z(z_1 - z_2) & \overline{\overline{I}} \cos k_z(z_1 - z_2) \end{bmatrix}$$

$$(2.23b)$$

The supermatrices $\overline{\overline{M}}'_\ell$ and $\overline{\overline{M}}''_\ell$ are substantially simpler than $\overline{\overline{M}}_\ell$.

We also consider the supermatrix $\overline{\overline{M}}_s$ in those cases in which the admittance operator $\overline{\overline{Y}}_s$ diagonalizes for perpendicularly-polarized and parallel-polarized fields:

$$\overline{\overline{Y}}^{',''}_s = Y^{',''}_s \, \overline{\overline{I}} \tag{2.24}$$

For such cases, the connection supermatrices $\overline{\overline{M}}_s$ are

$$\overline{\overline{M}}^{',''}_s(\eta_-;Y^{',''}_s;\eta_+) = \begin{bmatrix} \overline{\overline{I}} & \overline{\overline{0}} \\[4mm] \eta_- Y^{',''}_s \overline{a}_z \times \overline{\overline{I}} & \dfrac{\eta_-}{\eta_+} \overline{\overline{I}} \end{bmatrix} \tag{2.25}$$

When the effective permittivity of the shield material is large compared to that of the surrounding medium (which is usually free space), the condition $k_t^2 \ll |k|^2$ is valid for values of $\overline{k}_t$ corresponding to real angles of incidence. In such cases, the approximation $k_z \simeq k$ holds and may be used to simplify $\overline{\overline{M}}_\ell$, $\overline{\overline{M}}'_\ell$, and $\overline{\overline{M}}''_\ell$. We find that

$$\overline{\overline{M}}_\ell \simeq \overline{\overline{M}}'_\ell \simeq \overline{\overline{M}}''_\ell \simeq \begin{bmatrix} \overline{\overline{I}} \cos k(z_1 - z_2) & j\overline{a}_z \times \overline{\overline{I}} \sin k(z_1 - z_2) \\[4mm] -j\overline{a}_z \times \overline{\overline{I}} \sin k(z_1 - z_2) & \overline{\overline{I}} \cos k(z_1 - z_2) \end{bmatrix} \tag{2.26}$$

We conclude this section by considering the conditions under which an electrically thin layer may be modeled as an equivalent sheet admittance. The connection supermatrix $\overline{\overline{M}}_t$ for a layer in free space is

$$\overline{\overline{M}}_t = \overline{\overline{M}}_s(\eta_o;\overline{\overline{0}};\eta) \cdot \overline{\overline{M}}_\ell(0;k;d_\ell) \cdot \overline{\overline{M}}_s(\eta;\overline{\overline{0}};\eta_o) \qquad (2.27)$$

We define the equivalent sheet admittance $\overline{\overline{Y}}_{seq}$ by the relation

$$\overline{\overline{M}}_s(\eta_o;\overline{\overline{Y}}_{seq};\eta_o) = \overline{\overline{M}}_\ell^{-1}(0;k_o;d_\ell) \cdot \overline{\overline{M}}_t \qquad (2.28)$$

The factor $\overline{\overline{M}}_\ell^{-1}(0;k_o;d_\ell)$ is inserted to account for the physical distance d_ℓ occupied by the layer. Expanding the product in eq. (2.27) and substituting in eq. (2.28) yields the following four equations expressing the equivalence:

$$\overline{\overline{I}} = C_o C_\ell \overline{\overline{I}} + \frac{\eta_o}{\eta} S_o S_\ell \overline{\overline{U}}_o \cdot \overline{\overline{U}}_\ell \qquad (2.29a)$$

$$\overline{\overline{0}} = C_\ell S_o \overline{\overline{U}}_o - \frac{\eta}{\eta_o} S_\ell C_o \overline{\overline{U}}_\ell \qquad (2.29b)$$

$$\overline{a}_z \times \eta_o \overline{\overline{Y}}_{seq} = \frac{\eta_o}{\eta} C_o S_\ell \overline{\overline{U}}_\ell - S_o C_\ell \overline{\overline{U}}_o \qquad (2.29c)$$

$$\overline{\overline{I}} = C_o C_\ell \overline{\overline{I}} + \frac{\eta}{\eta_o} S_o S_\ell \overline{\overline{U}}_o \cdot \overline{\overline{U}}_\ell \qquad (2.29d)$$

in which

$$C_o = \cos k_{zo} d_\ell \qquad (2.30a)$$

$$C_\ell = \cos k_{zd} d_\ell \qquad (2.30b)$$

$$S_o = \sin k_{zo} d_\ell \qquad (2.30c)$$

$$S_\ell = \sin k_{zd} d_\ell \qquad (2.30d)$$

$$\overline{\overline{U}}_o = \frac{-1}{jk_o k_{zo}} \, \overline{a}_z \times (\overline{k}_t \overline{k}_t + k_{zo}^2 \overline{\overline{I}}) \tag{2.30e}$$

$$\overline{\overline{U}}_\ell = \frac{-1}{jkk_{zd}} \, \overline{a}_z \times (\overline{k}_t \overline{k}_t + k_{zd}^2 \overline{\overline{I}}) \tag{2.30f}$$

and $k_{zo}^2 = k_o^2 - k_t^2$, $k_{zd}^2 = k^2 - k_t^2$. Now if quantities of order $(kd)^2$ and higher are neglected, we find that eqs. (2.29a) and (2.29d) are satisfied as they stand; eq. (2.29c) yields the well-known result [7,8]

$$\eta_o \overline{\overline{Y}}_{seq} = jk_o d_\ell (\varepsilon_r - 1) \overline{\overline{I}} \tag{2.31}$$

as we expect; but eq. (2.29b) reduces to

$$\overline{\overline{0}} = jk_o d_\ell \left(1 - \frac{\varepsilon_o}{\varepsilon}\right) \overline{a}_z \times \left(\frac{\overline{k}_t \overline{k}_t}{k_o^2} - \frac{k_t^2}{k_o^2} \overline{\overline{I}}\right) \tag{2.32}$$

which is not true in general. It is obviously true if $\overline{k}_t = 0$, i.e., at normal incidence.

The condition (2.32) is also true when the electromagnetic field is polarized perpendicular to the plane of incidence. This is so because (cf. eq. (2.21c))

$$(\overline{k}_t \overline{k}_t - k_t^2 \overline{\overline{I}}) \cdot \overline{k}_t \overline{k}_t \cdot \overline{\overline{H}}_t = 0 \tag{2.33}$$

as is apparent by inspection. We now inquire under what conditions the expression (2.31) is valid for parallel-polarized fields. We consider the problem of reflection and transmission of a parallel-polarized plane electromagnetic wave by an electrically thin dielectric layer and by a sheet admittance in free space. We readily obtain the following results:

<u>thin layer</u>: $R'' = \left[\frac{jk_o d}{2} (\varepsilon_r - 1)\cos\theta - \frac{jk_t^2 d}{2k_o} \sec\theta (1 - \frac{1}{\varepsilon_r})\right] T''$ (2.34a)

30

$$T'' = [1 + \frac{jk_o d}{2}(\varepsilon_r - 1)\cos\theta + \frac{jk_t^2 d}{2k_o}\sec\theta(1 - \frac{1}{\varepsilon_r})]^{-1} \qquad (2.34b)$$

admittance sheet: $R'' = \frac{\eta_o}{2} Y_s'' \cos\theta \ T'' \qquad\qquad\qquad (2.34c)$

$$T'' = (1 + \frac{\eta_o}{2} Y_s'' \cos\theta)^{-1} \qquad\qquad\qquad (2.34d)$$

where $k_t^2 = k_o^2 \sin^2\theta$. It is apparent upon comparison of (2.34a) and (2.34b) with (2.34c) and (2.34d) that if Y_s'' is given by eq. (2.31), then we must require that for the approximation of a thin layer by an admittance sheet to be valid,

$$\tan^2\theta \ll |\varepsilon_r| \qquad\qquad\qquad (2.35)$$

where, in general,

$$\varepsilon_r \equiv \frac{1}{j\omega\varepsilon_o}(\sigma + j\omega\varepsilon) \qquad\qquad\qquad (2.36)$$

We therefore conclude that the characterization of an electrically thin layer as an equivalent sheet admittance is valid for perpendicular-polarized fields generally, and for parallel-polarized fields in which

$$\frac{k_t^2/k_o^2}{1 - k_t^2/k_o^2} \ll |\varepsilon_r| \qquad\qquad\qquad (2.37)$$

where k_o^2 denotes $\omega^2\mu_o\varepsilon_{out}$, ε_{out} being the permittivity of the medium outside the sheet admittance.

SECTION III

PLANAR GRAPHITE COMPOSITE SHIELDS

1.   INTRODUCTION

In this section we shall consider the problem of electromagnetic wave transmission through a planar layer of graphite composite in the frequency and time domains. A brief description of graphite composite materials has already been given in Section I of this report; we summarize here certain facts pertaining to these materials which are relevant to our electromagnetic analysis.

(a)   A layer of graphite composite is a layup of anisotropic laminae assembled into a "cross-ply" configuration. Therefore, the layer is itself probably anisotropic in behavior. However, some limited experimental data which has been previously mentioned [2] indicates that the anisotropy is weak. Therefore, we shall model the graphite composite as an isotropic material.

(b)   The conductivity of graphite composites appears to be roughly one-fourth that of pure graphite [1]. This value is 7.14×10^4 mho m^{-1}; we shall use a value of conductivity equal to 1.5×10^4 mho m^{-1} for the composite material in our numerical work.

(c)   Graphite composite is nonmagnetic and we shall use a value for permeability equal to that of free space in our numerical work.

In the next section, we develop the boundary connection operator for a planar graphite composite layer in free space. Then in paragraph 3, the problem of electromagnetic wave reflection and transmission by such a layer is solved in the frequency domain. The transmission of a transient EMP signal through the layer is considered in paragraph 4.

2. THE BOUNDARY CONNECTION SUPERMATRIX FOR A PLANAR GRAPHITE COMPOSITE LAYER IN FREE SPACE

The conductivity of a graphite composite is sufficiently high that the material may be considered to be a good conductor for frequencies throughout and beyond the EMP spectrum. Consequently, displacement currents may be neglected in comparison to conduction currents in the material, so that

$$k^2 = \omega^2 \mu_g \varepsilon_g - j\omega\mu_g \sigma_g \simeq -j\omega\mu_g \sigma_g \tag{3.1}$$

in which μ_g, ε_g, and σ_g denote respectively the permeability, permittivity, and conductivity of graphite composite. Furthermore, since $\sigma_g \gg \omega\varepsilon_o$ we neglect k_t^2 in comparison to k^2 in forming k_z^2: thus

$$k_z d \simeq kd = (1-j)d/\delta \tag{3.2}$$

where d is the thickness of the layer and $\delta = (2/\omega\mu_g \sigma_g)^{1/2}$ is the skin depth of the material. The boundary connection supermatrix for the graphite composite layer in free space is thus given by eq. (2.27), with $\overline{\overline{M}}_\ell$ given by eq. (2.26) and $k = (1-j)d/\delta$

$$\overline{\overline{M}}_t = \begin{bmatrix} \overline{\overline{I}} \cos(1-j)d/\delta & -j\,\dfrac{\eta}{\eta_o}\,\overline{a}_z \times \overline{\overline{I}} \sin(1-j)d/\delta \\[2em] j\,\dfrac{\eta_o}{\eta}\,\overline{a}_z \times \overline{\overline{I}} \sin(1-j)d/\delta & \overline{\overline{I}} \cos(1-j)d/\delta \end{bmatrix} \tag{3.3}$$

in which $\eta = \sqrt{j\omega\mu_g/\sigma_g}$ is the characteristic impedance of the graphite composite.

In the low-frequency limit $(d/\delta \ll 1)$

$$\overline{\overline{M}}_t \simeq \begin{bmatrix} \overline{\overline{I}} & -jk_o d\,\overline{a}_z \times \overline{\overline{I}} \\[2em] \eta_o \sigma_g d\,\overline{a}_z \times \overline{\overline{I}} & \overline{\overline{I}} \end{bmatrix} \tag{3.4}$$

33

and when $d/\delta \gg 1$

$$\bar{\bar{M}}_t \simeq \frac{1}{2} e^{(1+j)d/\delta} \begin{bmatrix} \bar{\bar{I}} & -\frac{\eta}{\eta_o} \bar{a}_z \times \bar{\bar{I}} \\ \frac{\eta_o}{\eta} \bar{a}_z \times \bar{\bar{I}} & \bar{\bar{I}} \end{bmatrix} \qquad (3.5)$$

Additionally, we note that

$$\frac{\eta_o}{\eta} \approx \sqrt{-j} \left[\frac{\eta_o \sigma_g d}{k_o d} \right]^{1/2} \qquad (3.6a)$$

$$\frac{\eta}{\eta_o} \approx \sqrt{j} \left[\frac{k_o d}{\eta_o \sigma_g d} \right]^{1/2} \qquad (3.6b)$$

3. PLANE-WAVE REFLECTION AND TRANSMISSION BY A PLANAR GRAPHITE COMPOSITE
    LAYER

The geometry of the problem to be considered in this section is shown
in Fig. (3.1). A plane electromagnetic wave of frequency ω is incident
upon a planar graphite composite layer of thickness d, from the region
$z < 0$; the angle of incidence is θ. The medium outside the layer is
free space. The reflected and transmitted fields are to be determined
as functions of the wave frequency.

The incident wave in the region $z < 0$ is given by

$$\bar{E}_{inc} = [E'_0 \bar{a}_y + E''_0 (\bar{a}_x \cos\theta - \bar{a}_z \sin\theta)] e^{-jk_o(x\sin\theta + z\cos\theta)} \qquad (3.7a)$$

$$\eta_o \bar{H}_{inc} = [E'_0 (\bar{a}_z \sin\theta - \bar{a}_x \cos\theta) + E''_0 \bar{a}_y] E^{-jk_o(x\sin\theta + z\cos\theta)} \qquad (3.7b)$$

in which E'_0 and E''_0 denote the amplitudes of the perpendicular-polarized
and parallel-polarized components of the incident-wave electric field.
The reflected wave in the region $z < 0$ is

34
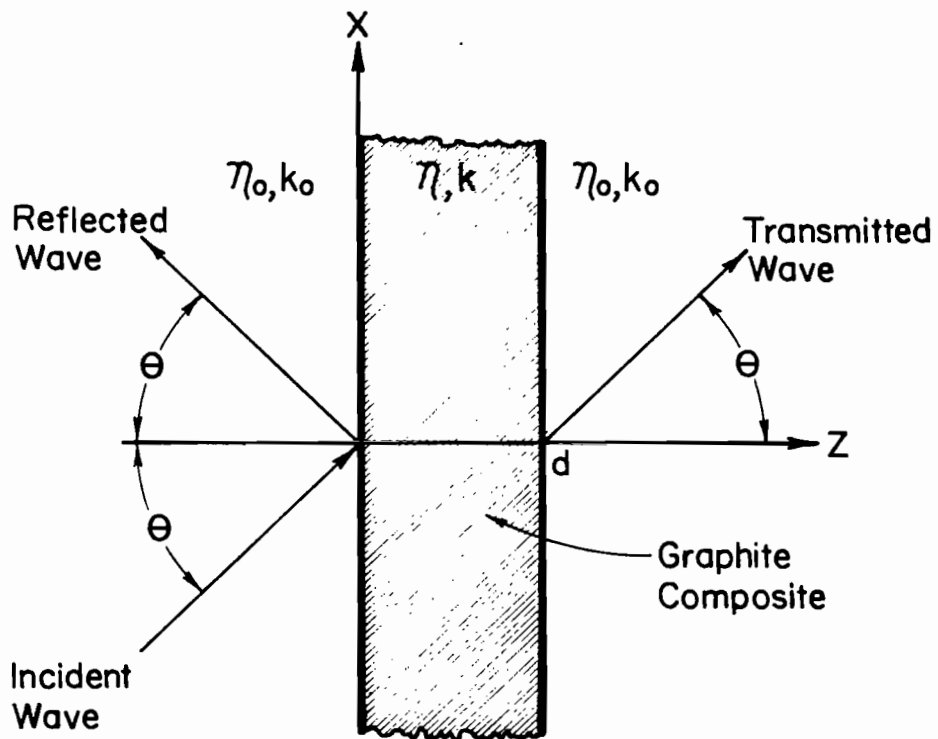
Figure 3.1.   Reflection and transmission of a plane wave by a planar
graphite composite layer: geometry of the problem

$$\bar{E}_{ref} = [R'E_0'\bar{a}_y - R''E_0''(\bar{a}_x\cos\theta + \bar{a}_z\sin\theta)]e^{-jk_o(x\sin\theta - z\cos\theta)} \qquad (3.8a)$$

$$\eta_o\bar{H}_{ref} = [R'E_0'(\bar{a}_x\cos\theta + \bar{a}_z\sin\theta) + R''E_0''\bar{a}_y]E^{-jk_o(x\sin\theta - z\cos\theta)} \qquad (3.8b)$$

and the transmitted wave in the region z > d is

$$\bar{E}_{trans} = [T'E_0'\bar{a}_y + T''E_0''(\bar{a}_x\cos\theta - \bar{a}_z\sin\theta)]e^{-jk_o[x\sin\theta + (z-d)\cos\theta]}$$

$$(3.9a)$$

$$\eta_o\bar{H}_{trans} = [T'E_0'(\bar{a}_z\sin\theta - \bar{a}_x\cos\theta) + T''E_0''\bar{a}_y]e^{-jk_o[x\sin\theta + (z-d)\cos\theta]}$$

$$(3.9b)$$

in which R', R'', T', and T'' are the reflection and transmission coefficients

for the perpendicular-polarized and parallel-polarized parts of the field.

The tangential components of the fields at z = 0 and z = d are

$$\tilde{\bar{E}}_t'(0) = (1 + R')E_0' \bar{a}_y$$

$$\eta_o \tilde{\bar{H}}_t''(0) = -\cos\theta(1 - R')E_0' \bar{a}_x$$

$$\tilde{\bar{E}}_t''(0) = \cos\theta(1 - R'')E_0'' \bar{a}_x$$

$$\eta_o \tilde{\bar{H}}_t'(0) = (1 + R'')E_0'' \bar{a}_y$$

$$\tilde{\bar{E}}_t'(d) = T'E_0' \bar{a}_y \qquad (3.10)$$

$$\eta_o \tilde{\bar{H}}_t''(d) = -\cos\theta \, T'E_0' \bar{a}_x$$

$$\tilde{\bar{E}}_t''(d) = \cos\theta T''E_0'' \bar{a}_x$$

$$\eta_o \tilde{\bar{H}}_t'(d) = T''E_0'' \bar{a}_y$$

Connecting these fields across the graphite composite layer using the boundary connection supermatrix given in eq. (3.3) yields two sets of equations which may be solved for the reflection and transmission coefficients. We have

$$
\begin{bmatrix}
-C - j \dfrac{n}{n_o} \cos\theta\ S & 1 \\[2ex]
\cos\theta\ C + j \dfrac{n_o}{n} S & \cos\theta
\end{bmatrix}
\begin{bmatrix}
R' \\[2ex]
T'
\end{bmatrix}
=
\begin{bmatrix}
C - j \dfrac{n}{n_o} \cos\theta\ S \\[2ex]
\cos\theta\ C - j \dfrac{n_o}{n} S
\end{bmatrix}
\tag{3.11a}
$$

$$
\begin{bmatrix}
\cos\theta\ C + j \dfrac{n}{n_o} S & \cos\theta \\[2ex]
C + j \dfrac{n_o}{n} \cos\theta\ S & -1
\end{bmatrix}
\begin{bmatrix}
R'' \\[2ex]
T''
\end{bmatrix}
=
\begin{bmatrix}
\cos\theta\ C - j \dfrac{n}{n_o} S \\[2ex]
-C + j \dfrac{n_o}{n} \cos\theta\ S
\end{bmatrix}
\tag{3.11b}
$$

in which $C \equiv \cos(1-j)d/\delta$, $S \equiv \sin(1-j)d/\delta$. Solving eqs. (3.11), we obtain expressions for R', T', R'', and T'' as follows:

$$
R' = \frac{1}{D'}\ jS\left(\frac{n}{n_o} \cos^2\theta - \frac{n_o}{n}\right)
\tag{3.12a}
$$

$$
T' = \frac{2}{D'}\ \cos\theta
\tag{3.12b}
$$

$$
R'' = \frac{1}{D''}\ jS\left(\frac{n_o}{n} \cos^2\theta - \frac{n}{n_o}\right)
\tag{3.12c}
$$

$$
T'' = \frac{2}{D''}\ \cos\theta
\tag{3.12d}
$$

in which

$$
D' = 2\cos\theta\ C + jS\left(\frac{n}{n_o} \cos^2\theta + \frac{n_o}{n}\right)
\tag{3.13a}
$$

$$
D'' = 2\cos\theta\ C + jS\left(\frac{n_o}{n} \cos^2\theta + \frac{n}{n_o}\right)
\tag{3.13b}
$$

Now, $|\eta/\eta_o|^2 = k_o/\eta_o\sigma_g \ll 1$. Neglecting this quantity with respect to unity, which is consistent with neglecting the displacement currents with respect to the conduction currents in the graphite composite, we obtain the following expressions for the transmission coefficients:

$$T' = (C + \frac{j}{2}\frac{\eta_o}{\eta}\sec\theta\ S)^{-1} \qquad (3.14a)$$

$$T'' = (C + \frac{j}{2}\frac{\eta_o}{\eta}\cos\theta\ S)^{-1} \qquad (3.14b)$$

Further approximations to the transmission coefficients are useful. In particular, it is easy to show that for the graphite composite, the condition $d/\delta \ll \eta_o\sigma_g d$ will hold for frequencies throughout and beyond the EMP spectrum. As a consequence, the approximation

$$T' \simeq \frac{2\cos\theta}{\eta_o\sigma_g d}(1-j)\frac{d}{\delta}\csc(1-j)\frac{d}{\delta} \qquad (3.15)$$

is valid for all angles of incidence θ, and the approximation

$$T'' \simeq \frac{2\sec\theta}{\eta_o\sigma_g d}(1-j)\frac{d}{\delta}\csc(1-j)\frac{d}{\delta} \qquad (3.16)$$

is valid for angles of incidence up to a point only a few hundredths of a degree from $90°$. Eqs. (3.15) and (3.16) show that the effect on the transmission coefficients of changing the wave frequency (and thus d/δ) is almost completely separable from the effects of changing $\eta_o\sigma_g d$ and θ. Therefore, we may express T' and T'' in terms of their values at $d/\delta = 0$ approximately, as follows:

$$\begin{bmatrix} T' \\ T'' \end{bmatrix} \simeq \begin{bmatrix} T'_0 \\ T''_0 \end{bmatrix}(1-j)\frac{d}{\delta}\csc(1-j)\frac{d}{\delta} \qquad (3.17)$$

in which

$$\begin{bmatrix} T_0' \\[2mm] T_0'' \end{bmatrix} = \frac{2}{\eta_o \sigma_g d} \begin{bmatrix} \cos\theta \\[2mm] \sec\theta \end{bmatrix} \qquad (3.18)$$

Numerical results pertinent to the analysis carried out in this section are presented in Figs. 3.2 and 3.3. In Fig. 3.2, T_0' and T_0'' are plotted as functions of θ for various values of the conductivity-thickness product $\sigma_g d$ (note that if $\sigma_g = 1.5 \times 10^4$ mho m^{-1}, $\sigma_g d = 15 d_{mm}$, where d_{mm} is the layer thickness in millimeters). A plot of the magnitude and phase of $(1-j)x \csc(1-j)x$ as a function of $x = d/\delta$ is given in Fig. 3.3. Since the data in Figs. 3.2 and 3.3a are presented in logarithmic form, the curves may be used to evaluate T' and T'' for various combinations of values of $\sigma_g d$, θ, and d/δ simply by adding the appropriate quantities. It should be noted that since the magnitudes of T' and T'' decrease as the frequency is increased, the graphite composite layer acts as a low-pass filter. This point is important for understanding the transient behavior of a transmitted EMP signal, which is considered in the next paragraph.

4. EMP TRANSIENT PROPAGATION THROUGH A PLANAR GRAPHITE COMPOSITE LAYER

By using the approximate formulas for the transmission coefficients in the frequency domain which were developed in the previous section and given in eqs. (3.15) and (3.16), we may readily evaluate the temporal behavior of the transmitted wave. Making the formal substitution $s = j\omega$ in T' and T'', we construct a Laplace integral for the transmitted field as follows:

$$E_{trans}(\tau) = \frac{1}{2\pi j} \int_{\Gamma_B} E_o(s)\, \frac{2}{\eta_o \sigma_g d} \begin{pmatrix} \cos\theta \\ \sec\theta \end{pmatrix} \frac{\sqrt{s\tau_d}}{\sinh\sqrt{s\tau_d}}\, e^{s\tau}\, ds \qquad (3.19)$$

Figure 3.2. T_o' and T_o'' vs. θ
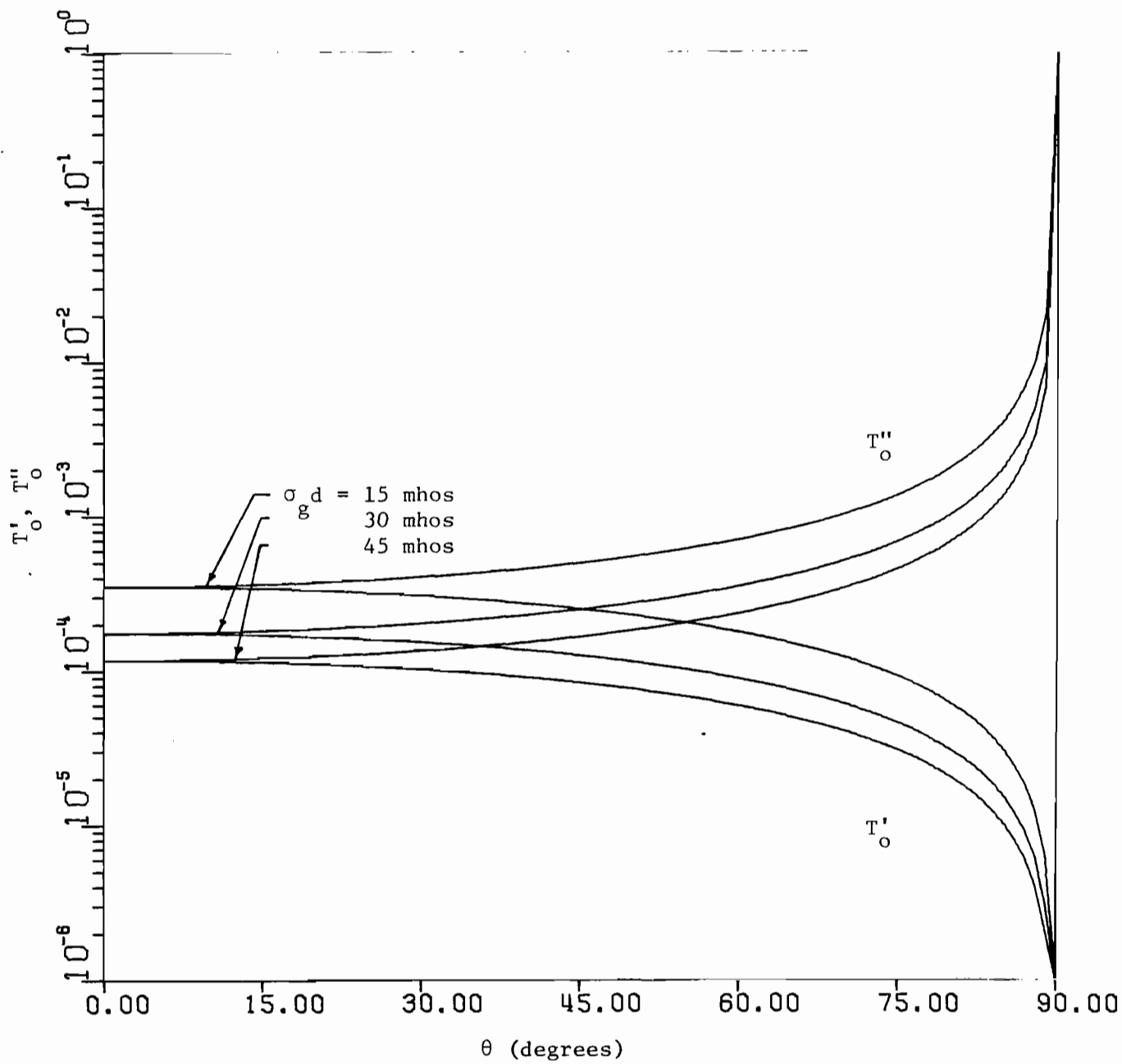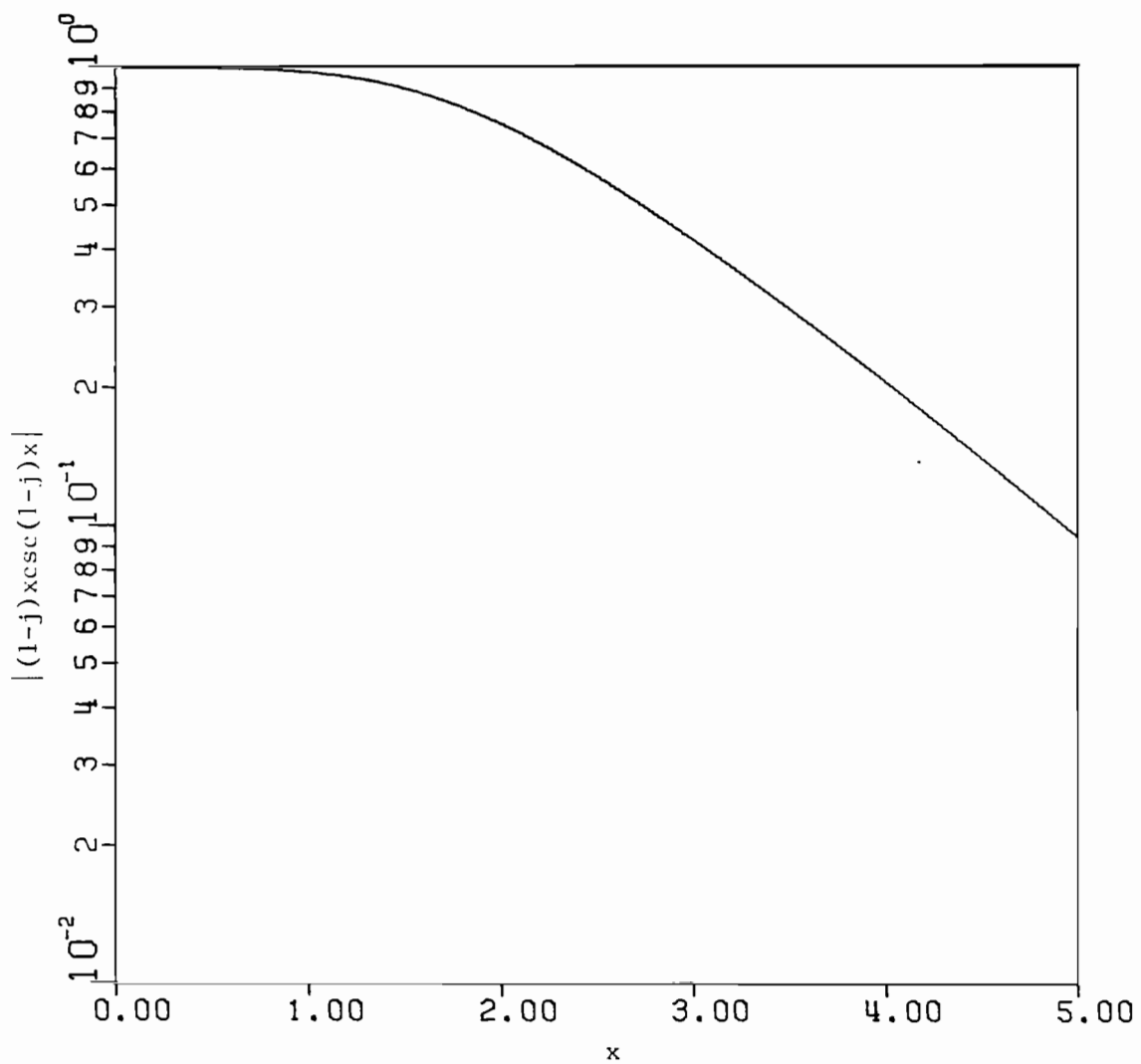
Figure 3.3a.   Magnitude of $(1-j)x\csc(1-j)x$ vs. x
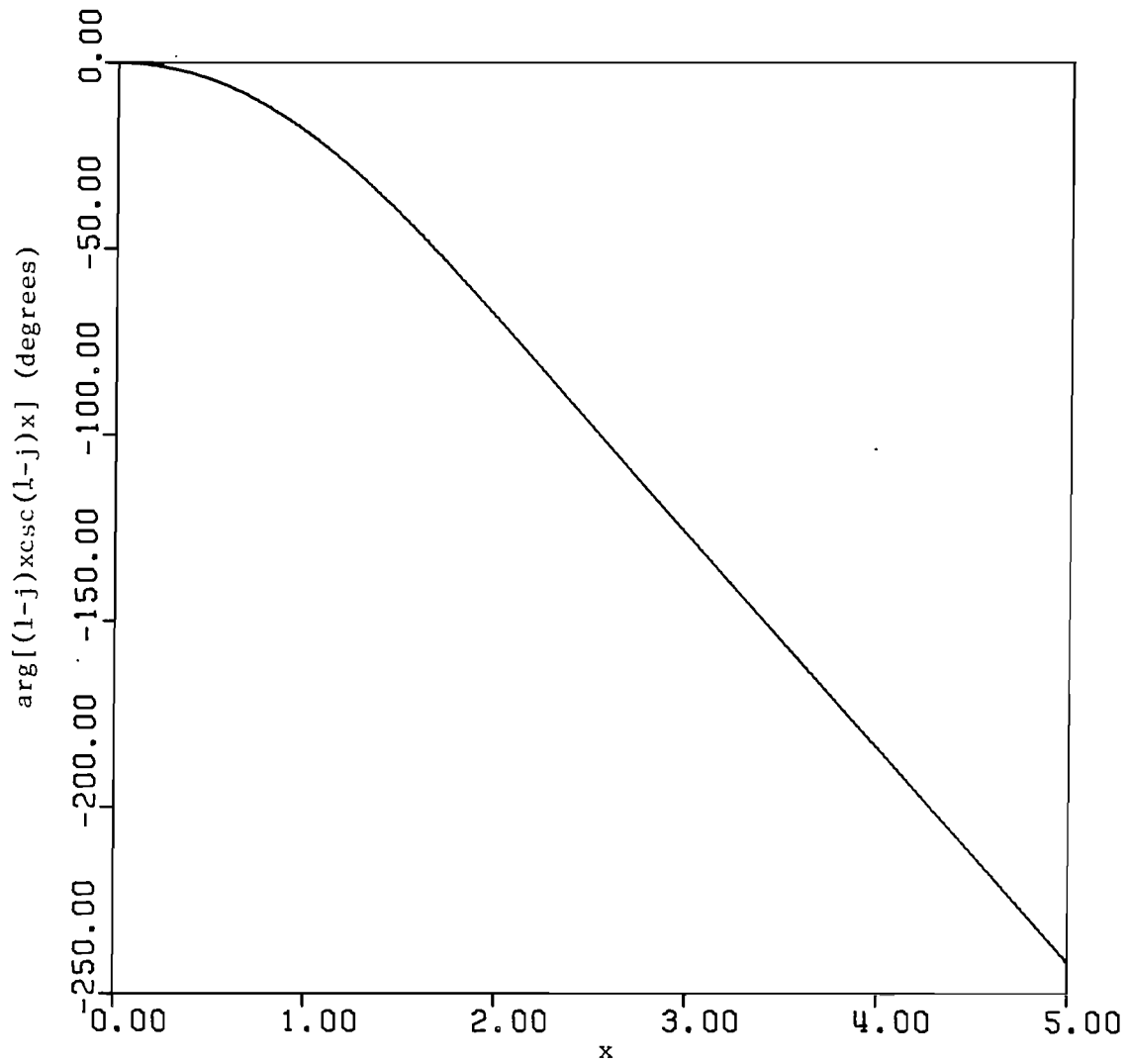
Figure 3.3b. Phase of (1-j)xcsc(1-j)x vs. x

in which Γ_B denotes the usual Bromwich contour, τ_d is the shield diffusion time, defined by

$$\tau_d = \mu_g \sigma_g d^2 \qquad (3.20)$$

and

$$\tau = t - \frac{1}{c} [x\sin\theta + (z-d)\cos\theta] \qquad (3.21)$$

$c = 1/\sqrt{\mu_o \varepsilon_o}$, the vacuum speed of light. In eq. (3.19), "$\cos\theta$" is to be used when the incident wave is polarized perpendicular to the plane of incidence, and "$\sec\theta$" is to be used for parallel polarization. $E_o(s)$ denotes the Laplace transform of the EMP signal discussed in Section I; it is

$$E_o(s) = A[\frac{1}{s+\alpha} - \frac{1}{s+\beta}] \qquad (3.22)$$

in which

$$A = (e^{-\alpha t_o} - e^{-\beta t_o})^{-1} = 1.1373... \qquad (3.23a)$$

$$t_o = \frac{1}{\beta-\alpha} \ln \frac{\beta}{\alpha} \qquad (3.23b)$$

$$\alpha = 4.80 \times 10^7 \qquad (3.23c)$$

$$\beta = 1.76 \times 10^9 \qquad (3.23d)$$

The integral in eq. (3.19) is readily evaluated using the Cauchy residue theorem. The poles of the integrand occur at $s = -\alpha$, $s = -\beta$, and

$$s = s_n = -\frac{n^2 \pi^2}{\tau_d} \qquad (n \geq 1) \qquad (3.24)$$

Furthermore, it is easy to show that Γ_B may be closed at infinity in the right half plane for $\tau < 0$, yielding a null result for $E(\tau)$, in accordance with causality; and for $\tau > 0$, Γ_B may be closed in the left half plane at infinity to yield for $E(\tau)$:

43

$$E(\tau) = \frac{2A}{\eta_o \sigma_g d} \begin{Bmatrix} \cos\theta \\ \sec\theta \end{Bmatrix} U(\tau) \left\{ \sqrt{\alpha\tau_d} \ \csc \ \sqrt{\alpha\tau_d} \ e^{-\alpha\tau} \right.$$

$$- \sqrt{\beta\tau_d} \ \csc \ \sqrt{\beta\tau_d} \ e^{-\beta\tau}$$

$$\left. + 2 \sum_{n=1}^{\infty} \frac{(-1)^n (n\pi)^2 (\alpha\tau_d - \beta\tau_d)}{(n^2\pi^2 - \alpha\tau_d)(n^2\pi^2 - \beta\tau_d)} \ e^{-n^2\pi^2\tau/\tau_d} \right\} \qquad (3.25)$$

$U(\tau)$ is the unit step function. The result in eq. (3.25) is based upon the assumption that all the poles of the integrand in eq. (3.19) are simple, i.e., that

$$(\alpha\tau_d \ \text{or} \ \beta\tau_d) \neq n^2\pi^2 \qquad (3.26)$$

for any $n \neq 0$. If this condition is violated, the appropriate limit of eq. (3.25) can be taken to yield the correct result.

Plots of $E(\tau)$ vs. τ, normalized by $(2/\eta_o \sigma_g d)$, are given for the case $\theta = 0°$ in Fig. 3.4, for three values of τ_d. The values chosen correspond if μ_g is chosen equal to the free-space value $4\pi \times 10^{-7}$ henry m^{-1} and $\sigma_g = 1.5 \times 10^4$ mho m^{-1}, to thicknesses d of 1, 2, and 3 mm. A non-normalized curve of the incident EMP signal is included for comparison. One will note the increasing attenuation of the peak value of the trans-mitted signal, the increasing time delay before the main buildup of the transmitted signal, and the increasing pulse width of the transmitted signal as d is increased. All these features are in keeping with the low-pass filter characteristic of the graphite composite layer which has been mentioned previously.
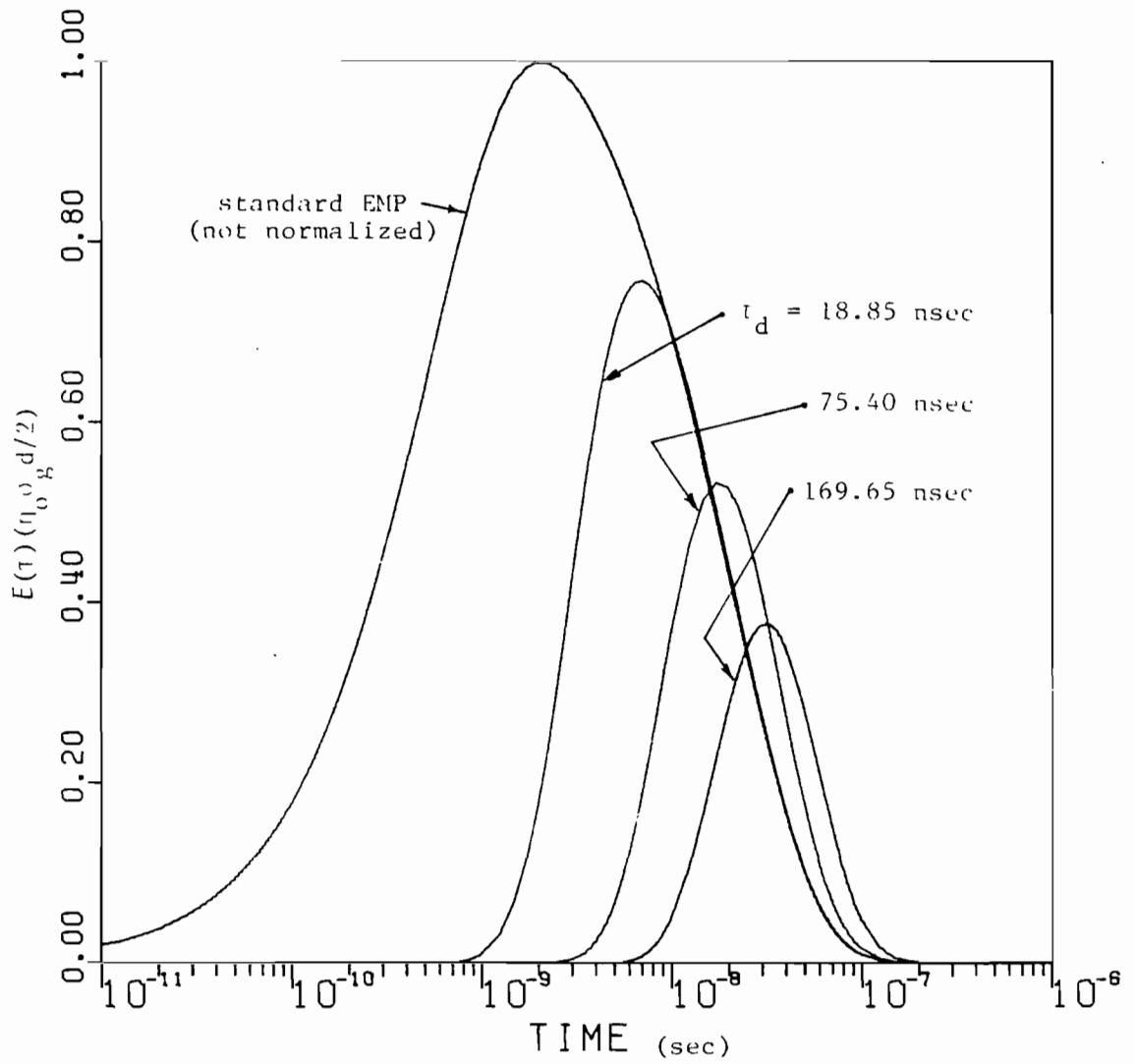
Figure 3.4.   Normalized transmitted EMP waveforms:
graphite slab, normal incidence

45

SECTION IV

CYLINDRICAL GRAPHITE COMPOSITE SHIELDS

1. INTRODUCTION

In this chapter we shall consider the problem of electromagnetic
field penetration into the interior of an infinitely long hollow cylindri-
cal shell of graphite composite. A similar problem has been recently
addressed by Schieber [9-12], who considered only cylindrical shells which
were electrically thin (i.e., the thickness of the shell was much less
than the skin depth of the shield material). He found that the axial
electric field at the center of the cylinder exhibited strong peaks as
the frequency of the incident wave was varied, these peaks occurring at
the transverse resonance frequencies of the cylinder. At these resonant
peaks, the axial field strength was equal to that of the incident wave,
so that the shielding effect of the cylinder was nil.

The shielding behavior of a thick cylindrical conducting shell was
studied by Wu and Tsai [5,13,14]. They found that when the cylindrical
shell thickness was at least equal to the skin depth of the shield
material at the resonant frequencies of the cylinder, the resonant peaks
in the axial field were significantly reduced. Resonance effects,
however, were still evident. To assess the importance of these resonances,
Wu and Tsai considered the temporal behavior of the axial electric field
when the cylindrical shell was illuminated by a normally incident TM_z-
polarized plane wave whose time dependence was that of the standard EMP
signal which has already been discussed. They found that the temporal
behavior of the axial field was only slightly affected by the cylindrical
resonances in a "worst case" analysis. In their example, the radius of'
the cylinder was 10 m and the product of the conductivity and shell

46

thickness was 0.1 mho. The reason for this behavior is, of course, that for cylinders of this size the lowest-order resonances occur for frequencies far out in the "tail" of the EMP spectrum, and so are only weakly excited. As the radius of the cylinder is decreased, the resonant frequencies are increased and their excitation becomes even weaker.

The cylindrical shells to be considered in this section have radii of 2 m or less (typical aircraft-fuselage sizes) and conductivity-thickness products of the order of 30 mhos. We therefore expect the resonance effects on the transient behavior of the internal fields induced by an EMP signal to be negligible. We introduce a new frequency-domain measure of shielding effectiveness for hollow bodies of resonant size or less which takes the entire internal field into account. This measure, based on a ratio of stored energies in the interior of the body, represents the space averages of the internal fields.

In the next paragraph, the problem of plane-wave scattering from a cylindrical shell of graphite composite is formulated in the frequency domain, using the ECS developed in the previous chapter for this material. We present results illustrating the energy shielding ratio as a function of frequency for several representative cases. Some time-domain considerations are discussed in paragraph 3 of this section.

2. FORMULATION OF THE PROBLEM: FREQUENCY-DOMAIN RESULTS

The geometry of the problem is shown in Fig. 4.1. An infinitely long cylindrical shell of graphite composite, whose inner and outer radii are a and b, respectively, is illuminated by a plane electromagnetic wave. The shell thickness d = b-a is small in comparison to the mean

47
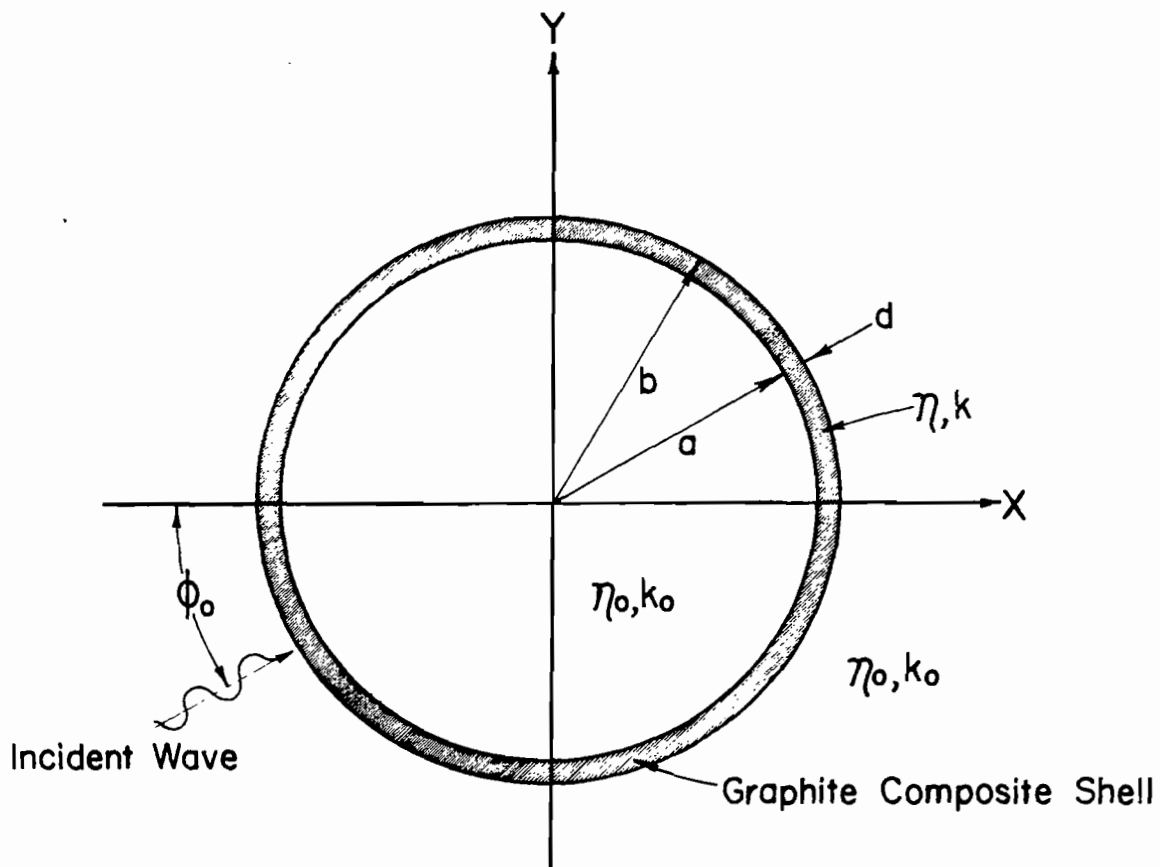
Figure 4.1. Plane-wave penetration of, and scattering by, a cylindrical shell of graphite composite: geometry of the problem

radius $\rho_o = \sqrt{ab}$. The medium outside and inside the shell is free space. For simplicity we consider only the case in which the propagation vector of the incident wave has no axial component and we shall investigate the two possible wave polarizations separately. The total fields may then be obtained by superposition.

Consider first the case in which the incident wave is polarized TM with respect to z. The field components present are E_z, H_ϕ, and H_ρ, where

$$E_z = -j\omega\mu_o \Psi \tag{4.1a}$$

$$H_\phi = -\frac{\partial \Psi}{\partial \rho} \tag{4.1b}$$

$$H_\rho = \frac{1}{\rho} \frac{\partial \Psi}{\partial \phi} \tag{4.1c}$$

and

$$\frac{1}{\rho} \frac{\partial}{\partial \rho} \left(\rho \frac{\partial \Psi}{\partial \rho} \right) + \frac{1}{\rho^2} \frac{\partial^2 \Psi}{\partial \phi^2} + k_o^2 \Psi = 0 \tag{4.2}$$

in the free-space regions. In the interior and exterior regions of the problem, appropriate expressions for Ψ are

$$0 \leq \rho < a: \quad \Psi = \frac{-E_o}{j\omega\mu_o} \sum_{n=-\infty}^{\infty} A_n J_n(k_o\rho) e^{jn(\phi-\phi')} \tag{4.3a}$$

$$b < \rho \leq \infty: \quad \Psi = \frac{-E_o}{j\omega\mu_o} \sum_{n=-\infty}^{\infty} [J_n(k_o\rho) + B_n H_n^{(2)}(k_o\rho)] e^{jn(\phi-\phi')} \tag{4.3b}$$

where A_n and B_n are to be determined, E_o is the amplitude of the incident electric field, and

$$\phi' = \phi_o + \pi/2 \tag{4.4}$$

ϕ_o is the angle of incidence shown in Fig. 4.1.

49

In order to evaluate the coefficients A_n and B_n, the tangential field components are connected across the graphite composite shell using the appropriate connection supermatrix, which is that given in eq. (3.3), modified for the change in the coordinate system ($\bar{a}_z$ is replaced by $\bar{a}_\rho$):

$$\bar{\bar{M}}_t = \begin{bmatrix} \bar{\bar{I}} \cos(1-j)d/\delta & -j \frac{n}{n_o} \bar{a}_\rho \times \bar{\bar{I}} \sin(1-j)d/\delta \\ \\ j \frac{n_o}{n} \bar{a}_\rho \times \bar{\bar{I}} \sin(1-j)d/\delta & \bar{\bar{I}} \cos(1-j)d/\delta \end{bmatrix} \qquad (4.5)$$

The spectra of the tangential field components at $\rho=a$ and $\rho=b$ are

$$\tilde{\bar{E}}_t(\rho=a) = E_o A_n J_n(k_o a) e^{-jn\phi'} \bar{a}_z \qquad (4.6a)$$

$$n_o \tilde{\bar{H}}_t(\rho=a) = -jE_o A_n J_n'(k_o a) e^{-jn\phi'} \bar{a}_\phi \qquad (4.6b)$$

$$\tilde{\bar{E}}_t(\rho=b) = E_o [J_n(k_o b) + B_n H_n^{(2)}(k_o b)] e^{-jn\phi'} \bar{a}_z \qquad (4.6c)$$

$$n_o \tilde{\bar{H}}_t(\rho=b) = -jE_o [J_n'(k_o b) + B_n H_n^{(2)'}(k_o b)] e^{-jn\phi'} \bar{a}_\phi \qquad (4.6d)$$

in which the primes (') denote differentiation with respect to the argument. For this problem, the spectral variable $\bar{k}_t = (n/\rho)\bar{a}_\phi$. Connecting these spectral components using $\bar{\bar{M}}_t$ as given in eq. (4.5) yields a pair of equations for A_n and B_n:

$$\begin{bmatrix} J_n(k_o a)C + \frac{n}{n_o} J_n'(k_o a)S & -H_n^{(2)}(k_o b) \\ \\ J_n'(k_o a)C - \frac{n_o}{n} J_n(k_o a)S & -H_n^{(2)'}(k_o b) \end{bmatrix} \begin{bmatrix} A_n \\ \\ B_n \end{bmatrix} = \begin{bmatrix} J_n(k_o b) \\ \\ J_n'(k_o b) \end{bmatrix} \qquad (4.7)$$

Solving eq. (4.7) for A_n and B_n, we obtain

$$A_n = \frac{1}{D_n} \left(\frac{2j}{\pi k_o b} \right) \qquad (4.8a)$$

50

$$B_n = \frac{1}{D_n} \left\{ C[J_n(k_o a)J_n'(k_o b) - J_n'(k_o a)J_n(k_o b)] \right.$$

$$\left. + S[\frac{n}{n_o} J_n'(k_o a)J_n'(k_o b) + \frac{n_o}{n} J_n(k_o a)J_n(k_o b)] \right\} \qquad (4.8b)$$

where

$$D_n = C[J_n'(k_o a)H_n^{(2)}(k_o b) - J_n(k_o a)H_n^{(2)'}(k_o b)]$$

$$- S[\frac{n}{n_o} J_n'(k_o a)H_n^{(2)'}(k_o b) + \frac{n_o}{n} J_n(k_o a)H_n^{(2)}(k_o b)] \qquad (4.9)$$

C and S denote $\cos(1-j)d/\delta$ and $\sin(1-j)d/\delta$ respectively. A_n and B_n may be simplified if we assume that $k_o d \ll 1$ and $|n/n_o|^2 \ll 1$. These conditions hold throughout the EMP spectrum in the cases we consider; so we obtain

$$A_n \simeq [C + \frac{n_o \sigma g d}{2} (\pi k_o \rho_o)J_n(k_o \rho_o)H_n^{(2)}(k_o \rho_o) \frac{S}{(1-j)d/\delta}]^{-1} \qquad (4.10a)$$

$$B_n \simeq -A_n \frac{n_o \sigma g d}{2} (\pi k_o \rho_o)J_n^2(k_o \rho_o) \frac{S}{(1-j)d/\delta} \qquad (4.10b)$$

A useful frequency-domain measure of the shielding effectiveness of the graphite shell is the ratio of the time-average stored energy per unit length inside the shell ($0<\rho<a$) to the time-average stored energy per unit length in the same region with the shell removed. Since this ratio is obtained by integrating the stored energy density throughout the cylindrical volume, it represents an "averaged" shielding effect, and so may be more useful than, say, the axial field strength, as a shielding effectiveness measure for a closed surface. It is easy to show that the time-average stored energy per unit length inside the cylinder is

51

$$W = \frac{\pi \varepsilon_o E_o^2}{2} \sum_{n=-\infty}^{\infty} |A_n|^2 \int_0^a [J_n^2(k_o\rho)\left(1 + \frac{n^2}{k_o^2\rho^2}\right) + J_n'(k_o\rho)^2]\rho\,d\rho \qquad (4.11)$$

In the absence of the cylinder, the time-average stored energy in the same volume is simply $\varepsilon_o \pi a^2 E_o^2/2$; so performing the integrations in eq. (4.11) and normalizing the result yields the "energy shielding ratio" r_w:

$$r_w = \sum_{n=-\infty}^{\infty} |A_n|^2 \ [J_n'(k_o a)^2 + J_n(k_o a)^2\left(1 - \frac{n^2}{k_o^2 a^2}\right)$$

$$+ \frac{1}{k_o a} J_n(k_o a)J_n'(k_o a)] \qquad (4.12)$$

When $k_o a \ll 1$, $r_w \simeq \frac{1}{2}(|A_o|^2 + |A_1|^2)$, and we obtain an approximate low-frequency expression for r_w as follows:

$$r_w\Big|_{k_o a \ll 1} \simeq \frac{1}{2}\left\{ \left|C - j\eta_o\sigma_g d\ k_o\rho_o\ \frac{S}{(1-j)d/\delta}\ \ell n\ k_o\rho_o\right|^{-2} \right.$$

$$\left. + \left|C + j\ \frac{\eta_o\sigma_g d}{2}\ k_o\rho_o\ \frac{S}{(1-j)d/\delta}\right|^{-2}\right\} \qquad (4.13)$$

Curves of r_w as a function of frequency are given in Figs. 4.2-4.4 for various values of ρ_o, d, and σ_g. The values of ρ_o chosen correspond to typical aircraft; d = 1, 2, and 3 mm; and σ_g varies around the base value 1.5×10^4 mho m^{-1}.

The analysis for the case in which the incident wave is polarized TE to z is similarly carried out. The field components present are H_z, E_ϕ, and E_ρ, where

$$H_z = j\omega\varepsilon_o\ \Phi \qquad (4.14a)$$

$$E_\phi = -\frac{\partial\Phi}{\partial\rho} \qquad (4.14b)$$

$$E_\rho = \frac{1}{\rho}\frac{\partial\Phi}{\partial\phi} \qquad (4.14c)$$

Figure 4.2.   Energy shielding ratio r_w vs. frequency with a as parameter; d = 2 mm, σ_g = 1.5 x 10^4 mho m^{-1} .

53

Figure 4.3.   Energy shielding ratio r_w vs. frequency with σ_g as parameter; d = 2 mm, a = 1 m

Figure 4.4. Energy shielding ratio r_w vs. frequency with d as parameter; $a = 1$ m, $\sigma_g = 1.5 \times 10^4$ mho m^{-1}

55

and

$$\frac{1}{\rho}\frac{\partial}{\partial\rho}\left(\rho\frac{\partial\Phi}{\partial\rho}\right) + \frac{1}{\rho^2}\frac{\partial^2\Phi}{\partial\phi^2} + k_o^2\Phi = 0 \tag{4.15}$$

in the free-space regions. Φ is given in the interior and exterior regions by

$$0 \le \rho < a: \quad \Phi = \frac{E_o}{jk_o}\sum_{n=-\infty}^{\infty}A_n'J_n(k_o\rho)e^{jn(\phi-\phi')} \tag{4.16a}$$

$$b < \rho \le \infty: \quad \Phi = \frac{E_o}{jk_o}\sum_{n=-\infty}^{\infty}[J_n(k_o\rho) + B_n'H_n^{(2)}(k_o\rho)]e^{jn(\phi-\phi')} \tag{4.16b}$$

in which A_n' and B_n' are to be determined. Applying the connection operator $\overline{\overline{M}}_t$ given in eq. (4.5) to the field representations obtained from eqs. (4.14)-(4.16), we solve for A_n' and B_n', obtaining

$$A_n' = \frac{1}{D_n'}\left(\frac{2j}{\pi k_o b}\right) \tag{4.17a}$$

$$B_n' = \frac{1}{D_n'}\left\{C[J_n(k_o a)J_n'(k_o b) - J_n'(k_o a)J_n(k_o b)]\right.$$

$$\left. + S[\frac{\eta_o}{\eta}J_n'(k_o a)J_n'(k_o b) + \frac{\eta}{\eta_o}J_n(k_o a)J_n(k_o b)]\right\} \tag{4.17b}$$

where

$$D_n' = C[J_n'(k_o a)H_n^{(2)}(k_o b) - J_n(k_o a)H_n^{(2)'}(k_o b)]$$

$$- S[\frac{\eta_o}{\eta}J_n'(k_o a)H_n^{(2)'}(k_o b) + \frac{\eta}{\eta_o}J_n(k_o a)H_n^{(2)}(k_o b)] \tag{4.18}$$

Approximate expressions for A_n' and B_n', valid if $k_o d \ll 1$ and $|\eta/\eta_o|^2 \ll 1$ as we assume, are

$$A_n' = [C + \frac{\eta_o \sigma_g d}{2} (\pi k_o \rho_o) J_n'(k_o \rho_o) H_n^{(2)'}(k_o \rho_o) \frac{S}{(1-j)d/\delta}]^{-1} \qquad (4.19a)$$

$$B_n' = -A_n' \frac{\eta_o \sigma_g d}{2} (\pi k_o \rho_o) J_n'(k_o \rho_o)^2 \frac{S}{(1-j)d/\delta} \qquad (4.19b)$$

The energy shielding ratio for this polarization, r_w', is given by

$$r_w' = \sum_{n=-\infty}^{\infty} |A_n'|^2 \; [J_n'(k_o a)^2 + J_n(k_o a)^2 \left(1 - \frac{n^2}{k_o^2 a^2}\right)$$

$$+ \frac{1}{k_o a} J_n(k_o a) J_n'(k_o a)] \qquad (4.20)$$

In the case $k_o a \ll 1$, $r_w' \simeq \frac{1}{2}(|A_o'|^2 + |A_1'|^2)$, and we obtain an approximate low-frequency expression for r_w' as

$$r_w' \Big|_{k_o a \ll 1} \simeq \frac{1}{2} \left\{ |C + j \frac{\eta_o \sigma_g d}{2} k_o \rho_o \frac{S}{(1-j)d/\delta}|^{-2} \right.$$

$$\left. + |C - j \frac{\eta_o \sigma_g d}{2 k_o \rho_o} \frac{S}{(1-j)d/\delta}|^{-2} \right\} \qquad (4.21)$$

Curves of r_w' as a function of frequency are given in Figs. 4.5-4.7 for the same values of a, d, and σ_g used in the curves for r_w calculated previously.

It will be noted that when $d/\delta \ll 1$, $r_w \to 1$ as $k_o \rho_o \to 0$ but $r_w' \to \frac{1}{2}$ as $k_o \rho_o \to 0$. This is so because the TE electric field (which is normal to the cylinder axis) terminates on surface charges on the cylinder surface. Thus r_w' contains only a contribution from the internal magnetic field, while both electric and magnetic fields contribute to r_w. One will also note from eqs. (4.13) and (4.21) and Figs. 4.2-4.7 that the principal "break frequency" for both r_w and r_w' is approximately $1/\pi \mu_o \rho_o \sigma_g d$.
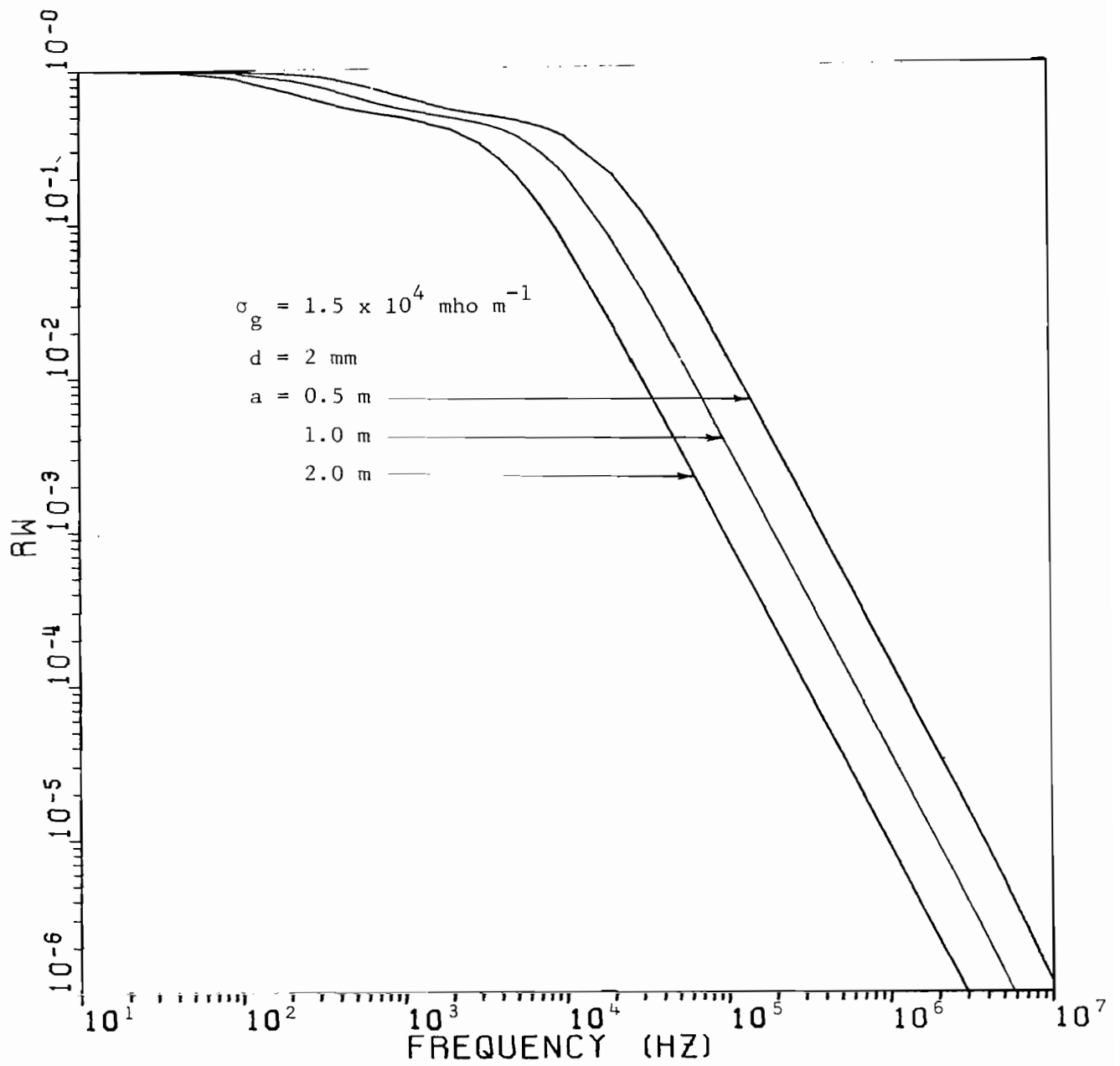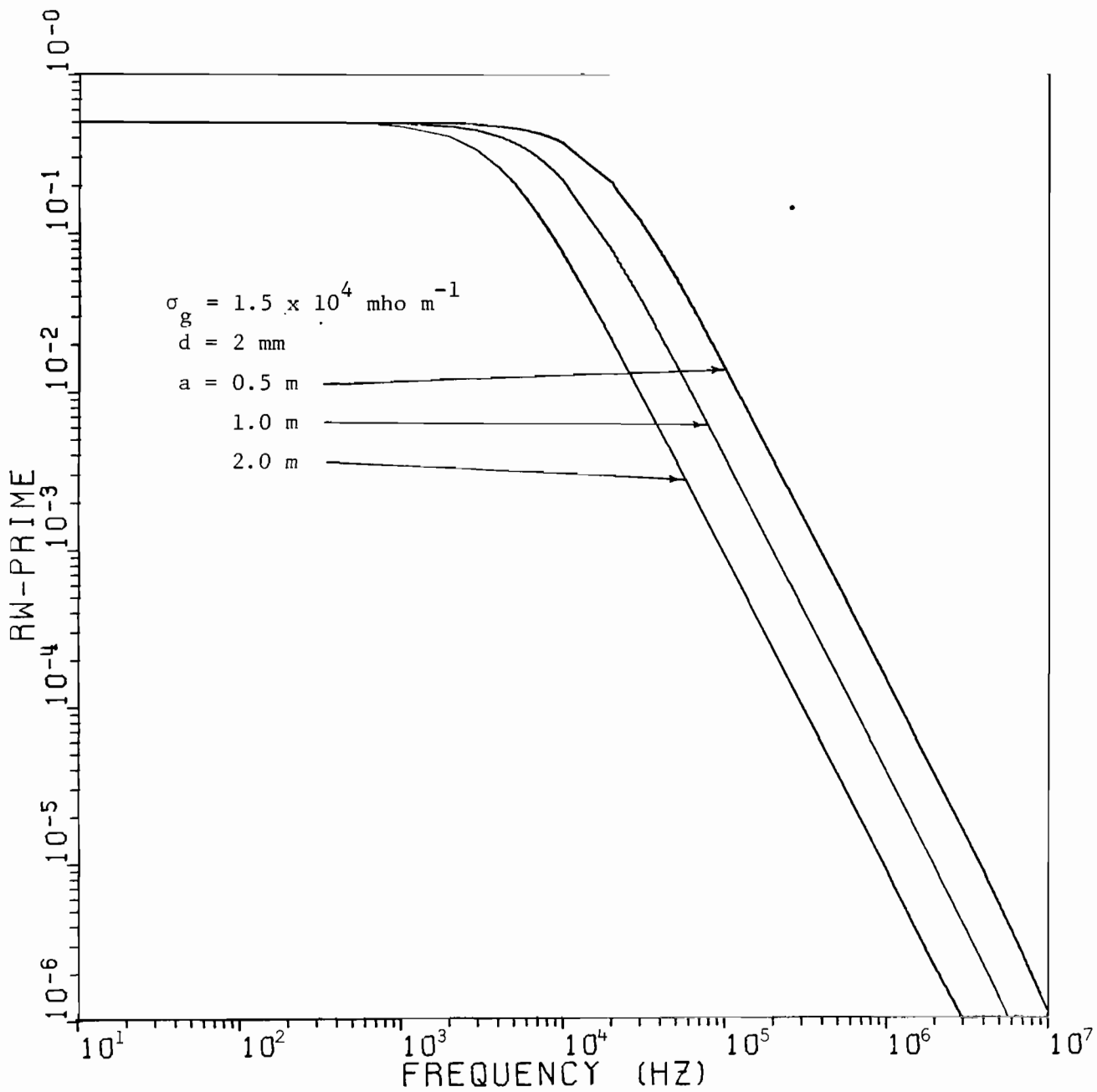
Figure 4.5. Energy shielding ratio r'_w vs. frequency with a as parameter; $d = 2$ mm, $\sigma_g = 1.5 \times 10^4$ mho m^{-1}
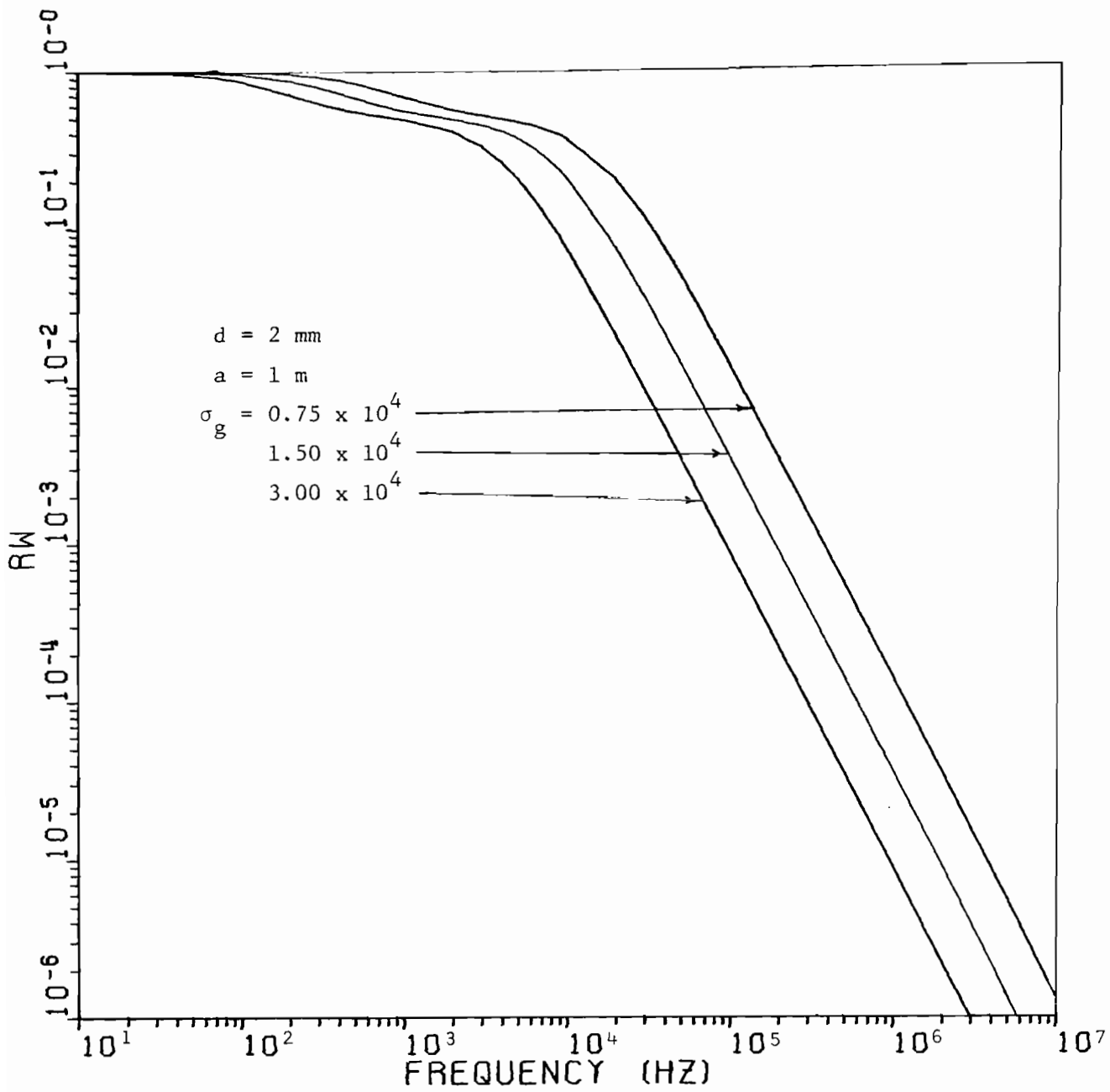
58
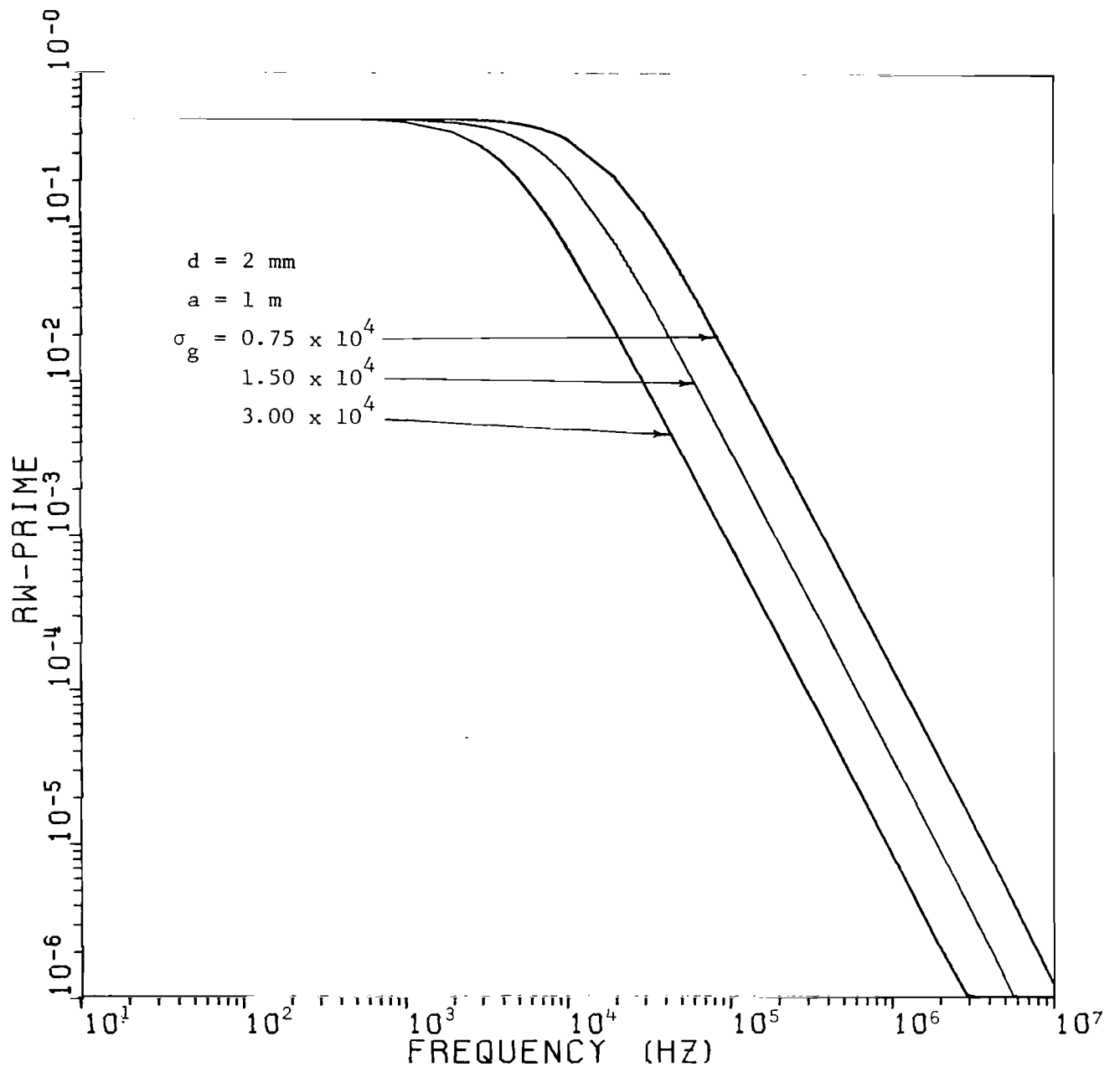
Figure 4.6. Energy shielding ratio r_w' vs. frequency with σ_g as parameter; $d = 2$ mm, $a = 1$ m

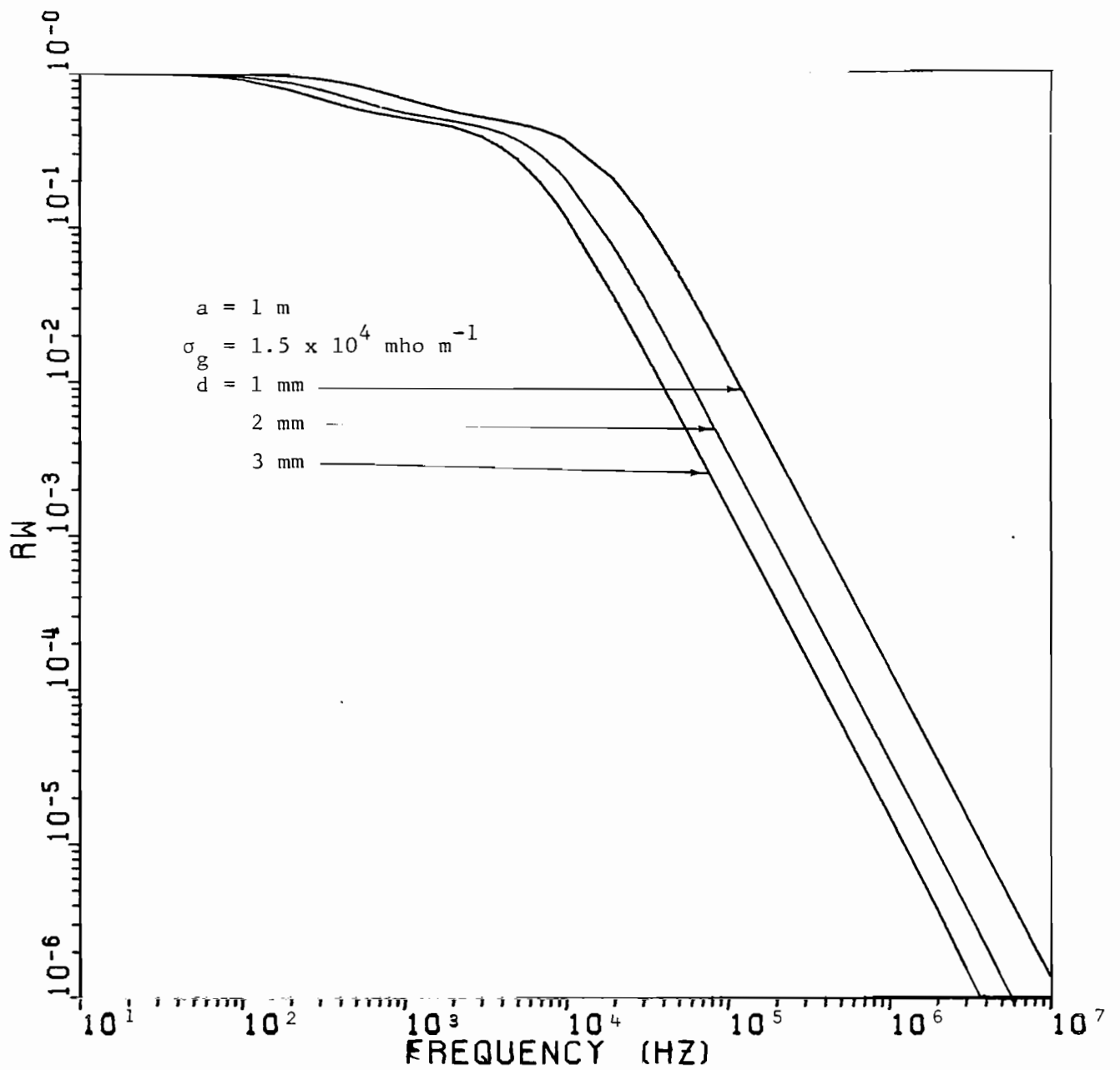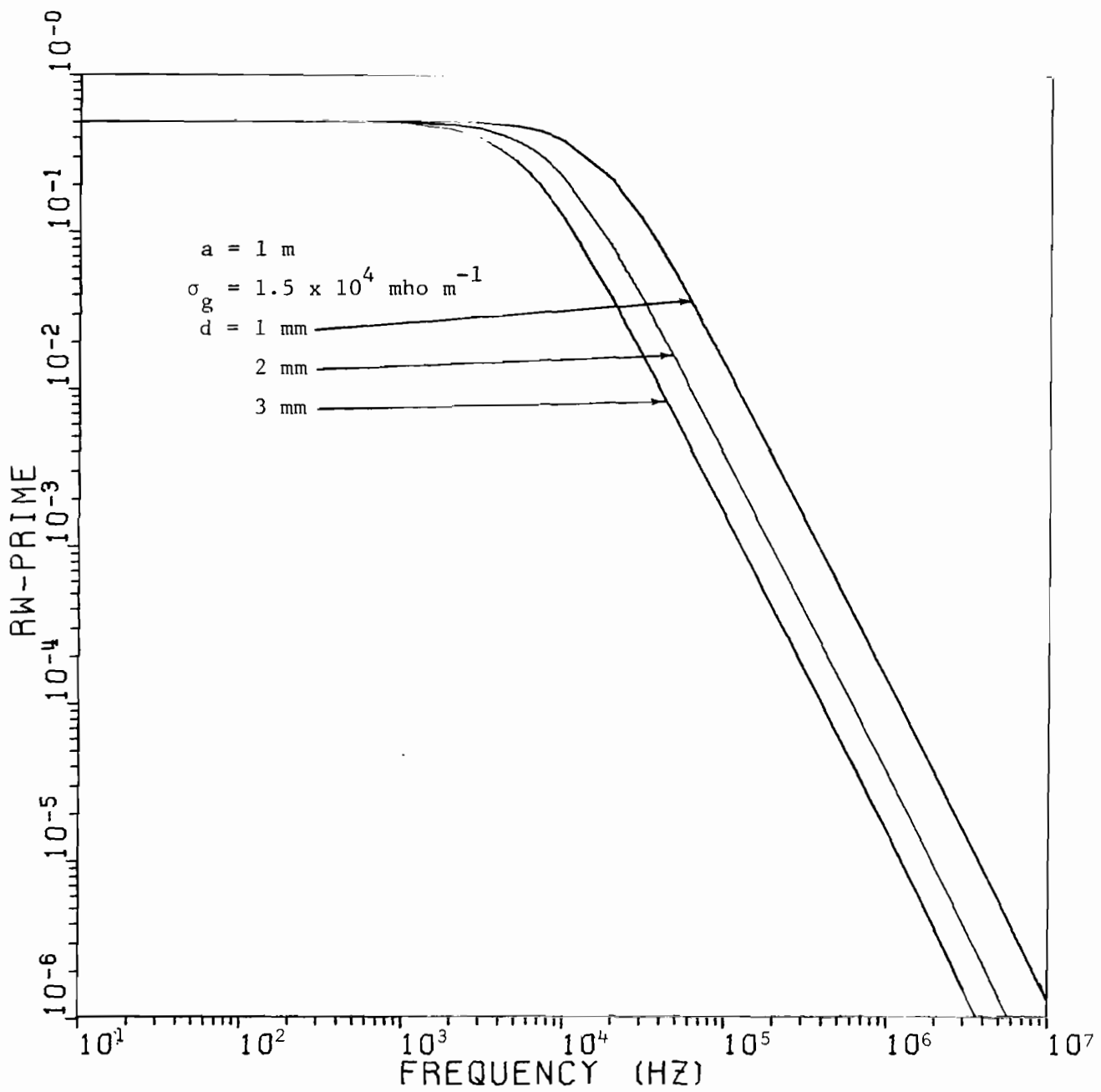Figure 4.7. Energy shielding ratio r_w' vs. frequency with d as parameter; $a = 1$ m, $\sigma_g = 1.5 \times 10^4$ mho m^{-1}

3. TIME-DOMAIN SHIELDING

In the frequency domain the ratio of the internal magnetic field H_{int} to the incident magnetic field H_{inc} is readily shown at low frequencies to be

$$\frac{H_{int}}{H_{inc}} = [C + j \frac{\eta_o \sigma_g d}{2} k_o \rho_o \frac{s}{(1-j)d/\delta}]^{-1} \qquad (4.22)$$

for either polarization. We now construct a Laplace integral for the internal field as follows (the incident waveform is the standard EMP double exponential):

$$H_{int}(t) = \frac{2dA}{\eta_o \rho_o} \frac{1}{2\pi j} \int_{\Gamma_B} (\frac{1}{s+\alpha} - \frac{1}{s+\beta}) \frac{e^{st} \, ds}{\sqrt{s\tau_d} \sinh \sqrt{s\tau_d} + \frac{2d}{\rho_o} \cosh \sqrt{s\tau_d}} \qquad (4.23)$$

in which all quantities have been previously defined. Now $2d/\rho_o \ll 1$ in the cases which we consider, so that the poles of the integrand, in addition to those at $s = -\alpha$ and $s = -\beta$, are approximately located at $s = -2d/\rho_o \tau_d$ and $-n^2 \pi^2 / \tau_d$ ($n \geq 1$). Thus we obtain for the internal magnetic field the approximate expression

$$H_{int}(t) \simeq \frac{2dA}{\rho_o \eta_o} [\frac{e^{-\beta t}}{\sqrt{\beta\tau_d} \sin \sqrt{\beta\tau_d}} - \frac{e^{-\alpha t}}{\sqrt{\alpha\tau_d} \sin \sqrt{\alpha\tau_d}}$$

$$+ 2(\beta-\alpha)\tau_d \sum_{n=1}^{\infty} \frac{(-1)^n e^{-n^2\pi^2 t/\tau_d}}{(\alpha\tau_d - n^2\pi^2)(\beta\tau_d - n^2\pi^2)}$$

$$+ \left(\frac{1}{\alpha\tau_d} - \frac{1}{\beta\tau_d}\right) e^{-(2d/\rho_o \tau_d)t}] \, U(t) \qquad (4.24)$$

in which we have made use of the assumption $\alpha\tau_d \gg 2d/\rho_o$. This assumption is easily satisfied in the cases we consider.

For late times, the dominant contribution to $H_{int}(t)$ is the last term in (4.24) (cf. ref. [15]):

$$H_{int}(t) \rightarrow \frac{2Ad}{\eta_o \rho_o} \left[\frac{1}{\alpha \tau_d} - \frac{1}{\beta \tau_d} \right] e^{-(2d/\rho_o \tau_d)t} \qquad (4.25)$$

A plot of $\eta_o H_{int}(t)$ vs. t for three values of τ_d is shown in Fig. 4.8[†]. The three values of τ_d chosen correspond to thicknesses d of 1, 2, and 3 mm if $\sigma_g = 1.5 \times 10^4$ mho m^{-1} and $\dot{\mu}_g = \mu_o$. The radius ρ_o is taken to be 1 m in each case. The contribution of the expression in (4.25) at late times is readily apparent.

Comparing Fig. 4.8 with Fig. 3.4, one will observe the "integrating" or "low-pass" character of the cylindrical geometry itself. Thus an incident signal is, in a sense, doubly low-pass filtered in passing into the interior of a cylindrical region shielded by a conducting shell. Contrasting behavior is evidenced by screened composite structures, which we shall consider in the next two sections.

[†] The reader is reminded that in Cal Comp plots such as Fig. 4.8, the axis labeling is such that the exponential factor (in this case 10^{-2}) is to be associated with the ordinate values, not with the axis label. Thus the maximum ordinate in Fig. 4.8 is 0.0025.
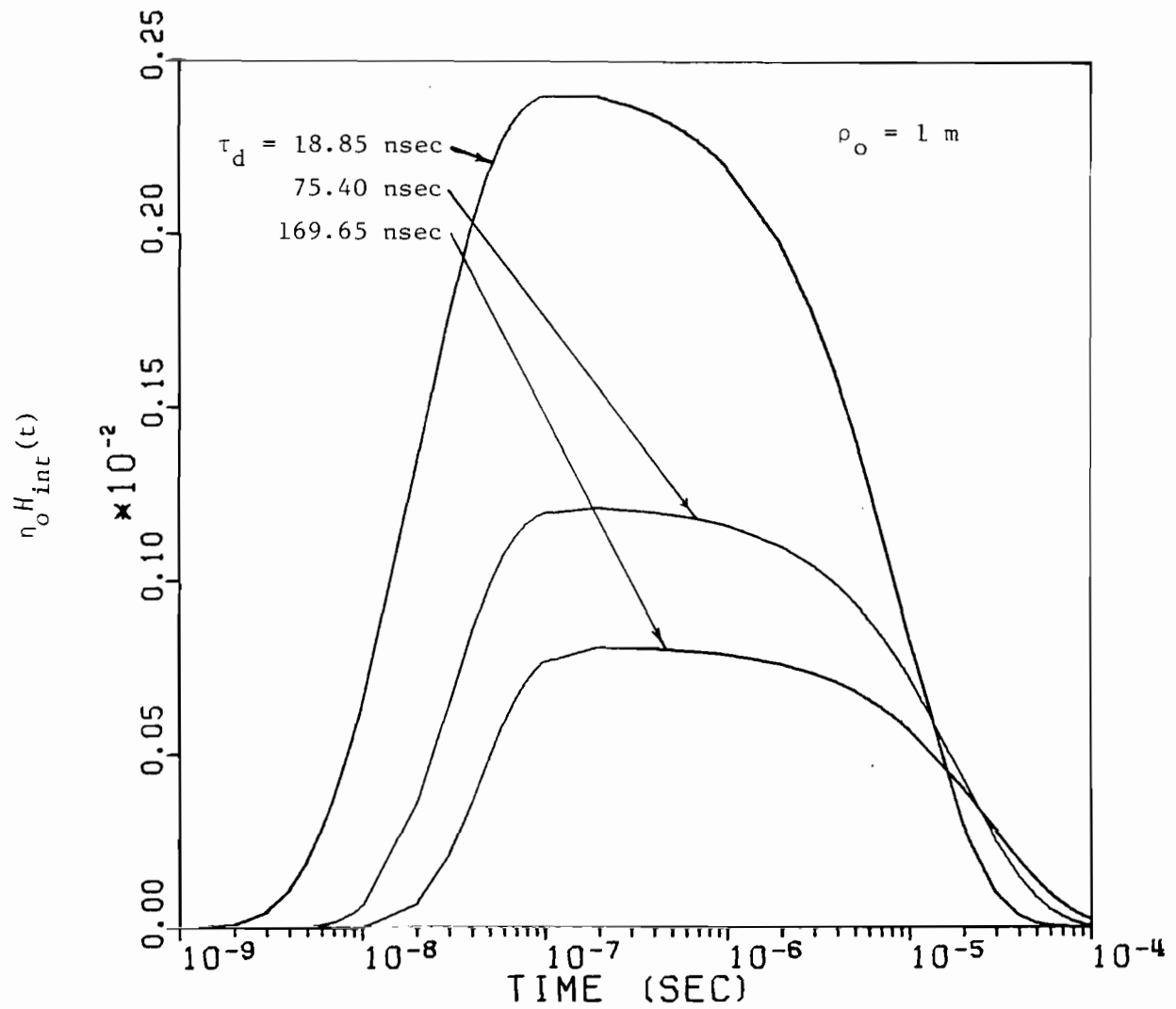
Figure 4.8. (η_o) times internal magnetic field for graphite cylindrical shell vs. t; $\rho_o = 1$ m

63

SECTION V

PLANAR WIRE-MESH COMPOSITE SHIELDS

1. INTRODUCTION

The characterization of a wire-mesh composite layer which we shall

develop in this chapter is that of a dielectric layer with an admittance

sheet on one of its surfaces. The presence of the dielectric layer in

the vicinity of the wire-mesh screen is necessary for the correct charac-

terization of the screen, since its periodic structure causes the screen

to carry with it a reactive field which "hugs" the screen and decays

exponentially in directions normal to the screen. Thus, a part of this

reactive field penetrates the dielectric layer and is affected by its

presence. The equivalent sheet admittance operator $\overline{\overline{Y}}_s$ which describes

the screen is therefore dependent upon both the dielectric properties

and the thickness of the composite layer of which it is a part.

The behavior of wire mesh screens in free space has been studied by

Kontorovich [4] and others [16-18] using the so-called "method of averaged

boundary conditions." This method is known to produce good results for

screens made of fine wire and having spatial periods much smaller than

the wavelength. More recently, Hill and Wait [19] have considered wire

mesh screens using Fourier expansions of the wire currents and have found

a computational technique which enables one to calculate the wire currents

relatively rapidly when the mesh size is small with respect to the wavelength.

We shall employ a method similar to, but an extension of, that used by

Hill and Wait to speed the convergence of the numerical solution for

the wire currents.

The screens which have been used to shield boron-epoxy composites are not generally fine enough to allow the unconcerned use of the thin-wire approximation which is basic to the present theory of wire-mesh screens. We shall, therefore, compare the results of our main analysis (which is based upon the thin-wire approximation) with the results obtained by considering the limit in which the screen is replaced by a conductor with a periodic distribution of small rectangular apertures in it. Using this comparison procedure, we can then establish bounds on the behavior of "thick-wire" mesh screens.

In paragraphs 2 and 3 of this section, we formulate the problem of plane-wave scattering by a fine wire-mesh screen in the surface of a dielectric layer of finite thickness. An equivalent sheet impedance for the screen is derived in paragraph 4, and the fields transmitted through the wire-mesh composite layer are considered in paragraph 5. The "per-forated screen" model is discussed in paragraph 6 and comparisons drawn between the two models.

2. FORMULATION OF THE PROBLEM

The geometry of the problem is shown in Fig. 5.1. A dielectric layer of relative permittivity ε_r (which may be complex) and relative permeability 1 is located in the region $0 \leq z \leq d$. A rectangular grid of conducting wires is embedded in the upper (z=0) surface of the layer: wires parallel to the y-axis are located at x=pa (p = 0,±1,...) and wires parallel to the x-axis are located at y = qb (q = 0,±1,...). The wire junctions are assumed to be bonded. The wire radius r is assumed to be small in comparison to the spacings a and b and to the wavelengths in
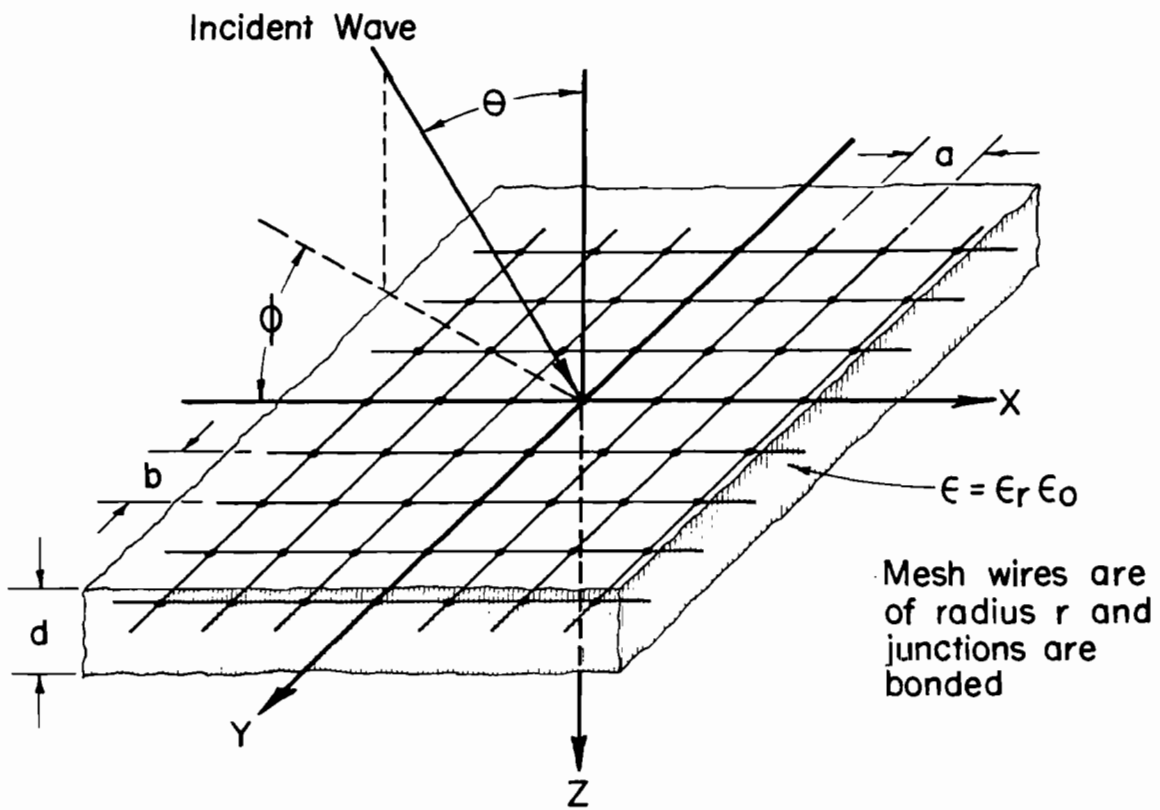
Figure 5.1. Reflection and transmission of a plane wave by a dielectric
layer with embedded wire-mesh screen: geometry of the
problem

free space and in the layer material; thus the wire currents are purely axial and the thin-wire approximations are valid. The wire impedance per unit length is given by

$$Z_w = \frac{\eta_w}{2\pi r} \frac{I_o(\tau_w r)}{I_1(\tau_w r)} \tag{5.1}$$

in which

$$\eta_w = (j\omega\mu_w/\sigma_w)^{1/2} \tag{5.2a}$$

$$\tau_w = (j\omega\mu_w\sigma_w)^{1/2} \tag{5.2b}$$

μ_w and σ_w denote respectively the wire permeability and conductivity, and $I_n(\cdot)$ denotes the modified Bessel function of the first kind. The time dependence is assumed to be $\exp(j\omega t)$.

The region outside the layer is free space. A plane electromagnetic wave is incident upon the layer from the region $z<0$. The incident electric field is given by

$$\bar{E}_{inc} = \bar{E}_o e^{-j\bar{k}_o\cdot\bar{r}} \tag{5.3}$$

in which $\bar{r}$ is the position vector, and

$$\bar{k}_o = k_o(\bar{a}_x \sin\theta \cos\phi + \bar{a}_y \sin\theta \sin\phi + \bar{a}_z \cos\theta) \tag{5.4}$$

$$\bar{E}_o = E_{o\theta}(\bar{a}_x \cos\theta \cos\phi + \bar{a}_y \cos\theta \sin\phi - \bar{a}_z \sin\theta)$$

$$+ E_{o\phi}(-\bar{a}_x \sin\phi + \bar{a}_y \cos\phi) \tag{5.5}$$

$E_{o\theta}$ and $E_{o\phi}$ denote respectively the amplitudes of the θ-polarized and ϕ-polarized components of the incident electric field, θ and ϕ are the incidence angles in spherical coordinates, and $k_o = \omega\sqrt{\mu_o\epsilon_o}$.

67

The wire currents I_x and I_y are expressed in terms of space-harmonic series as follows:

$$I_x(y = qb) = e^{-jk_{yo}qb} \sum_{m=-\infty}^{\infty} \tilde{I}_{xm} e^{-jk_{xm}x} \tag{5.6a}$$

$$I_y(x = pa) = e^{-jk_{xo}pa} \sum_{n=-\infty}^{\infty} \tilde{I}_{yn} e^{-jk_{yn}y} \tag{5.6b}$$

$\tilde{I}_{xm}$ and $\tilde{I}_{yn}$ denote the space-harmonic components of the currents I_x and I_y respectively, and

$$k_{xm} = k_o \sin\theta \cos\phi + 2\pi m/a \tag{5.7a}$$

$$k_{yn} = k_o \sin\theta \sin\phi + 2\pi n/b \tag{5.7b}$$

The electromagnetic field is expressed in terms of a vector function $\bar{\Psi}$ as follows:

$$\bar{H} = \nabla \times \bar{\Psi} \tag{5.8a}$$

$$\bar{E} = \frac{1}{j\omega\epsilon} [\nabla\nabla + k^2\bar{\bar{I}}] \cdot \bar{\Psi} \tag{5.8b}$$

where $\bar{\Psi} = \Psi_x \bar{a}_x + \Psi_y \bar{a}_y$ and

$$\nabla^2\bar{\Psi} + k^2\bar{\Psi} = 0 \tag{5.9}$$

with $k^2 = k_o^2 \epsilon_r$ and $\epsilon = \epsilon_o \epsilon_r$ for $0 \leq z \leq d$; and $k^2 = k_o^2$, $\epsilon = \epsilon_o$ elsewhere.

The periodic nature of the wire grid indicates that the various field quantities will be most conveniently expressed in terms of two-dimensional space harmonic series as

$$F(x,y,z) = \sum_{m=-\infty}^{\infty} \sum_{n=-\infty}^{\infty} \tilde{F}_{mn}(z) e^{-jk_{xm}x} e^{-jk_{yn}y} \tag{5.10}$$

We thus obtain for the tangential (x and y) space-harmonic components of $\bar{E}$ and $\bar{H}$ the following expressions:

$$\tilde{\bar{\bar{E}}}_{tmn} = \frac{1}{j\omega\epsilon} \, \bar{\bar{P}}_{mn} \cdot \tilde{\bar{\psi}}_{mn} \tag{5.11a}$$

$$\tilde{\bar{H}}_{tmn} = \frac{d}{dz} \, (\bar{a}_z \times \tilde{\bar{\psi}}_{mn}) \tag{5.11b}$$

in which

$$\bar{\bar{P}}_{mn} = \begin{bmatrix} k^2 - k_{xm}^2 & -k_{xm}k_{yn} \\ \\ -k_{xm}k_{yn} & k^2 - k_{yn}^2 \end{bmatrix} \tag{5.12}$$

In the dielectric layer, $\bar{\bar{P}}_{mn} = \bar{\bar{P}}_{dmn}$, $k^2 = k_o^2\epsilon_r$, and $\epsilon = \epsilon_o\epsilon_r$; elsewhere $\bar{\bar{P}}_{mn} = \bar{\bar{P}}_{omn}$, $k^2 = k_o^2$, and $\epsilon = \epsilon_o$. The space-harmonic components of the surface current density due to the currents in the grid wires are

$$\tilde{\bar{J}}_{smn} = \frac{\tilde{I}_{xm}}{b} \, \bar{a}_x + \frac{\tilde{I}_{yn}}{a} \, \bar{a}_y \tag{5.13}$$

We now construct appropriate solutions for $\bar{\psi}_{mn}$ in each of the three regions of the problem. We have

$$-\infty < z < 0: \quad \tilde{\bar{\psi}}_{mn} = \bar{A}_{mn} e^{jk_{zomn}z} + \bar{\pi}_{mn} e^{-jk_{zomn}z} \tag{5.14a}$$

$$0 < z < d: \quad \tilde{\bar{\psi}}_{mn} = \bar{B}_{mn}\cos k_{zdmn}z + \bar{C}_{mn}\sin k_{zdmn}z \tag{5.14b}$$

$$d < z < \infty: \quad \tilde{\bar{\psi}}_{mn} = \bar{D}_{mn} e^{-jk_{zomn}(z-d)} \tag{5.14c}$$

where $k_{zomn}^2 = k_o^2 - k_{xm}^2 - k_{yn}^2$ and $k_{zdmn}^2 = k_o^2\epsilon_r - k_{xm}^2 - k_{yn}^2$; $\bar{A}_{mn} - \bar{D}_{mn}$ are vector functions of m and n to be determined; and $\bar{\pi}_{mn}$ represents the incident wave:

$$\bar{\pi}_{mn} = j\omega\epsilon_o\delta_m\delta_n \, \bar{\bar{P}}_{omn}^{-1} \cdot \bar{E}_{ot} \tag{5.15}$$

δ_k denotes the Kronecker delta-function and $\bar{E}_{ot} = (\bar{\bar{I}} - \bar{a}_z\bar{a}_z) \cdot \bar{E}_o$ [cf. eq. (5.5)].

We are now in a position to construct the boundary-condition equations from which the unknowns $\bar{A}_{mn} - \bar{D}_{mn}$ may be determined in terms of $\bar{\pi}_{mn}$ and $\tilde{\bar{J}}_{smn}$. By ensuring continuity of tangential $\bar{E}$ at $z = 0$ and $z = d$, continuity of tangential $\ddot{\bar{H}}$ at $z = d$, and the appropriate discontinuity of tangential $\bar{H}$ at $z = 0$, we obtain the following system of equations:

$$\bar{\bar{P}}_o \cdot \bar{A} - \frac{1}{\epsilon_r} \bar{\bar{P}}_d \cdot \bar{B} = -\bar{\bar{P}}_o \cdot \bar{\pi} \tag{5.16a}$$

$$\bar{A} - \frac{k_{zd}}{jk_{zo}} \bar{C} = \bar{\pi} + \frac{1}{jk_{zo}} \tilde{\bar{J}}_s \tag{5.16b}$$

$$\frac{1}{\epsilon_r} \cos k_{zd}d \; \bar{\bar{P}}_d \cdot \bar{B} + \frac{1}{\epsilon_r} \sin k_{zd}d \; \bar{\bar{P}}_d \cdot \bar{C} - \bar{\bar{P}}_o \cdot \bar{D} = 0 \tag{5.16c}$$

$$k_{zd} \sin k_{zd}d \; \bar{B} - k_{zd} \cos k_{zd}d \; \bar{C} - jk_{zo} \bar{D} = 0 \tag{5.16d}$$

We have dropped the (m,n) subscripts in eq. (5.16) and in the following, for simplicity of notation. They will be reinserted where necessary for clarity.

It is sufficient for our purposes to solve eq. (5.16) for $\bar{A}$ and $\bar{D}$. We obtain, after some tedious but straightforward manipulations,

$$\bar{A} = \bar{\bar{F}} \cdot (\bar{\bar{\Lambda}} \cdot \bar{\pi} + \frac{1}{2jk_{zo}} \bar{\bar{\Gamma}} \cdot \tilde{\bar{J}}_s) \tag{5.17a}$$

$$\bar{D} = \bar{\bar{F}} \cdot (\bar{\pi} + \frac{1}{2jk_{zo}} \tilde{\bar{J}}_s) \sec k_{zd}d \tag{5.17b}$$

in which

$$\bar{\bar{F}} = [\bar{\bar{I}} + \frac{\xi}{2} \left(\frac{k_{zo}^2}{\epsilon_r} \bar{\bar{P}}_o^{-1} \cdot \bar{\bar{P}}_d + k_{zd}^2 \epsilon_r \bar{\bar{P}}_d^{-1} \cdot \bar{\bar{P}}_o \right)]^{-1} \tag{5.18a}$$

$$\bar{\bar{\Lambda}} = \frac{\xi}{2} \left(\frac{k_{zo}^2}{\epsilon_r} \bar{\bar{P}}_o^{-1} \cdot \bar{\bar{P}}_d - k_{zd}^2 \epsilon_r \bar{\bar{P}}_d^{-1} \cdot \bar{\bar{P}}_o \right) \tag{5.18b}$$

70

$$\bar{\bar{\Gamma}} = \bar{\bar{I}} + \xi \frac{k_{zo}^2}{\epsilon_r} \bar{\bar{P}}_o^{-1} \cdot \bar{\bar{P}}_d \qquad (5.18c)$$

and

$$\xi = \frac{j \tan k_{zd} d}{k_{zo} k_{zd}} \qquad (5.19)$$

$\bar{\bar{F}}$, $\bar{\bar{\Lambda}}$, and $\bar{\bar{\Gamma}}$ may also be expressed as follows:

$$\bar{\bar{F}} = a_f \bar{\bar{I}} + b_f \bar{\bar{K}}_y \qquad (5.20a)$$

$$\bar{\bar{\Lambda}} = a_\lambda \bar{\bar{I}} + b_\lambda \bar{\bar{K}}_x \qquad (5.20b)$$

$$\bar{\bar{\Gamma}} = a_\gamma \bar{\bar{I}} + b_\gamma \bar{\bar{K}}_x \qquad (5.20c)$$

in which

$$\bar{\bar{K}}_x = \begin{bmatrix} k_x^2 & k_x k_y \\ \\ k_x k_y & k_y^2 \end{bmatrix} \qquad (5.21a)$$

$$\bar{\bar{K}}_y = \begin{bmatrix} k_y^2 & -k_x k_y \\ \\ -k_x k_y & k_x^2 \end{bmatrix} \qquad (5.21b)$$

and

$$a_f = [1 + \frac{\xi}{2} \left(k_{zo}^2 \epsilon_r + \frac{k_{zd}^2}{\epsilon_r} \right)]^{-1} \qquad (5.22a)$$

$$b_f = \frac{-\xi}{2\epsilon_r} (\epsilon_r - 1)^2 a_f [1 + \frac{\xi}{2} (k_{zo}^2 + k_{zd}^2)]^{-1} \qquad (5.22b)$$

$$a_\lambda = - \frac{\xi}{2} k_o^2 (\epsilon_r - 1) \qquad (5.22c)$$

71

$$b_\lambda = \frac{\xi}{2\epsilon_r} (\epsilon_r^2 - 1) \qquad\qquad\qquad (5.22d)$$

$$a_\gamma = 1 + \xi \, k_{zo}^2 \qquad\qquad\qquad (5.22e)$$

$$b_\gamma = \frac{\xi}{\epsilon_r} (\epsilon_r - 1) \qquad\qquad\qquad \cdot \quad (5.22f)$$

In order to determine the still unknown wire currents and thereby complete the solution to the problem, we apply the boundary condition at the wire surfaces that the component of $\bar{E}$ parallel to a wire axis is equal to the wire current times its impedance per unit length. Since the wires have been assumed to be thin, it suffices to apply this condition at the tops of the wires, i.e.,

$$E_x(x, qb, -r) = Z_w I_x(y = qb) \qquad (q = 0, \pm 1, \ldots) \qquad (5.23a)$$

$$E_y(pa, y, -r) = Z_w I_y(x = pa) \qquad (p = 0, \pm 1, \ldots) \qquad (5.23b)$$

The conditions (5.23) lead directly to the following coupled set of equations:

$$\frac{1}{j\omega\epsilon_o} \sum_{n=-\infty}^{\infty} \frac{e^{-jk_{zomn}r}}{2jk_{zomn}} \, \bar{a}_x \cdot \bar{\bar{a}}_{mn} \cdot \tilde{\bar{J}}_{smn} - Z_w \tilde{I}_{xm}$$

$$= - \bar{a}_x \cdot \bar{\bar{b}} \cdot \bar{E}_{ot} \, \delta_m \qquad (m = 0, \pm 1, \ldots) \qquad (5.24a)$$

$$\frac{1}{j\omega\epsilon_o} \sum_{m=-\infty}^{\infty} \frac{e^{-jk_{zomn}r}}{2jk_{zomn}} \, \bar{a}_y \cdot \bar{\bar{a}}_{mn} \cdot \tilde{\bar{J}}_{smn} - Z_w \tilde{I}_{yn}$$

$$= -\bar{a}_y \cdot \bar{\bar{b}} \cdot \bar{E}_{ot} \, \delta_n \qquad (n = 0, \pm 1, \ldots) \qquad (5.24b)$$

in which

$$\bar{\bar{a}}_{mn} = \bar{\bar{P}}_{omn} \cdot \bar{\bar{F}}_{mn} \cdot \bar{\bar{\Gamma}}_{mn} \qquad\qquad\qquad (5.25a)$$

72

$$\bar{\bar{b}} = \bar{\bar{P}}_{ooo} \cdot (\bar{\bar{F}}_{oo} \cdot \bar{\bar{\Lambda}}_{oo} e^{-jk_{zooo}r} + \bar{\bar{I}}e^{jk_{zooo}r}) \cdot \bar{\bar{P}}_{ooo}^{-1} \qquad (5.25b)$$

Since $k_{zooo}r = k_o r\cos\theta \leq k_o r \ll 1$, we have

$$\bar{\bar{b}} \simeq \bar{\bar{P}}_{ooo} \cdot (\bar{\bar{F}}_{oo} \cdot \bar{\bar{\Lambda}}_{oo} + \bar{\bar{I}}) \cdot \bar{\bar{P}}_{ooo}^{-1} \qquad (5.26)$$

Equations (5.24) can now be solved for the wire currents, and the solution to the problem is formally complete. We address the problem of solving eq. (5.24) in the next paragraph.

3. GRID CURRENTS

Equations (5.24) may be rewritten as follows:

$$U_m \tilde{I}_{xm} + \sum_{n=-\infty}^{\infty} V_{mn} \tilde{I}_{yn} = R_o \delta_m \qquad (m = 0,\pm 1,\ldots) \qquad (5.27a)$$

$$W_n \tilde{I}_{yn} + \sum_{m=-\infty}^{\infty} X_{mn} \tilde{I}_{xm} = S_o \delta_n \qquad (n = 0,\pm 1,\ldots) \qquad (5.27b)$$

in which

$$U_m = Z_w - \frac{1}{j\omega\epsilon_o} \sum_{n=-\infty}^{\infty} a_{mn}^{(1,1)} \frac{e^{-jk_{zomn}r}}{2jk_{zomn}b} \qquad (5.28a)$$

$$V_{mn} = - \frac{1}{j\omega\epsilon_o} a_{mn}^{(1,2)} \frac{e^{-jk_{zomn}r}}{2jk_{zomn}a} \qquad (5.28b)$$

$$W_n = Z_w - \frac{1}{j\omega\epsilon_o} \sum_{m=-\infty}^{\infty} a_{mn}^{(2,2)} \frac{e^{-jk_{zomn}r}}{2jk_{zomn}a} \qquad (5.28c)$$

$$X_{mn} = - \frac{1}{j\omega\epsilon_o} a_{mn}^{(2,1)} \frac{e^{-jk_{zomn}r}}{2jk_{zomn}b} \qquad (5.28d)$$

$$R_o = E_{o\theta}(b^{(1,1)}\cos\theta\cos\phi + b^{(1,2)}\cos\theta\sin\phi)$$

$$+ E_{o\phi}(-b^{(1,1)}\sin\phi + b^{(1,2)}\cos\phi) \tag{5.28e}$$

$$S_o = E_{o\theta}(b^{(2,1)}\cos\theta\cos\phi + b^{(2,2)}\cos\theta\sin\phi)$$

$$+ E_{o\phi}(-b^{(2,1)}\sin\phi + b^{(2,2)}\cos\phi) \tag{5.28f}$$

$$a_{mn}^{(1,1)} = a_{fmn}[k_o^2(1 + \xi_{mn}k_{zomn}^2) - k_{xm}^2(1 + \xi_{mn}\frac{k_{zomn}^2}{\varepsilon_r})]$$

$$+ b_{fmn}k_o^2k_{yn}^2(1 + \xi_{mn}k_{zomn}^2) \tag{5.29a}$$

$$a_{mn}^{(1,2)} = a_{mn}^{(2,1)} = -a_{fmn}k_{xm}k_{yn}(1 + \xi_{mn}\frac{k_{zomn}^2}{\varepsilon_r})$$

$$- b_{fmn}k_o^2k_{xm}k_{yn}(1 + \xi_{mn}k_{zomn}^2) \tag{5.29b}$$

$$a_{mn}^{(2,2)} = a_{fmn}[k_o^2(1 + \xi_{mn}k_{zomn}^2) - k_{yn}^2(1 + \xi_{mn}\frac{k_{zomn}^2}{\varepsilon_r})]$$

$$+ b_{fmn}k_o^2k_{xm}^2(1 + \xi_{mn}k_{zomn}^2) \tag{5.29c}$$

$$b^{(1,1)} = 1 + a_{\lambda oo}a_{foo} + a_{foo}b_{\lambda oo}k_{xo}^2 + a_{\lambda oo}b_{foo}k_{yo}^2 \tag{5.29d}$$

$$b^{(1,2)} = b^{(2,1)} = k_{xo}k_{yo}(a_{foo}b_{\lambda oo} + a_{\lambda oo}b_{foo}) \tag{5.29e}$$

$$b^{(2,2)} = 1 + a_{\lambda oo}a_{foo} + a_{\lambda oo}b_{foo}k_{xo}^2 + a_{foo}b_{\lambda oo}k_{yo}^2 \tag{5.29f}$$

Equations (5.24) can be solved numerically for $\tilde{I}_{xm}$ and $\tilde{I}_{yn}$; however, Hill and Wait [19] have shown that in the case where the dielectric layer is absent (i.e., the wire grid is in free space), convergence of these equations can be extremely slow. They found that by incorporating a Kirchhoff's-law junction condition into the solution, the convergence

was radically improved. Anticipating a similar difficulty in the present situation, we shall modify eq. (5.24) by incorporating junction conditions which should speed the solution.

Consider the functions[†]

$$f_a(x) = \frac{-1}{2\pi j} \sum_{n=-\infty}^{\infty}{}' \frac{1}{n} e^{-2jn\pi x/a} \tag{5.30a}$$

$$g_a(x) = \frac{-a}{(2\pi)^2} \sum_{n=-\infty}^{\infty}{}' \frac{1}{n^2} e^{-2jn\pi x/a} \tag{5.30b}$$

which are shown in Fig. 5.2. $f_a(x)$ has a unit jump discontinuity at $x=0, \pm a, \ldots$; $g_a(x)$ has a unit discontinuity in slope at $x=0, \pm a, \ldots$. Let us write for $I_x(x, y = qb)$ and $I_y(x = pa, y)$:

$$I_x(x, y = qb) = e^{-jk_{yo}qb} e^{-jk_{xo}x} [\Delta f_a(x) + s_x g_a(x)$$

$$+ \sum_{m=-\infty}^{\infty} \tilde{I}_{xm}' e^{-2jm\pi x/a}] \tag{5.31a}$$

$$I_y(x = pa, y) = e^{-jk_{xo}pa} e^{-jk_{yo}y} [-\Delta f_b(y) + s_y g_b(y)$$

$$+ \sum_{n=-\infty}^{\infty} \tilde{I}_{yn}' e^{-2\pi jny/b}] \tag{5.31b}$$

The parameters Δ, s_x, and s_y are still to be determined; it will be noted, however, that Kirchhoff's current law is automatically satisfied at the wire junctions. The expressions given in eq. (5.31) are equivalent to

$$\tilde{I}_{xm} = \tilde{I}_{xm}' - \left[\frac{\Delta}{2\pi jm} + \frac{as_x}{(2\pi m)^2} \right] (1 - \delta_m) \tag{5.32a}$$

[†]The primes on the summation signs in eq. (5.30) and elsewhere indicate that the term n=0 is deleted.
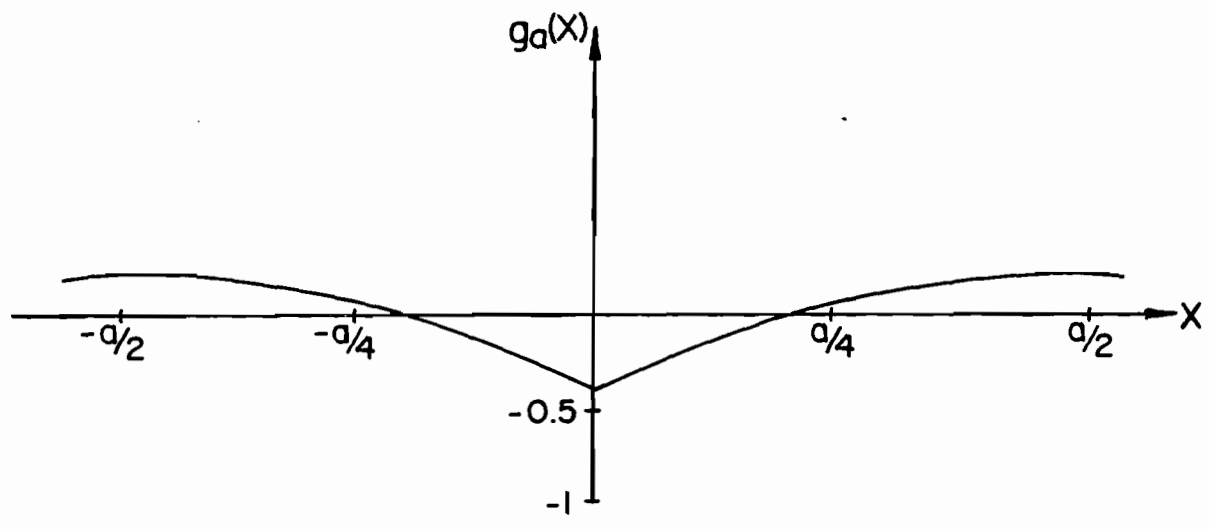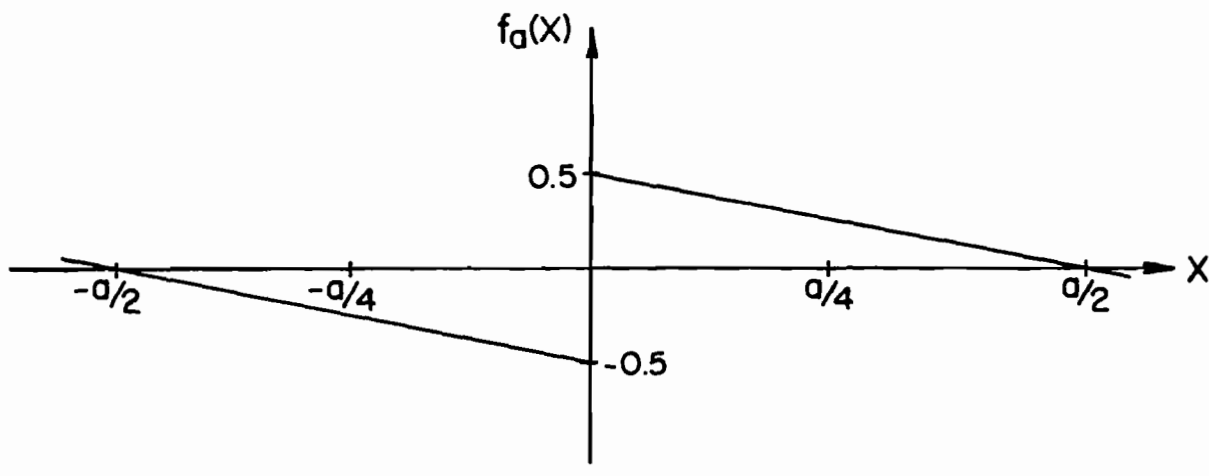
Figure 5.2.   Functions $f_a(x)$ and $g_a(x)$ vs. x

76

$$\tilde{I}_{yn} = \tilde{I}'_{yn} + \left[\frac{\Delta}{2\pi jn} - \frac{bs_y}{(2\pi n)^2}\right](1 - \delta_n) \qquad (5.32b)$$

It is now required that the charge density on each wire be continuous at the junctions, i.e.,

$$\left.\frac{\partial I_x}{\partial x}\right|_{x=pa-} = \left.\frac{\partial I_x}{\partial x}\right|_{x=pa+} \qquad (5.33a)$$

$$\left.\frac{\partial I_y}{\partial y}\right|_{y=qb-} = \left.\frac{\partial I_y}{\partial y}\right|_{y=qb+} \qquad (5.33b)$$

for all p,q. The conditions of (5.33) are obtained from the continuity equation. Imposing these conditions yields expressions for s_x and s_y in terms of Δ:

$$s_x = jk_{xo}\Delta \qquad (5.34a)$$

$$s_y = -jk_{yo}\Delta \qquad (5.34b)$$

If these expressions are introduced into eq. (5.32), we obtain

$$\tilde{I}_{xm} = \tilde{I}'_{xm} - \Delta(1-\delta_m)\left[\frac{1}{2\pi jm} + \frac{jk_{xo}a}{(2\pi m)^2}\right] \qquad (5.35a)$$

$$\tilde{I}_{yn} = \tilde{I}'_{yn} + \Delta(1-\delta_n)\left[\frac{1}{2\pi jn} + \frac{jk_{yo}b}{(2\pi n)^2}\right] \qquad (5.35b)$$

The final condition to be imposed is that the charge density on the "x-wires" be equal to that on the "y-wires" at the junctions. This requirement leads to the condition

$$\left.\frac{\partial I_x}{\partial x}\right|_{\substack{x=pa\\y=qb}} = \left.\frac{\partial I_y}{\partial y}\right|_{\substack{x=pa\\y=qb}} \qquad (5.36)$$

which yields the equation for Δ:

77

$$\Delta = \left[\frac{1}{b}\left(1 + \frac{k_{yo}^2 b^2}{12}\right) + \frac{1}{a}\left(1 + \frac{k_{xo}^2 a^2}{12}\right)\right]^{-1}$$

$$j\left[\sum_{n=-\infty}^{\infty} k_{yn}\tilde{I}_{yn}' - \sum_{m=-\infty}^{\infty} k_{xm}\tilde{I}_{xm}'\right] \tag{5.37}$$

This last condition may be interpreted physically by noting that it implies no potential difference between the wires at a junction. Kontorovich [4] used a more general condition than (5.36) to include the effect of a finite junction impedance. Inclusion of this effect in our analysis can be shown to modify eq. (5.37) by an additive term ζ in the first square brackets; and

$$\zeta = j\omega K Z_j \tag{5.38}$$

where Z_j is the junction impedance and K is a proportionality constant given by

$$K = \frac{1}{V_{pq}}\left[q_x(x=pa, y=qb) - q_y(x=pa, y=qb)\right] \tag{5.39}$$

V_{pq} is the junction potential difference and q_x and q_y denote respectively the linear charge densities on the "x-wires" and the "y-wires." It is tempting to proceed with incorporating this junction condition in our present analysis. However, we recognize that by initially formulating our problem with the x-wires and y-wires coplanar, the solution for the currents will converge to the result for which $\zeta=0$, no matter what value of ζ is initially assigned. Therefore, we shall consider only the bonded-junction limit in the present work, and reserve the case of finite junction impedance for further study.

Incorporating eqs. (5.35) into eq. (5.27) and simplifying, we obtain a new set of coupled equations for the "modified" space harmonics $\tilde{I}_{xm}'$ and $\tilde{I}_{yn}'$ as follows: together with eq. (5.37), we have

78

$$U_m \tilde{I}'_{xm} + \sum_{n=-\infty}^{\infty} V_{mn} \tilde{I}'_{yn} - P_m \Delta = R_o \delta_m \qquad (m = 0, \pm 1, \ldots) \qquad (5.40a)$$

$$W_n \tilde{I}'_{yn} + \sum_{m=-\infty}^{\infty} X_{mn} \tilde{I}'_{xm} + Q_n \Delta = S_o \delta_n \qquad (n = 0, \pm 1, \ldots) \qquad (5.40b)$$

in which

$$P_m = U_m \left[\frac{1}{2\pi jm} + \frac{jk_{xo}a}{(2m\pi)^2} \right] (1 - \delta_m)$$

$$- \sum_{n=-\infty}^{\infty}{}' V_{mn} \left[\frac{1}{2\pi jn} + \frac{jk_{yo}b}{(2n\pi)^2} \right] \qquad (5.41a)$$

$$Q_n = W_n \left[\frac{1}{2\pi jn} + \frac{jk_{yo}b}{(2n\pi)^2} \right] (1 - \delta_n)$$

$$- \sum_{m=-\infty}^{\infty}{}' X_{mn} \left[\frac{1}{2\pi jm} + \frac{jk_{xo}a}{(2m\pi)^2} \right] \qquad (5.41b)$$

The various summations required in the evaluation of the currents can be put into rapidly convergent form by adding to and subtracting from each summand its dominant behavior for large values of the summation index, and then performing the sum over the added dominant terms in closed form. We readily obtain

$$U_m = Z_w - \frac{q_m}{2\pi j\omega\epsilon_o} \ln(1 - e^{-2\pi r/b})^{-1} - \frac{a_{mo}^{(1,1)}}{j\omega\epsilon_o} \frac{e^{-jk_{zomo}r}}{2jk_{zomo}b}$$

$$- \frac{1}{j\omega\epsilon_o} \sum_{n=-\infty}^{\infty}{}' \left[a_{mn}^{(1,1)} \frac{e^{-jk_{zomn}r}}{2jk_{zomn}b} - \frac{q_m}{4|n|\pi} e^{-2|n|\pi r/b} \right] \qquad (5.42a)$$

79

$$W_n = Z_w - \frac{r_n}{2\pi j\omega\epsilon_o} \ell n(1 - e^{-2\pi r/a})^{-1} - \frac{a_{on}^{(2,2)}}{j\omega\epsilon_o} \frac{e^{-jk_{zoon}r}}{2jk_{zoon}a}$$

$$- \frac{1}{j\omega\epsilon_o} \sum_{m=-\infty}^{\infty}{}' \left[a_{mn}^{(2,2)} \frac{e^{-jk_{zomn}r}}{2jk_{zomn}a} - \frac{r_n}{4|m|\pi} e^{-2|m|\pi r/a} \right] \qquad (5.42b)$$

$$\sum_{n=-\infty}^{\infty}{}' \frac{V_{mn}}{n} = - \frac{s_m}{2\pi j\omega\epsilon_o} \ell n(1 - e^{-2\pi r/b})^{-1}$$

$$- \frac{1}{j\omega\epsilon_o} \sum_{n=-\infty}^{\infty}{}' \left[a_{mn}^{(1,2)} \frac{e^{-jk_{zomn}r}}{2njk_{zomn}a} - \frac{s_m}{4|n|\pi} e^{-2|n|\pi r/b} \right] \qquad (5.42c)$$

$$\sum_{m=-\infty}^{\infty}{}' \frac{X_{mn}}{m} = - \frac{t_n}{2\pi j\omega\epsilon_o} \ell n(1 - e^{-2\pi r/a})^{-1}$$

$$- \frac{1}{j\omega\epsilon_o} \sum_{m=-\infty}^{\infty}{}' \left[a_{mn}^{(2,1)} \frac{e^{-jk_{zomn}r}}{2mjk_{zomn}b} - \frac{t_n}{4|m|\pi} e^{-2|m|\pi r/a} \right] \qquad (5.42d)$$

in which

$$q_m = \lim_{|n|\to\infty} a_{mn}^{(1,1)} = k_o^2 - \frac{2k_{xm}^2}{1 + \epsilon_r} \qquad (5.43a)$$

$$r_n = \lim_{|m|\to\infty} a_{mn}^{(2,2)} = k_o^2 - \frac{2k_{yn}^2}{1 + \epsilon_r} \qquad (5.43b)$$

$$s_m = \lim_{|n|\to\infty} a_{mn}^{(1,2)} \frac{b}{na} = \frac{-4\pi k_{xm}}{a(\epsilon_r + 1)} \qquad (5.43c)$$

$$t_n = \lim_{|m|\to\infty} a_{mn}^{(2,1)} \frac{a}{mb} = \frac{-4\pi k_{yn}}{b(\epsilon_r + 1)} \qquad (5.43d)$$

The above results hold when d > 0. (If d = 0, the correct results are obtained by setting $\epsilon_r = 1$).

We are now in a position to calculate the wire currents in a relatively efficient manner, and from the currents to construct all the field quantities of interest in the problem. Our principal interest, however, is in developing a relatively simple characterization of the screen embedded in the surface of the composite, in the form of an equivalent sheet impedance. This problem is addressed in the next paragraph.

4. EQUIVALENT SHEET IMPEDANCE OF THE GRID

In this paragraph we derive an equivalent sheet impedance for the wire grid embedded in the surface of the dielectric layer. The relation which we seek is

$$\tilde{\bar{E}}_{too} = \bar{\bar{Z}}_s \cdot \tilde{\bar{J}}_{soo} = \bar{\bar{Y}}_s^{-1} \cdot \tilde{\bar{J}}_{soo} \tag{5.44}$$

which relates the space-averaged tangential electric field at the grid to the space-averaged surface current density [cf. eq. (2.16)].

From eqs. (5.11a), (5.14a), and (5.17a) we obtain

$$\tilde{\bar{E}}_{too}(z=0) = \frac{1}{j\omega\epsilon_o} \bar{P}_{ooo} \cdot (\bar{A}_{oo} + \bar{\pi}_{oo})$$

$$= \frac{1}{j\omega\epsilon_o} (\bar{\bar{P}}_{ooo} \cdot \bar{\bar{F}}_{oo} \cdot \bar{\bar{\Lambda}}_{oo} + \bar{\bar{P}}_{ooo}) \cdot \bar{\pi}_{oo}$$

$$- \frac{\eta_o}{2k_o^2} \sec\theta \, \bar{\bar{P}}_{ooo} \cdot \bar{\bar{F}}_{oo} \cdot \bar{\bar{\Gamma}}_{oo} \cdot \tilde{\bar{J}}_{soo} \tag{5.45}$$

and using eqs. (5.15) and (5.25),

$$\tilde{\bar{E}}_{too}(z=0) = \bar{\bar{b}} \cdot \bar{\bar{E}}_{ot} - \frac{\eta_o}{2k_o^2} \sec\theta \, \bar{\bar{a}}_{oo} \cdot \tilde{\bar{J}}_{soo} \tag{5.46}$$

81

Now substituting eq. (5.44) in (5.46), we have

$$\bar{\bar{Z}}_s \cdot \tilde{\bar{J}}_{soo} = \bar{\bar{b}} \cdot \bar{E}_{ot} - \frac{\eta_o}{2k_o^2} \sec\theta \, \bar{\bar{a}}_{oo} \cdot \tilde{\bar{J}}_{soo} \qquad (5.47)$$

The system of eqs. (5.27), or (5.37) and (5.40), can, in principle at least, be reduced to a system of the form

$$\tilde{\tilde{U}}I_{xo} + \tilde{\tilde{V}}I_{yo} = R_o \qquad (5.48a)$$

$$\tilde{\tilde{X}}I_{xo} + \tilde{\tilde{W}}I_{yo} = S_o \qquad (5.48b)$$

or, equivalently,

$$\begin{bmatrix} b\tilde{U} & a\tilde{V} \\ b\tilde{X} & a\tilde{W} \end{bmatrix} \begin{bmatrix} \tilde{I}_{xo}/b \\ \tilde{I}_{yo}/a \end{bmatrix} = \begin{bmatrix} R_o \\ S_o \end{bmatrix} \qquad (5.49)$$

Now,

$$\begin{bmatrix} R_o \\ S_o \end{bmatrix} = \bar{\bar{b}} \cdot \bar{E}_{ot} \qquad (5.50)$$

and defining

$$\bar{\bar{Z}}_g = \begin{bmatrix} b\tilde{U} & a\tilde{V} \\ b\tilde{X} & a\tilde{W} \end{bmatrix} \qquad (5.51)$$

we obtain

$$\bar{\bar{Z}}_g \cdot \tilde{\bar{J}}_{soo} = \bar{\bar{b}} \cdot \bar{E}_{ot} \qquad (5.52)$$

Substituting eq. (5.52) into eq. (5.47) yields

$$\bar{\bar{Z}}_s = \bar{\bar{Z}}_g - \frac{\eta_o}{2k_o^2} \sec\theta \, \bar{\bar{a}}_{oo} \qquad (5.53)$$

82

which is the relation required. It is evident that the problem of finding

the equivalent transfer impedance $\overline{\overline{Z}}_s$ has been reduced to determining the

impedance $\overline{\overline{Z}}_g$. This can always be done numerically, of course: calculating

the currents $\tilde{I}_{xo}$ and $\tilde{I}_{yo}$ from (5.37) and (5.40) for given $E_{o\theta}$ and $E_{o\phi}$

permits the evaluation of $\tilde{U}$, $\tilde{V}$, $\tilde{W}$, and $\tilde{X}$; however, we recognize that

in the applications we have intended to consider, the mesh dimensions

will always be much smaller than the wavelengths involved. As a

consequence, an approximate analytic solution can be obtained.

The approximate solution is based on the fact that in the low-

frequency limit, the system of equations (5.40) together with the

auxiliary condition (5.37) has proven to converge using only one modified

space-harmonic in I_x and I_y (discussion of the appropriate numerical

results is deferred to paragraph 7 of this section). Therefore, in

this limit, we have

$$\tilde{U} = U_o + k_{xo} f \, P_o \tag{5.54a}$$

$$\tilde{V} = V_{oo} - k_{yo} f \, P_o \tag{5.54b}$$

$$\tilde{X} = X_{oo} - k_{xo} f \, Q_o \tag{5.54c}$$

$$\tilde{W} = W_o + k_{yo} f \, Q_o \tag{5.54d}$$

in which

$$f = j\left[\frac{1}{b}\left(1 + \frac{k_{yo}^2 b^2}{12}\right) + \frac{1}{a}\left(1 + \frac{k_{xo}^2 a^2}{12}\right)\right]^{-1} \tag{5.55}$$

Thus, if

$$\overline{\overline{Z}}_s = \begin{bmatrix} Z_{sxx} & Z_{sxy} \\ Z_{syx} & Z_{syy} \end{bmatrix} \tag{5.56}$$

83

then

$$Z_{sxx} = Z_w b - \frac{1}{j\omega\epsilon_o} \sum_{n=-\infty}^{\infty} \frac{e^{-jk_{zoon}r}}{2jk_{zoon}} \left\{ a_{on}^{(1,1)} \right.$$

$$\left. - k_{xo}\frac{b}{a} f\left[\frac{1}{2\pi jn} + \frac{jk_{yo}b}{(2\pi n)^2}\right]a_{on}^{(1,2)} \right\} \tag{5.57a}$$

$$Z_{sxy} = \frac{-fk_{yo}}{j\omega\epsilon_o} \sum_{n=-\infty}^{\infty}{}' a_{on}^{(1,2)} \frac{e^{-jk_{zoon}r}}{2jk_{zoon}} \left[\frac{1}{2\pi jn} + \frac{jk_{yo}b}{(2\pi n)^2}\right] \tag{5.57b}$$

$$Z_{syx} = \frac{-fk_{xo}}{j\omega\epsilon_o} \sum_{m=-\infty}^{\infty}{}' a_{mo}^{(2,1)} \frac{e^{-jk_{zomo}r}}{2jk_{zomo}} \left[\frac{1}{2\pi jm} + \frac{jk_{xo}a}{(2\pi m)^2}\right] \tag{5.57c}$$

$$Z_{syy} = Z_w a - \frac{1}{j\omega\epsilon_o} \sum_{m=-\infty}^{\infty}{}' \frac{e^{-jk_{zomo}r}}{2jk_{zomo}} \left\{ a_{mo}^{(2,2)} \right.$$

$$\left. - k_{yo}\frac{a}{b} f\left[\frac{1}{2\pi jm} + \frac{jk_{xo}a}{(2m\pi)^2}\right]a_{mo}^{(2,1)} \right\} \tag{5.57d}$$

In obtaining the above results we have used the approximation

$\exp(jk_o r \cos\theta) \simeq 1$. In order to simplify the results of eq. (5.56)

further, we take the limit as $k_o a$, $k_o b$, $k_d a$, $k_d b$, $k_{xo} a$, and $k_{yo} b$ all

approach zero, retaining only terms of first order in the final results.

We obtain, after some tedious manipulation,

$$Z_{sxx} \simeq Z_w b + j\eta_o \frac{k_o b}{2\pi} L_{1b} - j\eta_o \frac{k_o b}{2\pi} \frac{k_{xo}^2}{k_o^2} (1 + \frac{jf}{a})L_{2b} \tag{5.58a}$$

$$Z_{sxy} \simeq -\frac{\eta_o f k_{xo} k_{yo}}{2\pi k_o} L_{2b} \tag{5.58b}$$

$$Z_{syx} \simeq -\frac{\eta_o f k_{xo} k_{yo}}{2\pi k_o} L_{2a} \tag{5.58c}$$

$$Z_{syy} \simeq Z_w a + j\eta_o \frac{k_o a}{2\pi} L_{1a} - j\eta_o \frac{k_o a}{2\pi} \frac{k_{yo}^2}{k_o^2} (1 + \frac{jf}{b}) L_{2a} \qquad (5.58d)$$

in which

$$L_{1q} = \sum_{n=1}^{\infty} \frac{e^{-2n\pi r/q}}{n} = \ln(1 - e^{-2\pi r/q})^{-1} \qquad (5.59a)$$

$$L_{2q} = \sum_{n=1}^{\infty} \frac{e^{-2n\pi r/q}}{n} \left[\frac{1 + t_{nq}/\epsilon_r}{1 + \frac{1}{2} t_{nq}(\epsilon_r + \frac{1}{\epsilon_r})} \right] \qquad (5.59b)$$

$$t_{nq} = \tanh\left(\frac{2n\pi d}{q}\right) \qquad (5.59c)$$

where $q = a$ or b.

Let us now consider the eigenvalues of the impedance matrix $\bar{\bar{Z}}_s$ for the case of a square mesh, $a=b$. It is easy to show that the two eigenvalues Z_{s1} and Z_{s2} are given by

$$Z_{s1} = Z_w a + j\eta_o (\frac{k_o a}{2\pi}) \ln(1 - e^{-2\pi r/a})^{-1} \qquad (5.60a)$$

$$Z_{s2} = Z_{s1} - j\eta_o (\frac{k_o a}{2\pi}) \frac{k_{to}^2}{2k_o^2} L_{2a} \qquad (5.60b)$$

where $k_{to}^2 = k_{xo}^2 + k_{yo}^2 = k_o^2 \sin^2\theta$. Consideration of the eigenvalue equation

$$(\bar{\bar{Z}}_s - Z_{si}\bar{\bar{I}}) \cdot \tilde{\bar{J}}_{soo} = 0 \qquad (5.61)$$

for $i = 1,2$ reveals that

$$\text{for } Z_s = Z_{s1}: \qquad \bar{k}_{to} \cdot \tilde{\bar{J}}_{soo} = 0 \qquad (5.62a)$$

$$\text{for } Z_s = Z_{s2}: \qquad \bar{k}_{to} \times \tilde{\bar{J}}_{soo} = 0 \qquad (5.62b)$$

where $\bar{k}_{to} = k_{xo}\bar{a}_x + k_{yo}\bar{a}_y$. The conditions of eq. (5.62) are immediately

85

recognized as those corresponding to perpendicular and parallel polarization respectively; therefore

$$Z_{s1} = Z'_s = 1/Y'_s \qquad (5.63)$$

is the equivalent sheet impedance for a perpendicular-polarized field, and

$$Z_{s2} = Z''_s = 1/Y''_s \qquad (5.64)$$

is the equivalent sheet impedance for a parallel-polarized field.

Several features of these results are worthy of some discussion. These are:

(a) Z'_s and Z''_s (or Y'_s and Y''_s) are <u>isotropic</u>, i.e., they do not depend upon the angle ϕ. This result is not surprising, since a bonded wire mesh in free space is known to behave isotropically [4,19] at low frequencies.

(b) Z'_s and Z''_s are not equal except when $\bar{k}_{to} = \bar{0}$; thus the wire mesh is <u>fundamentally different</u> from a simple surface admittance layer in this respect.

(c) Z''_s is dependent upon k_{to}^2, so the wire mesh is <u>spatially dispersive</u>. This result also agrees with the known results for the wire mesh in free space.

(d) Z''_s depends upon ε_r and d. Physically, this occurs because for parallel polarization a normal component of electric field is present which penetrates the dielectric layer. The real importance of this result is that the behavior of the grid depends upon its surroundings. As a consequence, the total behavior of the grid and the dielectric layer cannot be found by considering these components separately.

86

(e)   The function L_{2a} is bounded as follows:

$$\ln(1 - e^{-2\pi r/a})^{-1} \geq L_{2a} \geq \frac{2}{1 + \varepsilon_r} \ln(1 - e^{-2\pi r/a})^{-1}$$

The upper bound follows from setting $\varepsilon_r = 1$ and/or $d = 0$ in (5.59b); the lower bound follows from letting d/a become large in that equation.

(f)   With regard to the observation made in 5 above, it must be emphasized that $|\varepsilon_r|$ cannot be too large, since the condition $(k_d a/2\pi) \ll 1$ must hold in order for our approximate analysis to be valid.

The thickness of the dielectric layer can be simply accounted for by defining an equivalent relative permittivity ε_{eqr} as follows:

$$\varepsilon_{eqr} = \frac{2}{L_{2a}} \ln(1 - e^{-2\pi r/a})^{-1} - 1 \tag{5.65}$$

ε_{eqr} will depend upon d/a, ε_r, and (weakly) upon r/a; and

$$Z_s'' = Z_w a + j\eta_o (\frac{k_o a}{2\pi})[1 - \frac{k_{to}^2}{k_o^2(1 + \varepsilon_{eqr})}]\ln(1 - e^{-2\pi r/a})^{-1} \tag{5.66}$$

where $1 \leq \varepsilon_{eqr} \leq \varepsilon_r$. We have calculated curves of ε_{eqr} vs. d/a for various values of ε_r and r/a; the results are shown in Fig. 5.3. It is evident from these numerical results that when d/a is greater than unity, $\varepsilon_{eqr} \simeq \varepsilon_r$; and since this is the situation which normally prevails in wire-mesh composite applications, we shall set $\varepsilon_{eqr} = \varepsilon_r$ in the remainder of this Note.

A generalization of this result is obvious: if a wire grid is embedded between two dielectric layers of relative permittivity ε_{r1} and ε_{r2} and the thicknesses of both of the layers exceeds a, then the equivalent surface transfer impedances of the grid will be simply

87

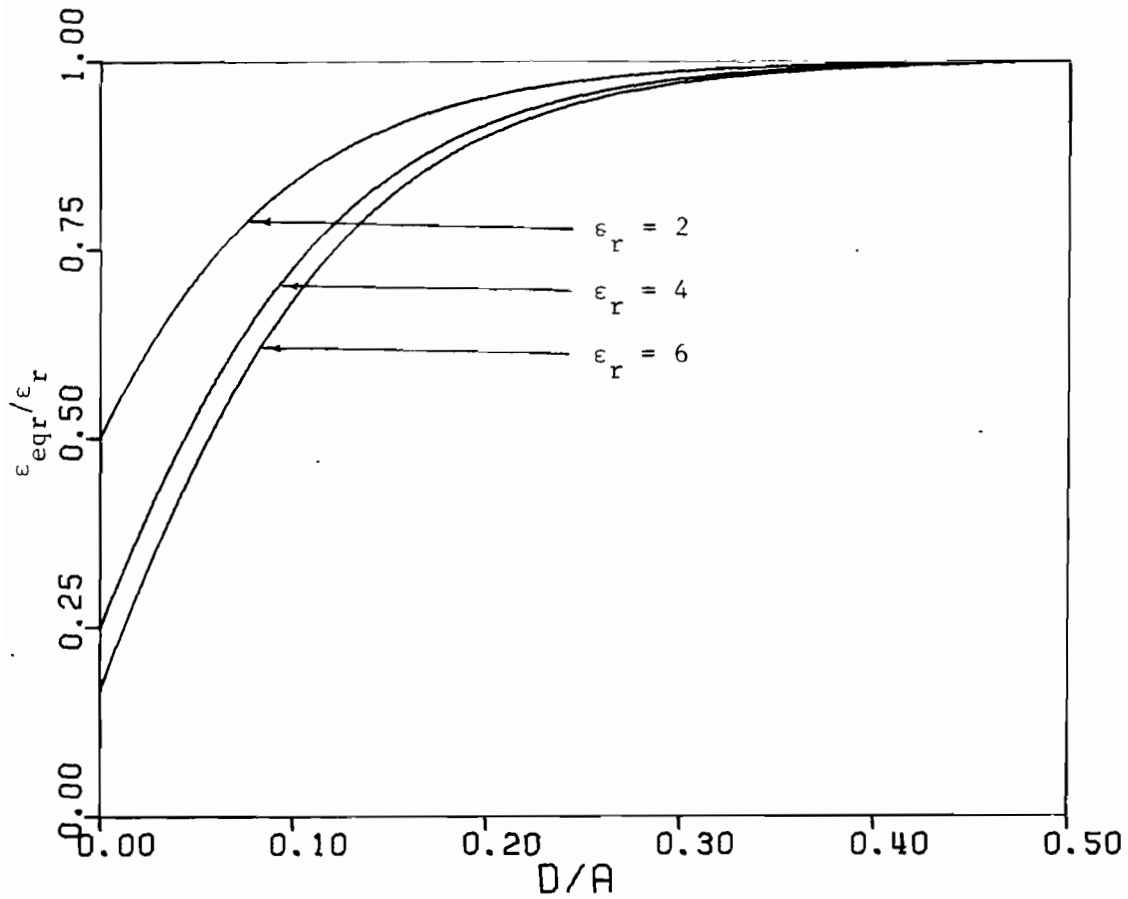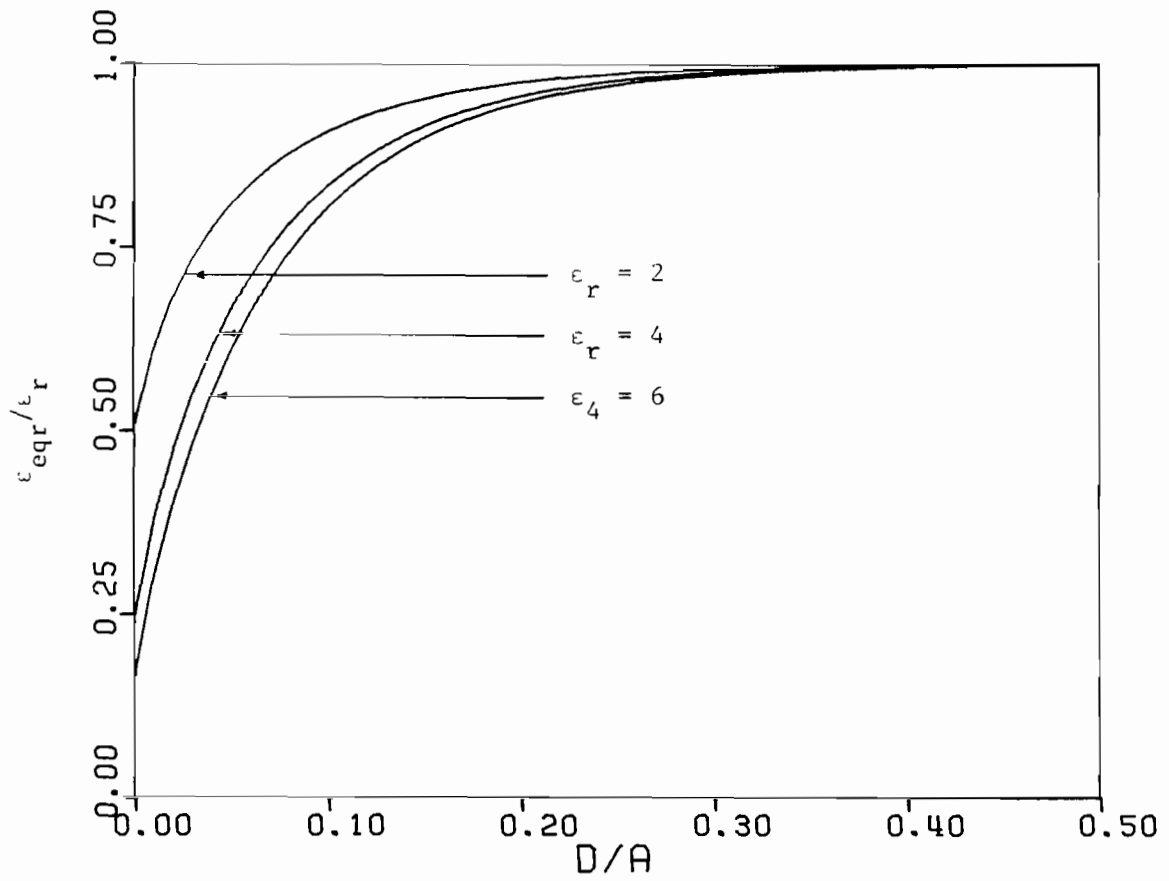Figure 5.3a. ε_{eqr} vs. d/a for ε_r = 2, 4, 6; r/a = 0.25

Figure 5.3b. ε_{eqr} vs. d/a for ε_r = 2, 4, 6; r/a = 0.025

$$Z'_s = Z_w a + \frac{j\omega\mu_o a}{2\pi} \ln(1 - e^{-2\pi r/a})^{-1} \qquad (5.67a)$$

$$Z''_s = Z_w a + \frac{j\omega\mu_o a}{2\pi} \ln(1 - e^{-2\pi r/a})^{-1} \left[1 - \frac{k_{to}^2}{k_o^2(\varepsilon_{r1} + \varepsilon_{r2})}\right] \qquad (5.67b)$$

The physical reason behind these results is simply that the reactive field of the wire grid decays exponentially in the directions normal to the grid as $\exp(-2\pi|z|/a)$; and if the layer boundaries are sufficiently far removed from the grid, these boundaries are not "felt" by the reactive field.

It is convenient to express the equivalent sheet impedance for a square mesh in dyadic form as

$$\bar{\bar{Z}}_s = \hat{Z}_{s1}\bar{\bar{I}} + \hat{Z}_{s2} \frac{(-j\bar{k}_{to})(-j\bar{k}_{to})}{k_o^2} \qquad (5.68)$$

or in dyadic operator form as

$$\bar{\bar{Z}}_s = \hat{Z}_{s1}\bar{\bar{I}} + \hat{Z}_{s2} \frac{\nabla_t \nabla_t}{k_o^2} \qquad (5.67)$$

in which

$$\hat{Z}_{s1} = Z_w a + j\eta_o \frac{k_o a}{2\pi} L_{1a} \qquad (5.70a)$$

$$\hat{Z}_{s2} = j\eta_o \frac{k_o a}{4\pi} L_{2a} \qquad (5.70b)$$

and ∇_t denotes the transverse or surface del operator. The eigenoperators for perpendicular and parallel polarization are then given by

$$Z'_s = \hat{Z}_{s1} \qquad (5.71a)$$

$$Z''_s = \hat{Z}_{s1} + \hat{Z}_{s2}\nabla_t^2/k_o^2 \qquad (5.71b)$$

90

We have used the fact that ∇_t is equivalent in the space domain to $-j\bar{k}_{to}$ in the Fourier spectral domain to construct the result (5.69) from (5.68) and (5.71b) from (5.67b). Curves of $Z'_s = R_s + jX_s$ are shown plotted as functions of frequency for typical screen parameters in Fig. 5.4.

In the next paragraph we shall consider the problem of transmission of a plane electromagnetic wave through a planar layer of the wire–mesh composite, using the equivalent sheet impedance $\overline{\overline{Z}}_s$ which has been developed in this paragraph.

5.   THE TRANSMITTED FIELD

Having developed an equivalent sheet impedance operator to characterize the wire–mesh screen, we may make use of the boundary-connection formalism developed in Section II to solve the problem of transmission of a plane electromagnetic wave through a planar wire–mesh composite shield[†]. The boundary connection relation for our problem is (cf. eq. (2.19))

$$\begin{bmatrix} \tilde{\tilde{E}}_t(0-) \\ \\ \eta_o \tilde{\tilde{H}}_t(0-) \end{bmatrix} = \begin{bmatrix} \overline{\overline{M}}_{t11} & \overline{\overline{M}}_{t12} \\ \\ \overline{\overline{M}}_{t21} & \overline{\overline{M}}_{t22} \end{bmatrix} \cdot \begin{bmatrix} \tilde{\tilde{E}}_t(d+) \\ \\ \eta_o \tilde{\tilde{H}}_t(d+) \end{bmatrix} \tag{5.72}$$

in which

$$\overline{\overline{M}}_{t11} = \overline{\overline{I}} \cos k_{zd} d \tag{5.73a}$$

$$\overline{\overline{M}}_{t12} = -\frac{1}{\sqrt{\varepsilon_r}} \overline{\overline{U}} \sin k_{zd} d \tag{5.73b}$$

[†]We could, of course, calculate the transmitted field directly from the analysis in paragraph 2 of this section. However, in the frequency range of interest for EMP studies, the approach based on the equivalent $\overline{\overline{Z}}_s$ is much simpler.
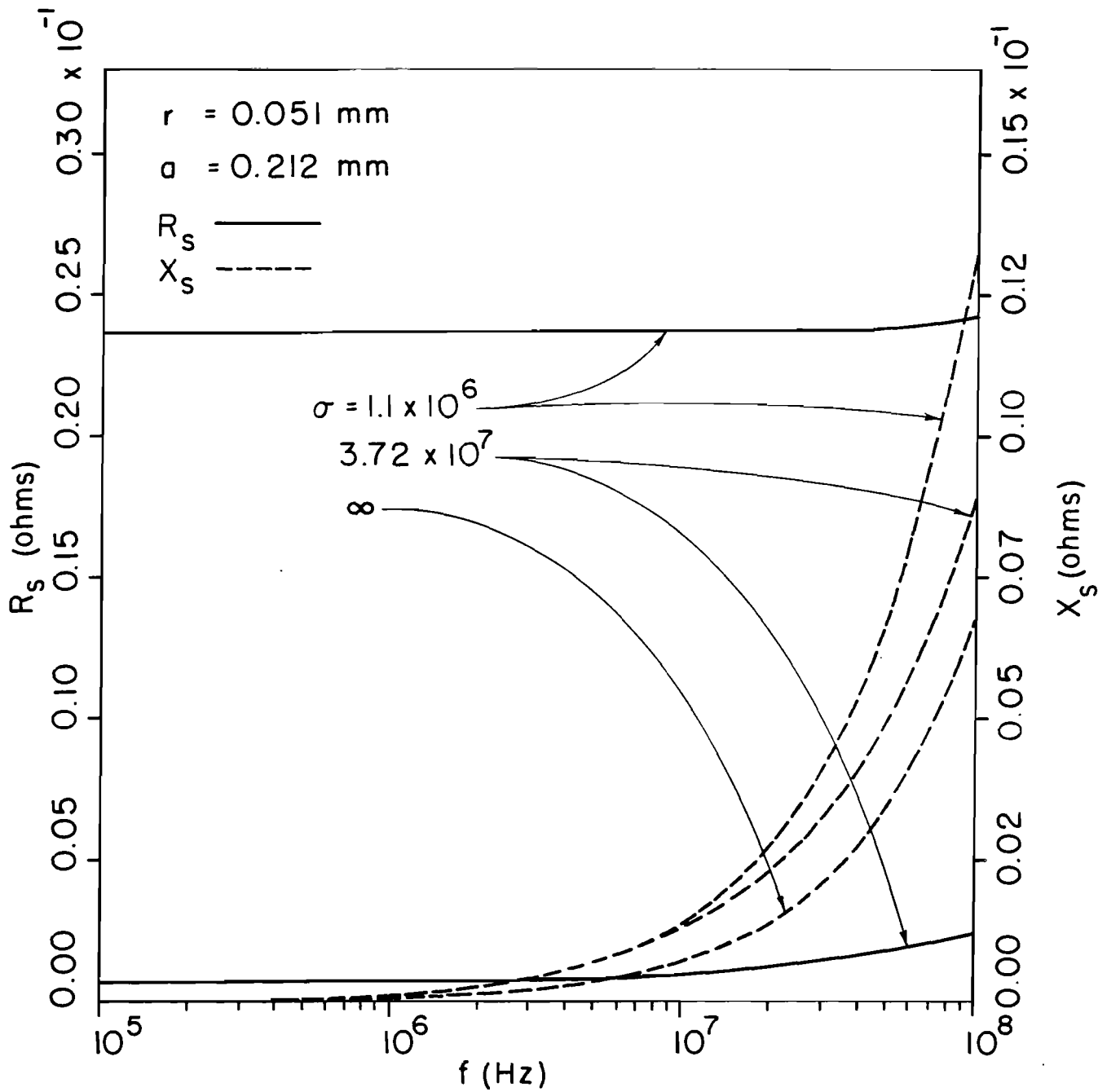
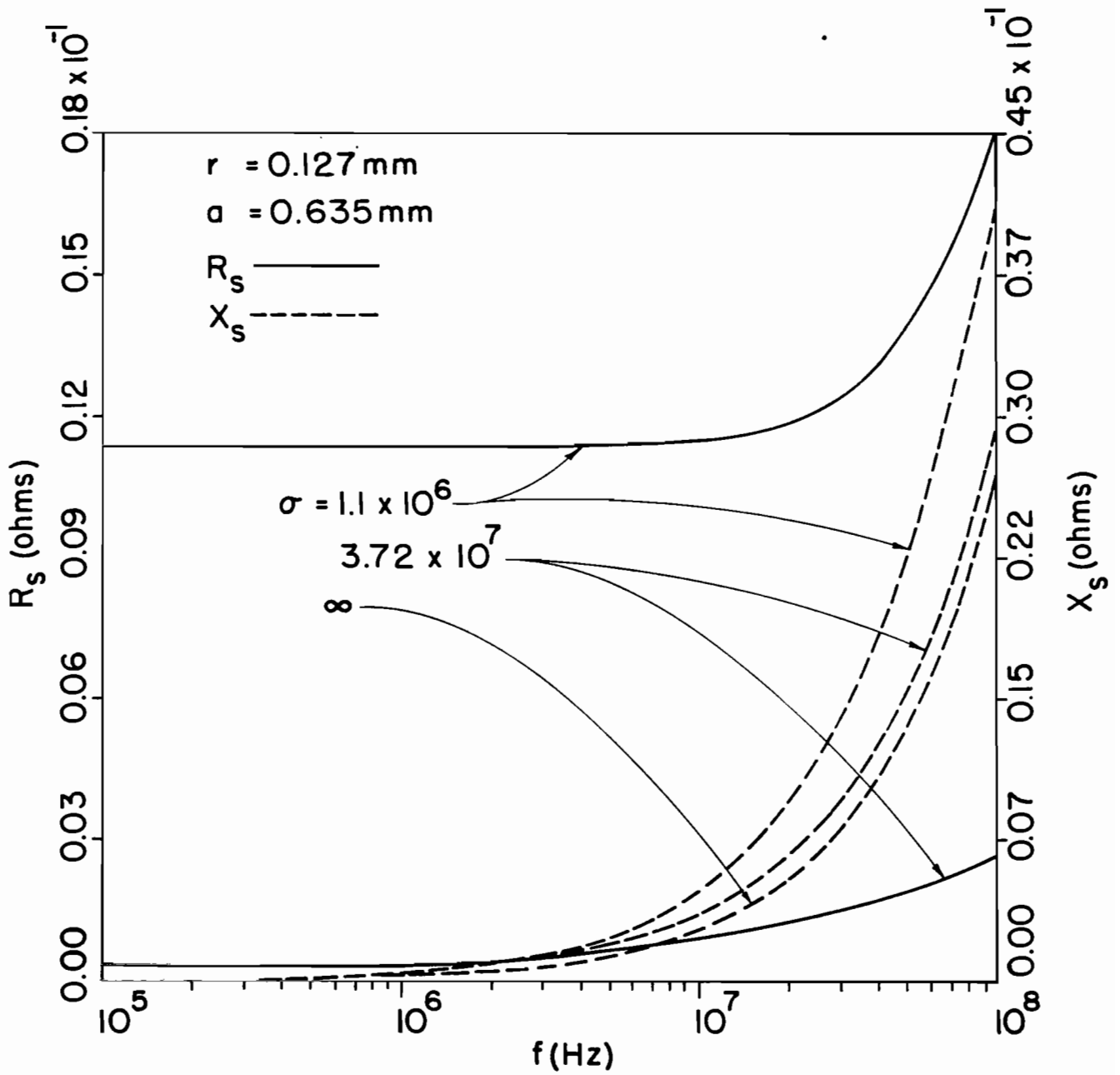Figure 5.4a. Curves of R_s and X_s ($Z'_s = R_s + jX_s$) vs. frequency; r = 0.051 mm, a = 0.212 mm

Figure 5.4b. Curves of R_s and X_s ($Z'_s = R_s + jX_s$) vs. frequency;
r = 0.127 mm, a = 0.635 mm

93

$$\bar{\bar{M}}_{t21} = \eta_o \cos k_{zd}d \; \bar{a}_z \times \bar{\bar{Z}}_s^{-1} + \sqrt{\epsilon_r} \; \bar{\bar{U}} \sin k_{zd}d \qquad (5.73c)$$

$$\bar{\bar{M}}_{t22} = \bar{\bar{I}} \cos k_{zd}d - \frac{\eta_o}{\sqrt{\epsilon_r}} \sin k_{zd}d \; (\bar{a}_z \times \bar{\bar{Z}}_s^{-1}) \cdot \bar{\bar{U}} \qquad (5.73d)$$

and $\bar{\bar{U}}$ is given in eq. (2.9) with $k = k_o\sqrt{\epsilon_r}$ and $k_z = k_{zd}$.

For perpendicular polarization, the elements $\bar{\bar{M}}'_{tij}$ are, when $k_{zd}d \ll 1$,

$$\bar{\bar{M}}'_{t11} = \bar{\bar{I}} \qquad (5.74a)$$

$$\bar{\bar{M}}'_{t12} = -jk_o d \; \bar{a}_z \times \bar{\bar{I}} \qquad (5.74b)$$

$$\bar{\bar{M}}'_{t21} = [\eta_o(Z'_s)^{-1} + j \frac{k_{zd}^2 d}{k_o}]\bar{a}_z \times \bar{\bar{I}} \qquad (5.74c)$$

$$\bar{\bar{M}}'_{t22} = [1 + jk_o d \; \eta_o(Z'_s)^{-1}]\bar{\bar{I}} \qquad (5.74d)$$

and for parallel polarization, we have

$$\bar{\bar{M}}''_{t11} = \bar{\bar{I}} \qquad (5.75a)$$

$$\bar{\bar{M}}''_{t12} = - \frac{jk_{zd}^2 d}{k_o \epsilon_r} \bar{a}_z \times \bar{\bar{I}} \qquad (5.75b)$$

$$\bar{\bar{M}}''_{t21} = [\eta_o(Z''_s)^{-1} + jk_o \epsilon_r d]\bar{a}_z \times \bar{\bar{I}} \qquad (5.75c)$$

$$\bar{\bar{M}}''_{t22} = [1 + j \frac{k_{zd}^2 d}{k_o \epsilon_r} \eta_o(Z''_s)^{-1}]\bar{\bar{I}} \qquad (5.75d)$$

We have introduced the approximation $k_{zd}d \ll 1$ because such a relation

will hold for a composite panel of this type over the entire EMP frequency

range: for example, if $\epsilon_r = 4.0$ and $d = 2mm$, $k_{zd}d \le 0.0084$ at $f = 10^8$ Hz.

Now carrying out an analysis similar to that done in Chapter III, we obtain for the transmission coefficients T' and T" the expressions

$$T' = \left\{1 + [\frac{\eta_o}{2}(Z_s')^{-1} + \frac{jk_o d}{2}(\varepsilon_r - 1)]\sec\theta\right\}^{-1} e^{-jk_o d \cos\theta} \tag{5.76a}$$

$$T" = \left\{1 + [\frac{\eta_o}{2}(Z_s")^{-1} + \frac{jk_o d}{2}(\varepsilon_r - 1)]\cos\theta \right.$$

$$\left. + \frac{jk_o d}{2}\sin^2\theta(1 - \frac{1}{\varepsilon_r})[\sec\theta + \eta_o(Z_s")^{-1}]\right\}^{-1} e^{-jk_o d \cos\theta} \tag{5.76b}$$

to first order in $(k_o d)$. It is clear from eq. (5.76a) that for perpendicular polarization, the equivalent sheet admittance for the wire-mesh composite layer is

$$Y_{s,eq}' = (Z_s')^{-1} + \frac{jk_o d}{\eta_o}(\varepsilon_r - 1) \tag{5.77}$$

which is in agreement with the result given earlier in eq. (2.31). For parallel polarization the "equivalent" sheet admittance is

$$Y_{s,eq}" = (Z_s")^{-1} + \frac{jk_o d}{\eta_o}(\varepsilon_r - 1)$$

$$+ \frac{jk_o d}{\eta_o}\sin^2\theta \sec\theta(1 - \frac{1}{\varepsilon_r})[\sec\theta + \eta_o(Z_s")^{-1}] \tag{5.78}$$

The equivalent sheet admittances given above can be substantially simplified if we restrict our attention to realistic screen parameters and the EMP frequency range. For example, a screen with a = 0.635 mm (40 × 40 meshes to the inch) made of stainless-steel wire (conductivity 1.1×10^6 mho m^{-1}) of radius 0.05 mm yields a value of $|\eta_o(Z_s')^{-1}|$ greater than 3×10^3. Thus we may neglect terms proportional to $k_o d$; and

$$Y_{s,eq}' \simeq (Z_s')^{-1} \tag{5.79}$$

95

and, except for angles of incidence θ very close to 90°,

$$Y''_{s,eq} \simeq (Z''_s)^{-1} \qquad (5.80)$$

It is therefore apparent that the screened composite layer is essentially equivalent to the screen alone, insofar as its behavior as a shield is concerned. It should be noted, however, that the effect of the dielectric layer does indeed enter the results, in that Z''_s depends upon the relative permittivity of the layer. We give explicit expressions for $Y'_{s,eq}{}^{,''}$ for plane waves below:

$$Y'_{s,eq} \simeq [Z_w a + \frac{j\omega\mu_o a}{2\pi} \ln(1 - e^{-2\pi r/a})^{-1}]^{-1} \qquad (5.81a)$$

$$Y''_{s,eq} \simeq [Z_w a + \frac{j\omega\mu_o a}{2\pi} \ln(1 - e^{-2\pi r/a})^{-1}(1 - \frac{\sin^2\theta}{1 + \epsilon_r})]^{-1} \qquad (5.81b)$$

For fields other than plane waves, $\sin^2\theta$ should be replaced by k_{to}^2/k_o^2.

The transmission coefficients T' and T'' are given approximately by

$$T' \simeq e^{-jk_o d \cos\theta} \frac{2\cos\theta}{2\cos\theta + \eta_o (Z'_s)^{-1}} \qquad (5.82a)$$

$$T'' \simeq e^{-jk_o d \cos\theta} \frac{2\sec\theta}{2\sec\theta + \eta_o (Z''_s)^{-1}} \qquad (5.82b)$$

These very simple expressions will quickly yield numerical values for the frequency-domain transmitted field. Some representative curves of the magnitudes of T' and T'' as functions of frequency for various angles of incidence are shown in Figs. 5.5-5.8.

The problem of transmission of a transient EMP signal through the wire-mesh composite layer is of interest and may be easily attacked. For simplicity, we shall assume that $Z_w \simeq (\pi r^2 \sigma_w)^{-1}$, i.e., that the screen wires have radii small in comparison to the skin depth over the frequency
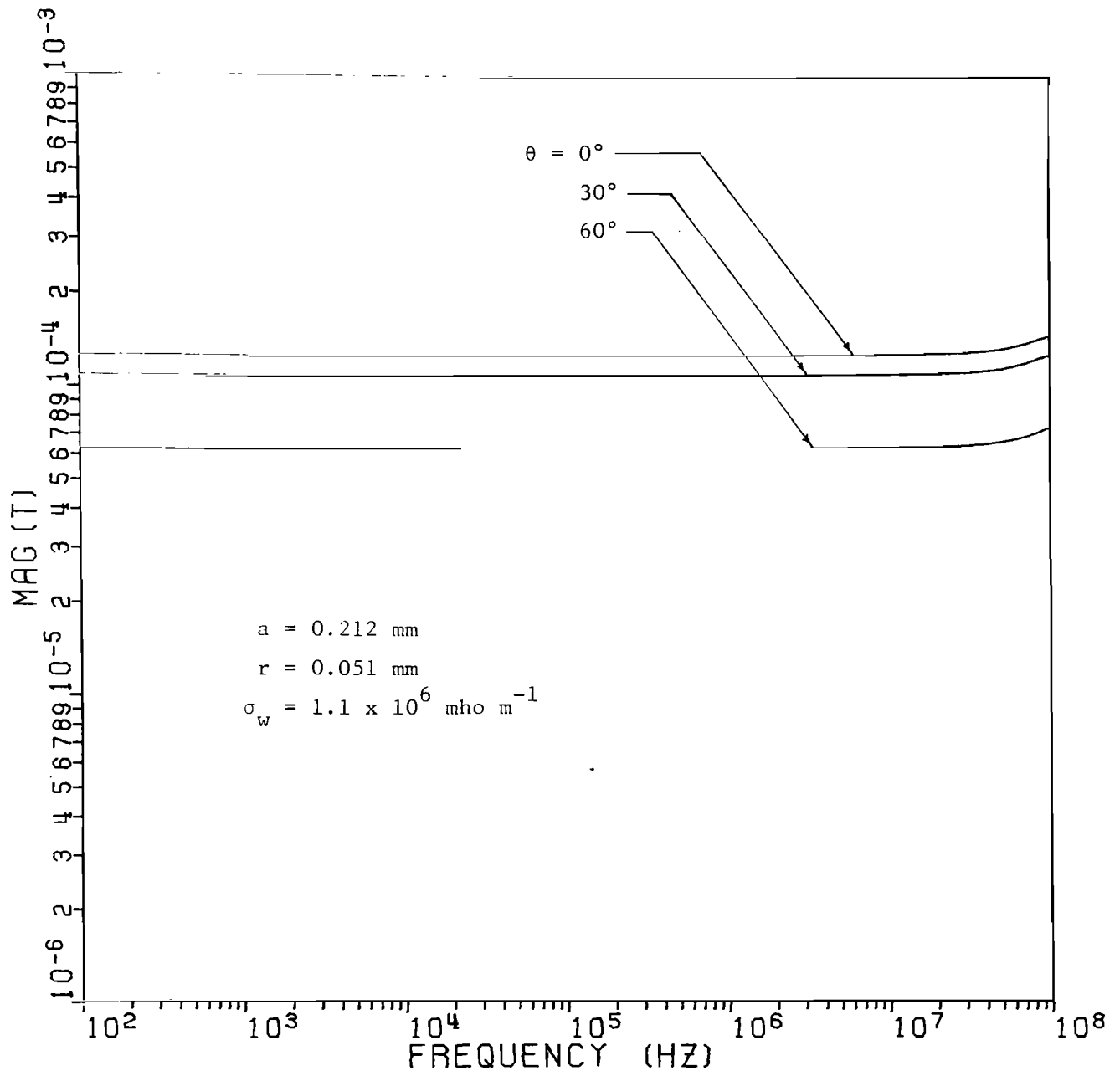
96

The figure is a semi-log plot. The vertical axis is labeled MAG (T) ranging from 10^{-6} to 10^{-3}. The horizontal axis is labeled FREQUENCY (HZ) ranging from 10^2 to 10^8. Curves are labeled $\theta = 0°$, $30°$, $60°$. Parameters shown on the plot:

$a = 0.212$ mm

$r = 0.051$ mm

$\sigma_w = 1.1 \times 10^6$ mho m^{-1}

Figure 5.5a. $|T'|$ vs. frequency; a = 0.212 mm, r = 0.051 mm, $\sigma_w = 1.1 \times 10^6$ mho m^{-1}; $\theta = 0°$, $30°$, $60°$.
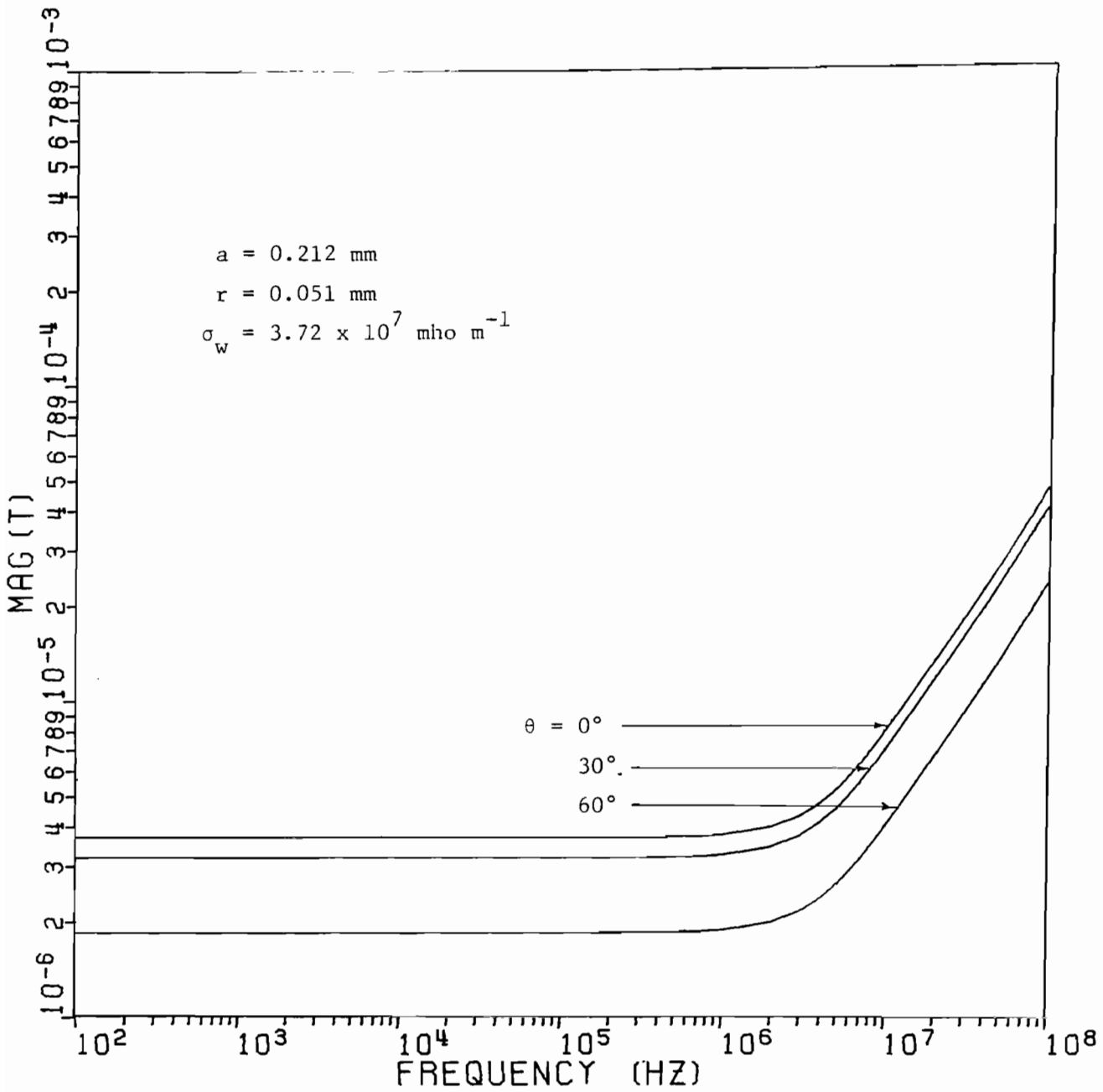
Figure 5.5b. $|T'|$ vs. frequency; a = 0.212 mm, r = 0.051 mm,
σ_w = 3.72 x 10^7 mho m^{-1}; θ = 0°, 30°, 60°
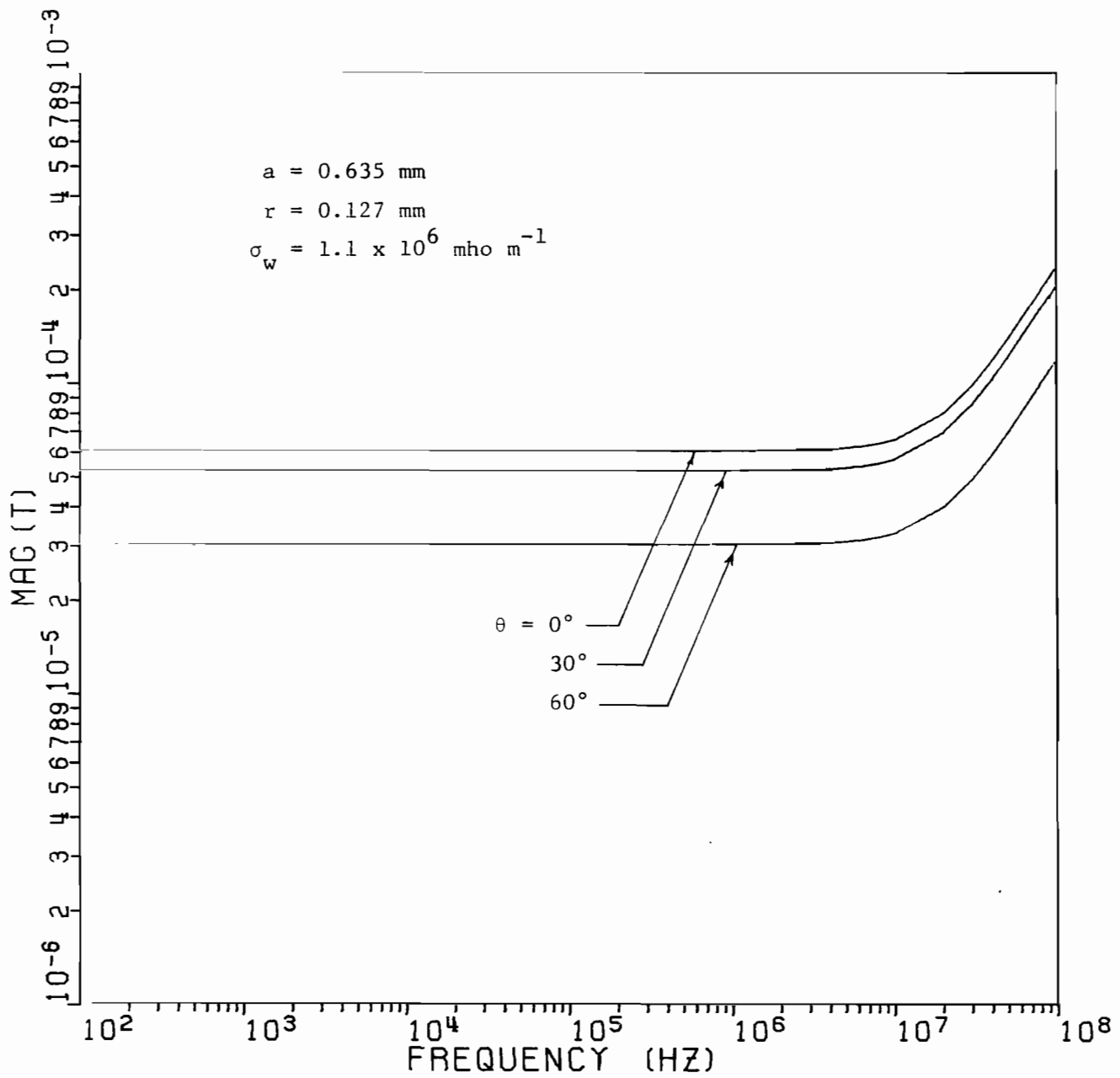
Figure 5.6a. $|T'|$ vs. frequency; a = 0.625 mm, r = 0.127 mm, $\sigma_w = 1.1 \times 10^6$ mho m^{-1}; $\theta = 0°$, 30°, 60°
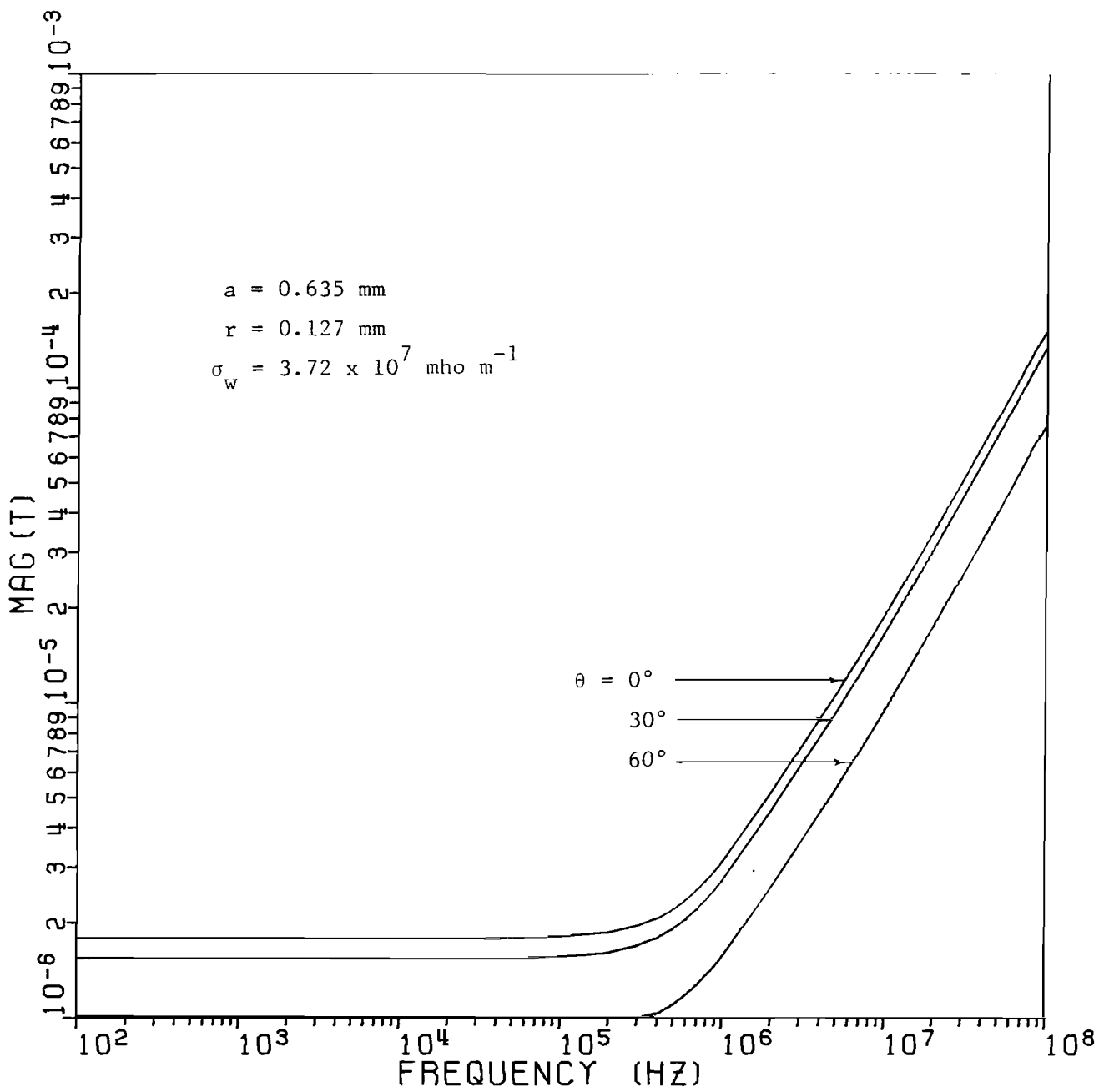
Figure 5.6b. $|T'|$ vs. frequency; a = 0.625 mm, r = 0.127 mm,
σ_w = 3.72 x 10^7 mho m^{-1}; θ = 0°, 30°, 60°

100
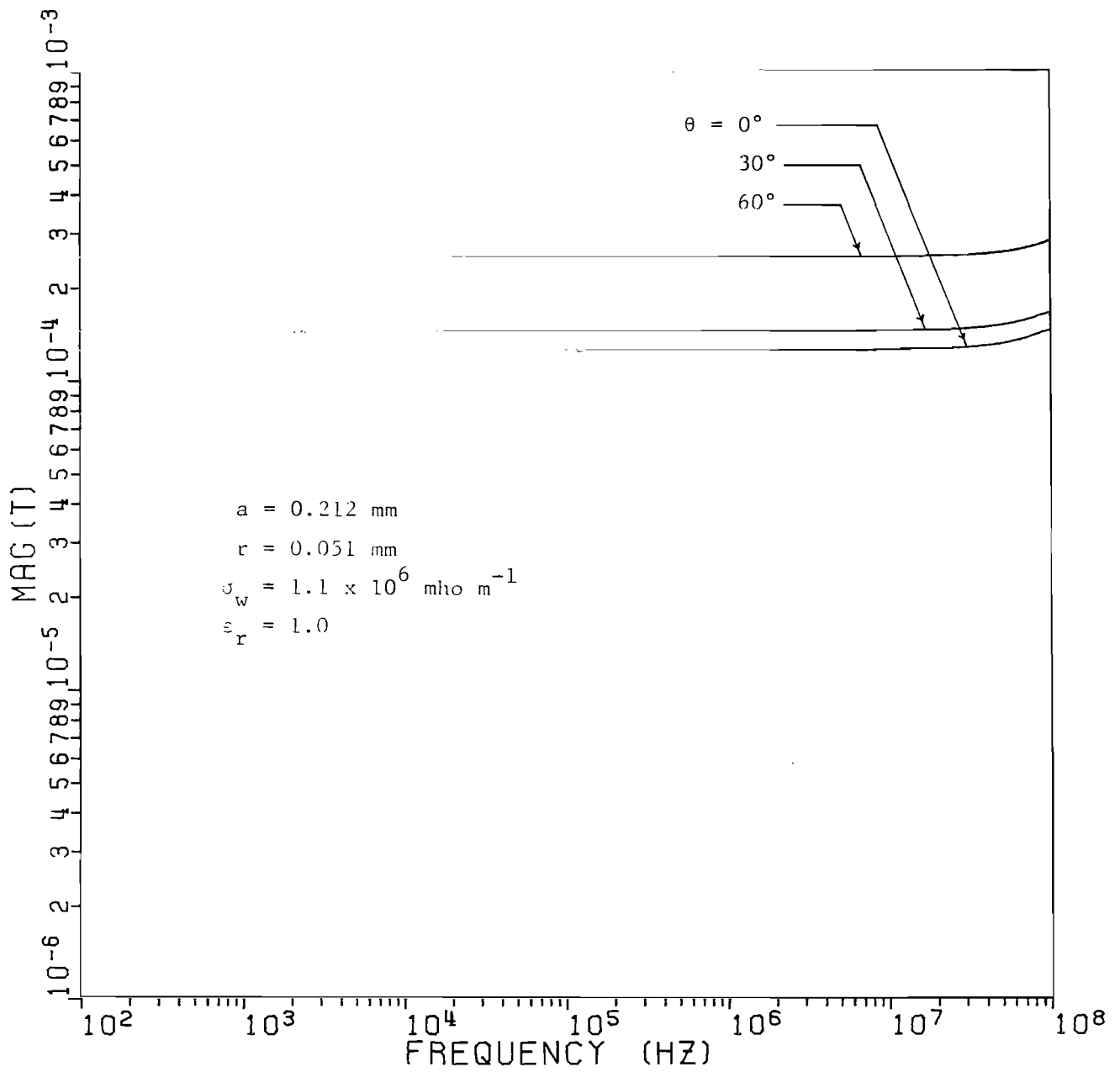
Figure 5.7a. $|T''|$ vs. frequency; a = 0.212 mm, r = 0.051 mm,
σ_w = 1.1 x 10^6 mho m^{-1}, ε_r = 1.0; θ = 0°, 30°, 60°
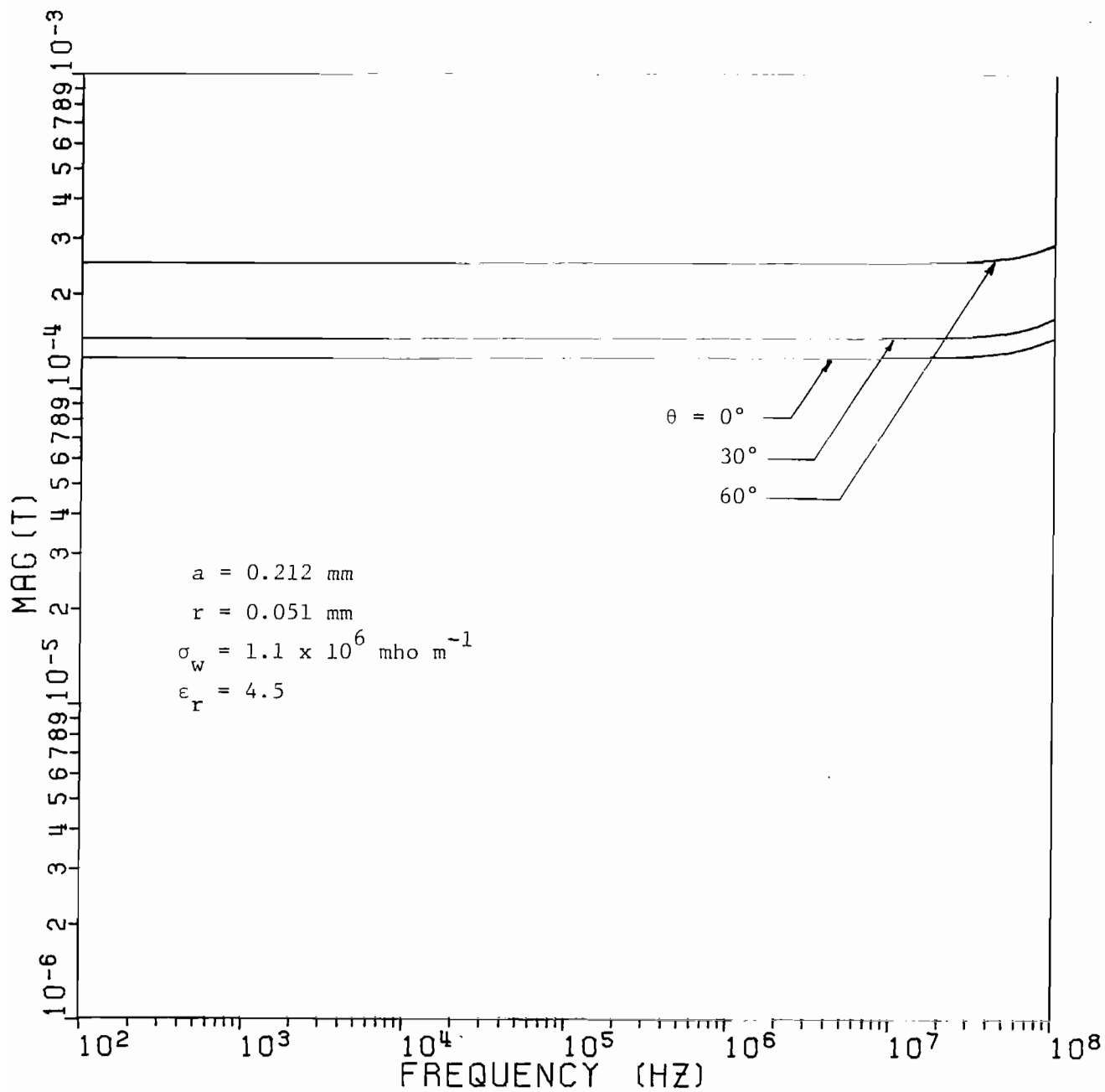
Figure 5.7b. $|T''|$ vs. frequency; $a = 0.212$ mm, $r = 0.051$ mm,
$\sigma_w = 1.1 \times 10^6$ mho m^{-1}, $\varepsilon_r = 4.5$; $\theta = 0°$, $30°$, $60°$

102
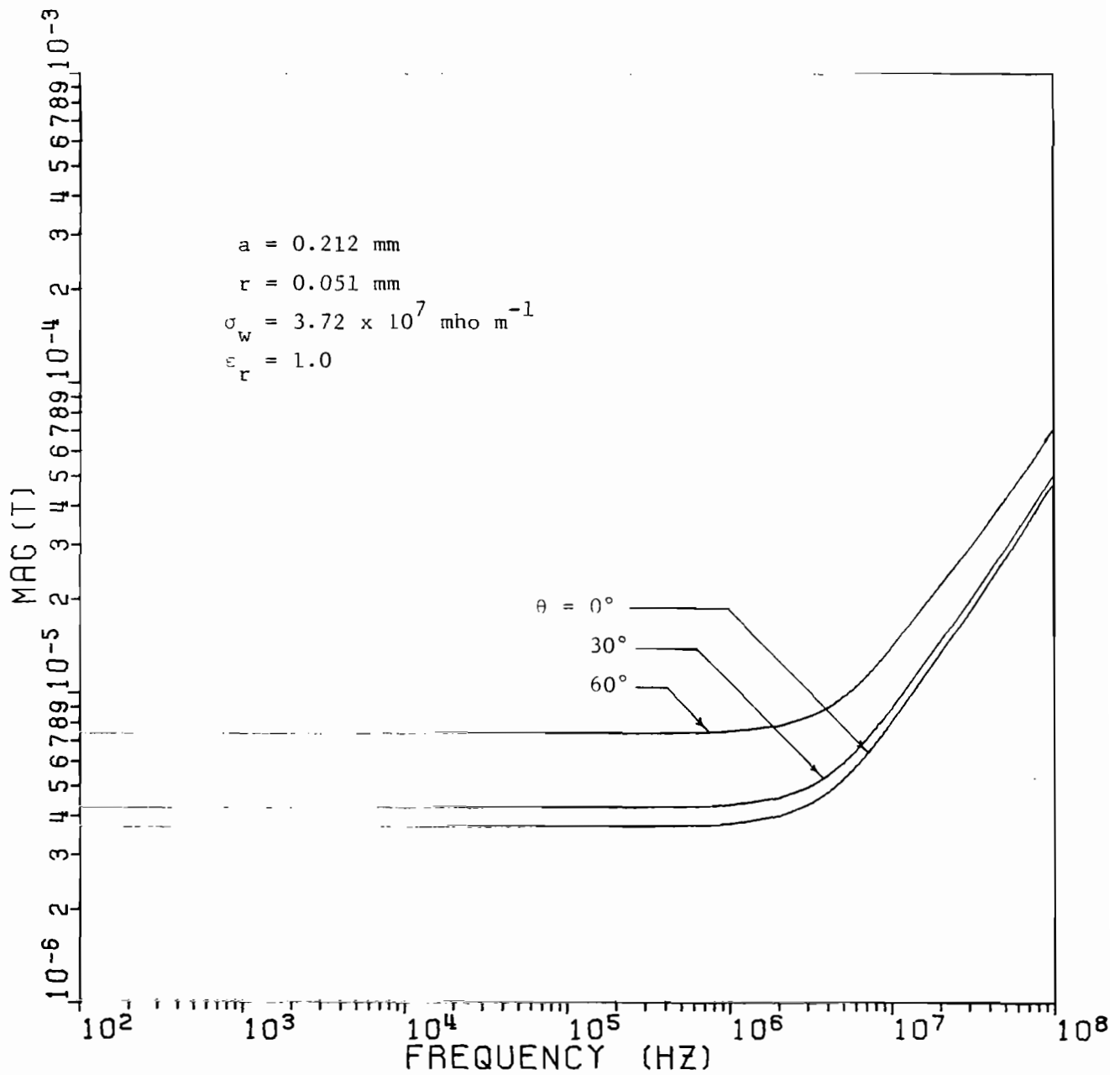
Figure 5.7c. $|T''|$ vs. frequency; a = 0.212 mm, r = 0.051 mm, σ_w = 3.72 x 10^7 mho m^{-1}, ε_r = 1.0; θ = 0°, 30°, 60°

Figure 5.7d. $|T''|$ vs. frequency; a = 0.212 mm, r = 0.051 mm, σ_w = 3.72 x 10^7 mho m^{-1}, ε_r = 4.5; θ = 0°, 30°, 60°

Figure 5.8a. $|T''|$ vs. frequency; a = 0.635 mm, r = 0.127 mm, σ_w = 1.1 x 10^6 mho m^{-1}, ε_r = 1.0; θ = 0°, 30°, 60°

Figure 5.8b. $|T''|$ vs. frequency; $a = 0.635$ mm, $r = 0.127$ mm, $\sigma_w = 1.1 \times 10^6$ mho m^{-1}, $\varepsilon_r = 4.5$; $\theta = 0°$, $30°$, $60°$

Figure 5.8c. $|T''|$ vs. frequency; $a = 0.635$ mm, $r = 0.127$ mm, $\sigma_w = 3.72 \times 10^7$ mho m^{-1}, $\varepsilon_r = 1.0$; $\theta = 0°$, $30°$, $60°$
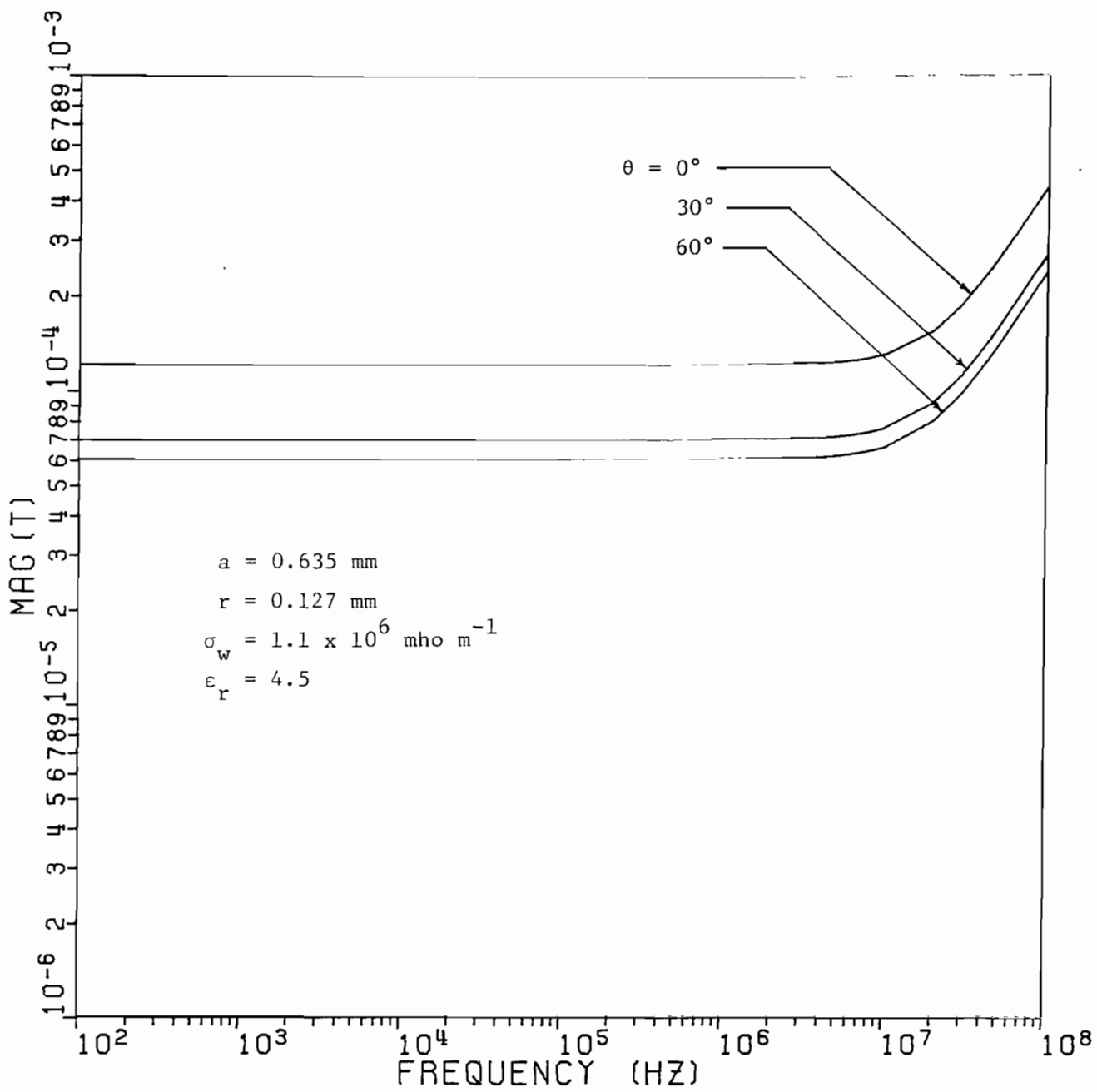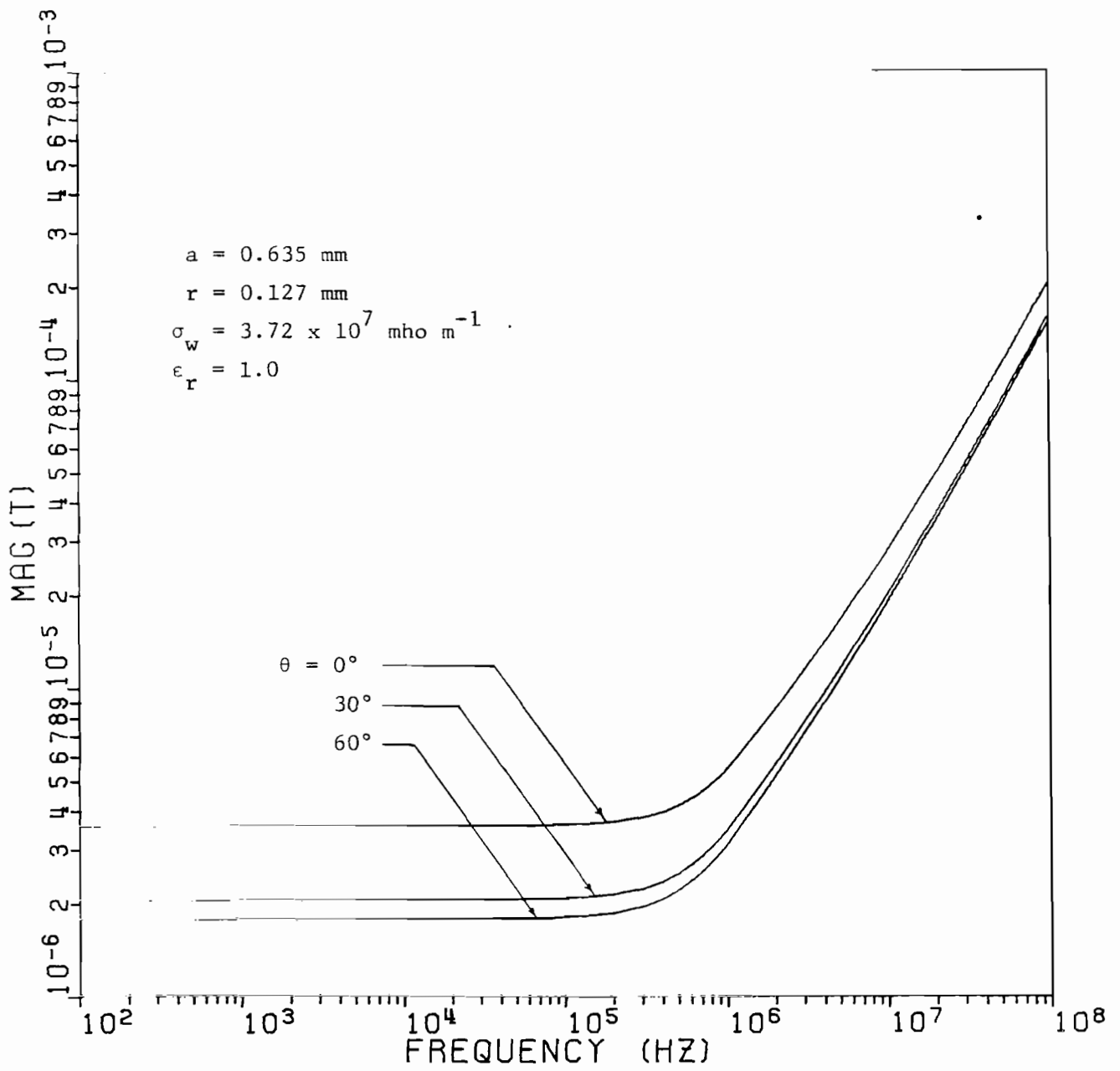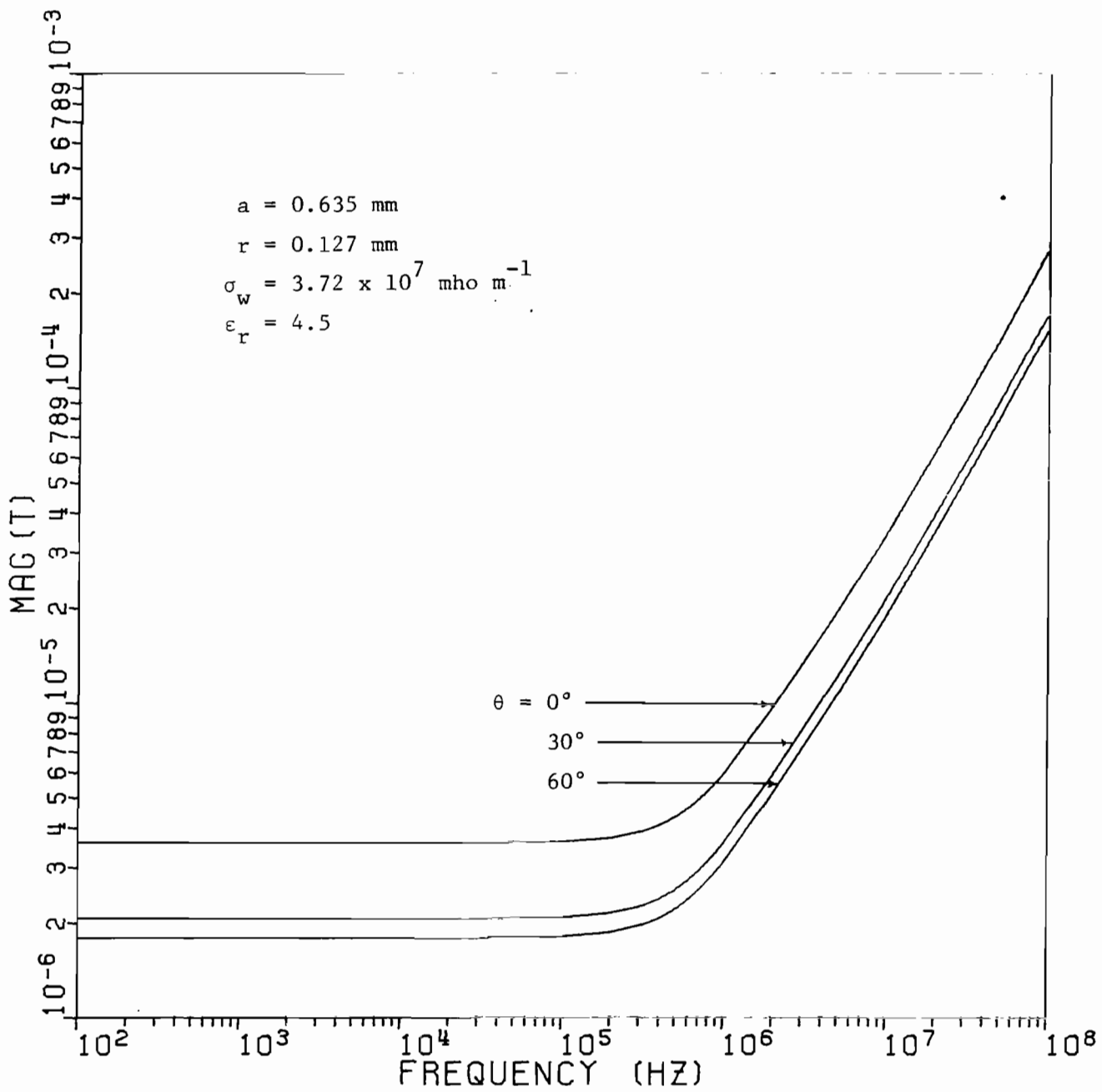
Figure 5.8d. $|T''|$ vs. frequency; $a = 0.635$ mm, $r = 0.127$ mm,
$\sigma_w = 3.72 \times 10^7$ mho m^{-1}, $\varepsilon_r = 4.5$; $\theta = 0°$, $30°$, $60°$

range of interest. This assumption will be reasonably valid over most of the frequency range occupied by an EMP signal, and will lead to a relatively simple analytical expression for the transmitted field. Setting up a Laplace integral for the transmitted fields $E_t'(\tau)$ and $E_t''(\tau)$, we easily obtain

$$
\begin{aligned}
E_t^{',''}(\tau) = {} & Ae^{-\alpha\tau}\left[\frac{\gamma^{',''} - \alpha}{\delta^{',''} + \gamma^{',''} - \alpha}\right] \\
& - Ae^{-\beta\tau}\left[\frac{\gamma^{',''} - \beta}{\delta^{',''} + \gamma^{',''} - \beta}\right] \\
& - Ae^{-(\delta^{',''} + \gamma^{',''})\tau}\left[\frac{\delta^{',''}(\beta-\alpha)}{(\delta^{',''} + \gamma^{',''} - \alpha)(\delta^{',''} + \gamma^{',''} - \beta)}\right]
\end{aligned}
\tag{5.83}
$$

in which A, α, and β have been previously defined, and

$$
\gamma' = \frac{2}{\mu_o r^2 \sigma_w \ell n(1-e^{-2\pi r/a})^{-1}}
\tag{5.84a}
$$

$$
\gamma'' = \gamma'(1 - \frac{\sin^2\theta}{1 + \varepsilon_r})^{-1}
\tag{5.84b}
$$

$$
\delta' = \frac{\pi c \; \sec\theta}{a \; \ell n(1-e^{-2\pi r/a})^{-1}}
\tag{5.84c}
$$

$$
\delta'' = \delta'\cos^2\theta(1 - \frac{\sin^2\theta}{1 + \varepsilon_r})^{-1}
\tag{5.84d}
$$

Now for angles of incidence not too close to 90°, δ' and δ'' are large in comparison to α, β, γ', and γ''. Therefore, an approximate expression for the transmitted field is

$$
\begin{aligned}
E_t^{',''}(\tau) = {} & \frac{\gamma^{',''}}{\delta^{',''}} E_o(\tau) \\
& + \frac{1}{\delta^{',''}}\left[\frac{dE_o}{d\tau} - \frac{dE_o}{d\tau}\Big|_{\tau=0} e^{-(\delta^{',''} + \gamma^{',''})\tau}\right]
\end{aligned}
\tag{5.85}
$$

109

in which $E_o(\tau)$ is given in eq. (1.1). The factors γ'/δ' and γ''/δ'' are given by

$$\frac{\gamma'}{\delta'} = \frac{2a}{\pi \, \eta_o r^2 \sigma_w} \cos\theta \qquad\qquad (5.86a)$$

$$\frac{\gamma''}{\delta''} = \frac{2a}{\pi \, \eta_o r^2 \sigma_w} \sec\theta \qquad\qquad (5.86b)$$

Note that the quantity $\pi r^2 \sigma_w/a$ plays the same role in these expressions as does the quantity $\sigma_g d$ in related formulas for the graphite composite case. Curves of $E_t(\tau)$ vs. τ at normal incidence are shown for two representative cases in Figs. 5.9 and 5.10.

The shapes of the $E_t(\tau)$ curves of Figs. 5.9 and 5.10 can be understood readily in terms of the "differentiating" or high-pass character of the bonded wire-mesh screen. The sheet impedance of the screen comprises both resistive and inductively reactive components, and thus increases in magnitude with increasing frequency. The effect of this behavior on the transmission coefficient in the frequency domain is evident in Figs. 5.5 through 5.8: configurations with $\sigma_w = 1.1 \times 10^6$ mho m^{-1} yield values of $|T'|$ and $|T''|$ which are nearly constant with respect to frequency over the range of interest, and the sheet impedance is primarily resistive. Increasing the wire conductivity to 3.72×10^7 mho m^{-1} decreases the resistive component of the sheet impedance, making the reactive component relatively more important. For the two mesh size/wire radius combinations considered, the transmission coefficient at low frequencies is higher for the case a = 0.212 mm, r = 0.051 mm than for the case a = 0.635 mm, r = 0.127 mm, as a consequence of the fact that the second configuration contains more metal per unit area, even though the mesh size is larger. On the other hand, the inductive reactance
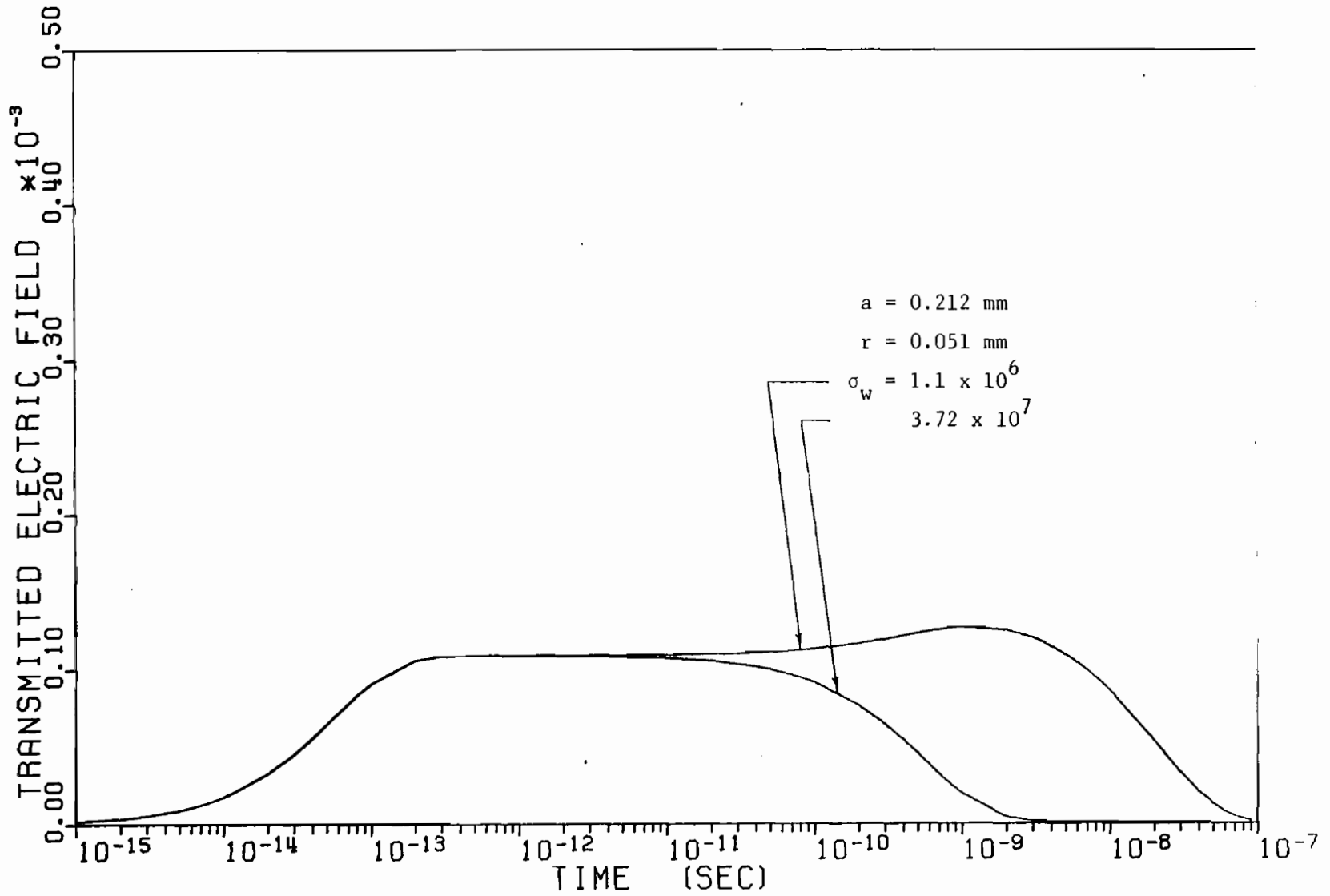
110

Figure 5.9. $E_t(\tau)$ vs. τ; a = 0.212 mm, r = 0.051 mm, σ_w = 1.1 x 10^6, 3.72 x 10^7 mho m^{-1}
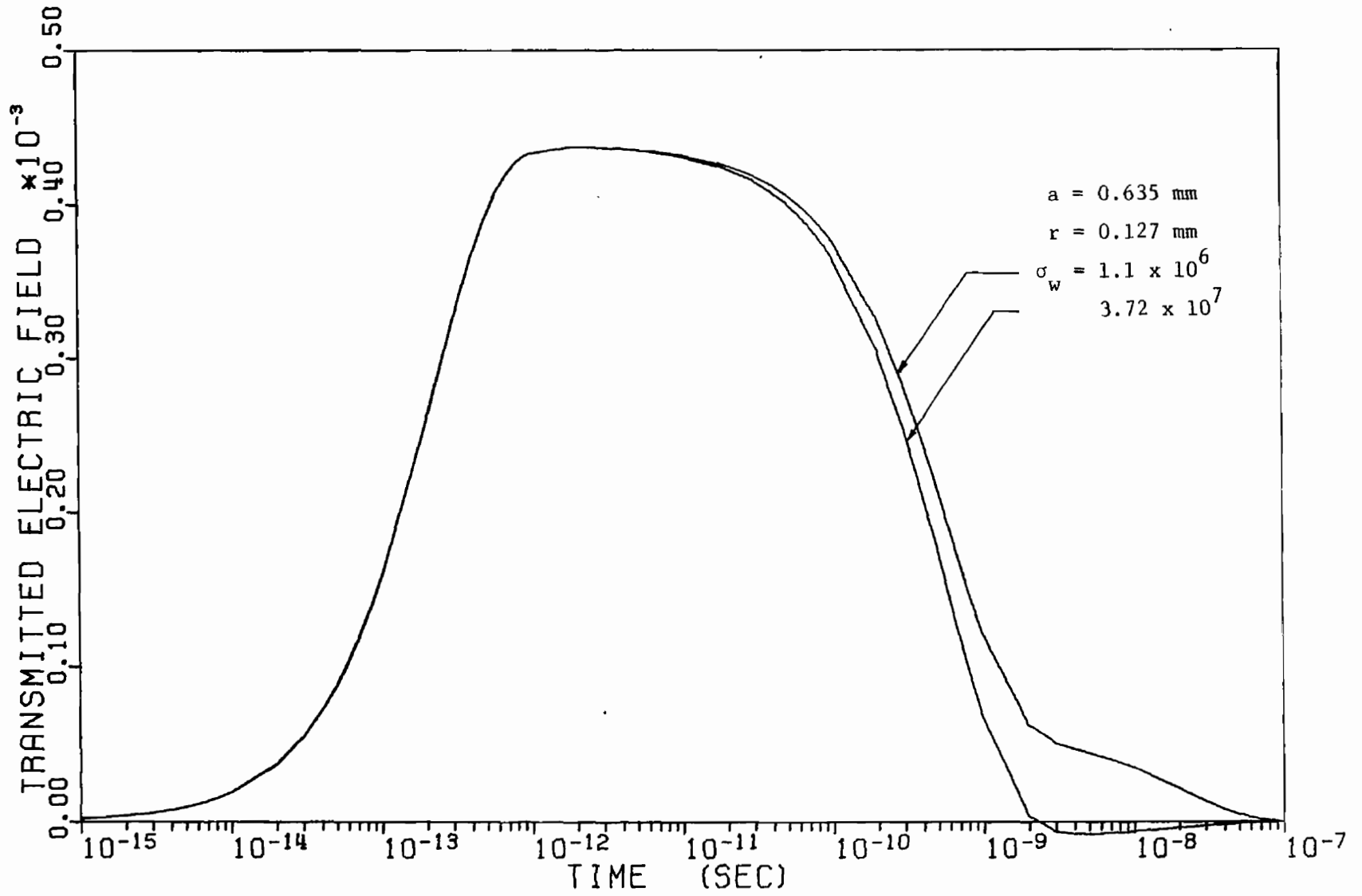
Figure 5.10. $E_t(\tau)$ vs. τ; a = 0.635 mm, r = 0.127 mm, σ_w = 1.1 x 10^6, 3.72 x 10^7 mho m^{-1}

of the 0.635/0.127 configuration is larger than that of the 0.212/0.051 mesh, for equal wire conductivity; the magnitude of the transmission coefficient for this case is correspondingly greater at higher frequencies.

The effect of this behavior on the time-domain transmitted electric field is evident in Figs. 5.9 and 5.10. The 0.212/0.051 mesh yields an $E_t(\tau)$ response which is nearly independent of σ_w up to $\tau = 5 \times 10^{-12}$ sec; this early-time behavior is principally a result of the inductive reactance of the sheet impedance. At later times the resistive component of the sheet impedance exerts the dominating influence on the transmitted field.

The 0.635/0.127 mesh, on the other hand, yields a much higher amplitude for the transmitted field at early times (again, up to $\tau = 5 \times 10^{-12}$ sec, the response is nearly independent of σ_w) as a consequence of its larger inductive reactance. The late-time amplitude is again dominated by the resistance of the screen, although some undershoot is apparent for $\tau > 2 \times 10^{-9}$ sec for the case of the larger wire conductivity.

The most interesting comparison to be made among the four curves presented is that between the two higher-conductivity cases. The finer mesh, <u>even though its equivalent conductivity-thickness product</u> $\pi r^2 \sigma_w/a$ <u>is smaller by a factor of 2 than that of the larger mesh</u>, yields a smaller transmitted field. This observation leads one to conclude that the conductivity-thickness product alone cannot be used as a measure of the effectiveness of mesh shields. The time-domain behavior of the incident fields must also be taken into account; in fact, an interesting problem for further study would be to <u>design</u> a screen to yield minimum transmitted field under a given set of constraints.

113

One should also compare the curves in Figs. 5.9 and 5.10 with those in Fig. 5.4 for the planar graphite composite layer. The pulse shapes have already been discussed. Of interest, however, is comparing the peak transmitted electric field amplitudes for the two types of composite. For example, a 2 mm thick graphite panel of conductivity $\sigma_g = 1.5 \times 10^4$ mho m^{-1} yields a peak transmitted electric field amplitude of 9.7×10^{-5}; the 0.635/0.127 mesh yields a peak value of 45×10^{-5}; and the 0.212/0.051 mesh, 15×10^{-5}. The screened panel would thus seem generally to be a poorer shield than the graphite panel, at least at early times. We will return to this type of comparison in the next section.

6. THE PERFORATED SCREEN MODEL FOR A WIRE MESH

In this paragraph we briefly consider the problem of transmission of a plane electromagnetic wave through a periodic square array of square apertures in a perfectly conducting plane, in order to compare the results to those previously obtained for the wire mesh. Our purpose is to gain some insight into the behavior of the mesh screen when the assumption $r/a \ll 1$ does not apply and the thin-wire approximation breaks down.

Let the screen be in the surface $z=0$ and let the apertures be square of side length h and centered at $(x = (m + 1/2)a, y = (n + 1/2)a)$ for $-\infty < m,n < \infty$. The geometry is shown in Fig. 5.11. It is well known (cf., e.g., [20]) that an electrically small aperture in a conducting screen can be modeled in terms of equivalent electric and magnetic dipoles. We therefore consider the electromagnetic field radiated by a planar array of electric and magnetic dipoles in free space located at $(x = (m+1/2)a, y = (n+1/2)a, z=0)$. The electric and magnetic dipole moments are assumed to be given by

114
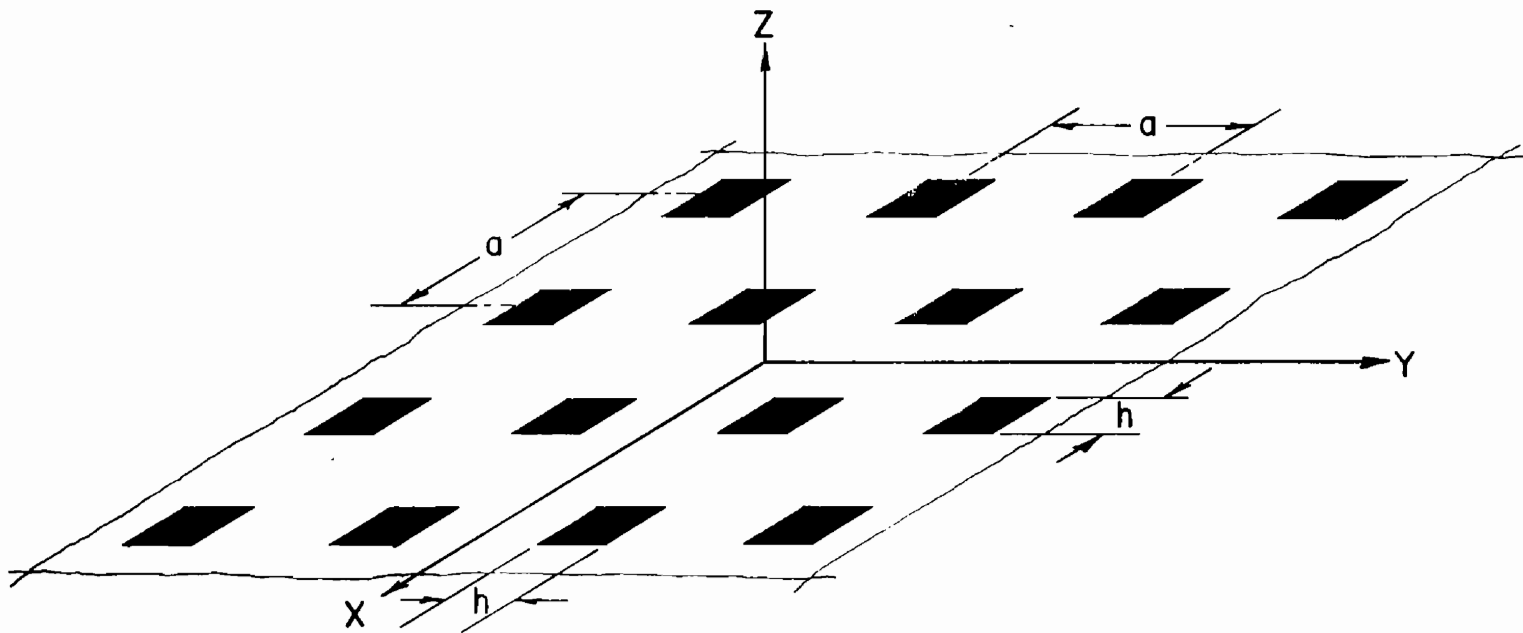
Figure 5.11. Perforated screen geometry

$$\bar{p}_e(x = ma + a/2, \ y = na + a/2) = p_{eoz}\bar{a}_z e^{-jk_{xo}a(m+1/2)}$$

$$\cdot \ e^{-jk_{yo}a(n+1/2)} \tag{5.87a}$$

$$\bar{p}_m(x = ma + a/2, \ y = na + a/2) = \bar{p}_{mo}e^{-jk_{xo}a(m+1/2)-jk_{yo}a(n+1/2)}$$

$$\tag{5.87b}$$

in which $\bar{p}_e$ denotes the electric dipole moment and $\bar{p}_m$ denotes the magnetic

dipole moment. p_{eoz} and $\bar{p}_{mo}$ are constants; furthermore $\bar{p}_{mo} = p_{mox}\bar{a}_x + p_{moy}\bar{a}_y$.

When the period of the array a is very small in comparison to the

free-space wavelength, the radiated electric field is easily shown to be

$$E_x = \frac{1}{2a^2}\left(\frac{k_{xo}p_{eoz}}{\omega\varepsilon_o} - p_{moy}\right)e^{-jk_{xo}x - jk_{yo}y - jk_{zo}z} \tag{5.88a}$$

$$E_y = \frac{1}{2a^2}\left(\frac{k_{yo}p_{eoz}}{\omega\varepsilon_o} + p_{mox}\right)e^{-jk_{xo}x - jk_{yo}y - jk_{zo}z} \tag{5.88b}$$

$$E_z = \frac{1}{2a^2 k_{zo}}\left[k_{xo}p_{moy} - k_{yo}p_{mox} - \frac{1}{2\omega\varepsilon_o}(k_{xo}^2 + k_{yo}^2)\right]e^{-jk_{xo}x-jk_{yo}y-jk_{zo}z}$$

$$\tag{5.88c}$$

in the region $z > 0$; also, $k_{zo}^2 = k_o^2 - k_{xo}^2 - k_{yo}^2$.

Now the dipole moments p_{eoz} and $\bar{p}_{mo}$ are given in terms of the fields

E_{zo} and $\bar{H}_{to}$ which would exist in the plane z=0 if the apertures were

closed by the relations

$$p_{eoz} = j\omega\varepsilon_o\alpha_e E_{zo} \tag{5.89a}$$

$$\bar{p}_{mo} = -j\omega\mu_o\alpha_m \bar{H}_{to} \tag{5.89b}$$

in which α_e and α_m denote respectively the electric and magnetic polariz-

116

abilities of the apertures. Latham [20] has calculated these polariz-

abilities; his results are

$$\alpha_e/a^3 = \frac{0.114 \ (h/a)^3}{1 + 0.104(h/a)^3} \qquad\qquad (5.90a)$$

$$\alpha_m/a^3 = \frac{0.260 \ (h/a)^3}{1 - 0.185(h/a)^3} \qquad\qquad (5.90b)$$

Let us now assume that a perpendicularly polarized plane wave is

incident upon the perforated screen from the region z<0. Then E_{zo} and

$\bar{H}_{to}$ are given by

$$E_{zo} = E'_{zo} = 0 \qquad\qquad (5.91a)$$

$$\bar{H}_{to} = \bar{H}'_{to} = \frac{-2E'_o \cos\theta}{\eta_o} \ (\bar{a}_x \ \cos\phi + \bar{a}_y \ \sin\phi) \qquad\qquad (5.91b)$$

in which E'_o denotes the electric field amplitude in the incident wave;

furthermore, $k_{xo} = k_o \sin\theta \ \cos\phi$, $k_{yo} = k_o \sin\theta \ \sin\phi$, and $k_{zo} = k_o \cos\theta$, in

which θ and ϕ are the incidence angles. The transmitted electric field

amplitude is now easily shown to be

$$E'_{trans} = jk_o a \cos\theta \ (\alpha_m/a^3) E'_o \qquad\qquad (5.92)$$

When a parallel-polarized plane wave is incident upon the screen,

the fields E_{zo} and $\bar{H}_{to}$ are

$$E_{zo} = E''_{zo} = -2E''_o \ \sin\theta \qquad\qquad (5.93a)$$

$$\bar{H}_{to} = \bar{H}''_{to} = \frac{2E''_o}{\eta} \ (-\bar{a}_x \ \sin\phi + \bar{a}_y \ \cos\phi) \qquad\qquad (5.93b)$$

where E''_o denotes the electric field amplitude in the incident wave. The

transmitted electric field amplitude is

$$E''_{trans} = jk_o a \ \sec\theta \ (\alpha_m/a^3)[1 - (\alpha_e/\alpha_m)\sin^2\theta]E''_o \qquad\qquad (5.94)$$

117

Now let us compare the expressions given in eqs. (5.92) and (5.94) with those obtained for the electric field transmitted through a perfectly conducting wire mesh screen, in the low-frequency limit. We have, from the results obtained in the previous paragraph,

$$E'_{trans} \simeq jk_o a \cos\theta \, \frac{1}{\pi} \, \ell n (1 - e^{-2\pi r/a})^{-1} \, E'_o \qquad (5.95a)$$

$$E''_{trans} \simeq jk_o a \sec\theta \, \frac{1}{\pi} \, \ell n (1 - e^{-2\pi r/a})^{-1} (1 - \frac{1}{2} \sin^2\theta) E''_o \qquad (5.95b)$$

Examining eqs. (5.92) and (5.95a) for E'_{trans}, we see that the expressions $\frac{1}{\pi} \ell n (1 - e^{-2\pi r/a})^{-1}$ and α_m/a^3 (cf. eq. (5.90b)) are to be compared. We shall compare them on the basis of equal optical coverage by letting h = a-2r. The two expressions are shown as functions of r/a in Fig. 5.12. The wire-mesh model factor is always larger than the perforated-screen factor; the former is accurate in the limit $r/a \to 0$, and the latter is accurate in the limit $r/a \to 0.5$. It is clear that the wire mesh model overestimates the transmitted field amplitude, and therefore underestimates the induced currents on the screen, for values of r/a which are not very small in comparison to unity.

Examining eqs. (5.94) and (5.95b) for E''_{trans}, we see that the relevant comparison is between the constant factor 0.5 for the wire-mesh model and the ratio α_e/α_m for the perforated-screen model. This ratio is shown as a function of r/a in Fig. 5.13. It is apparent that the mesh model overestimates the importance of the "$\sin^2\theta$" term in the transmission coefficient for parallel-polarized fields. The reason for this is probably the use of the thin-wire approximation in the analysis of the mesh model. In effect, the equivalent permittivity of the mesh for electric fields normal to the plane of the mesh, caused by induced line dipole moments on the wires, has been ignored. It is clear from our earlier analysis

118
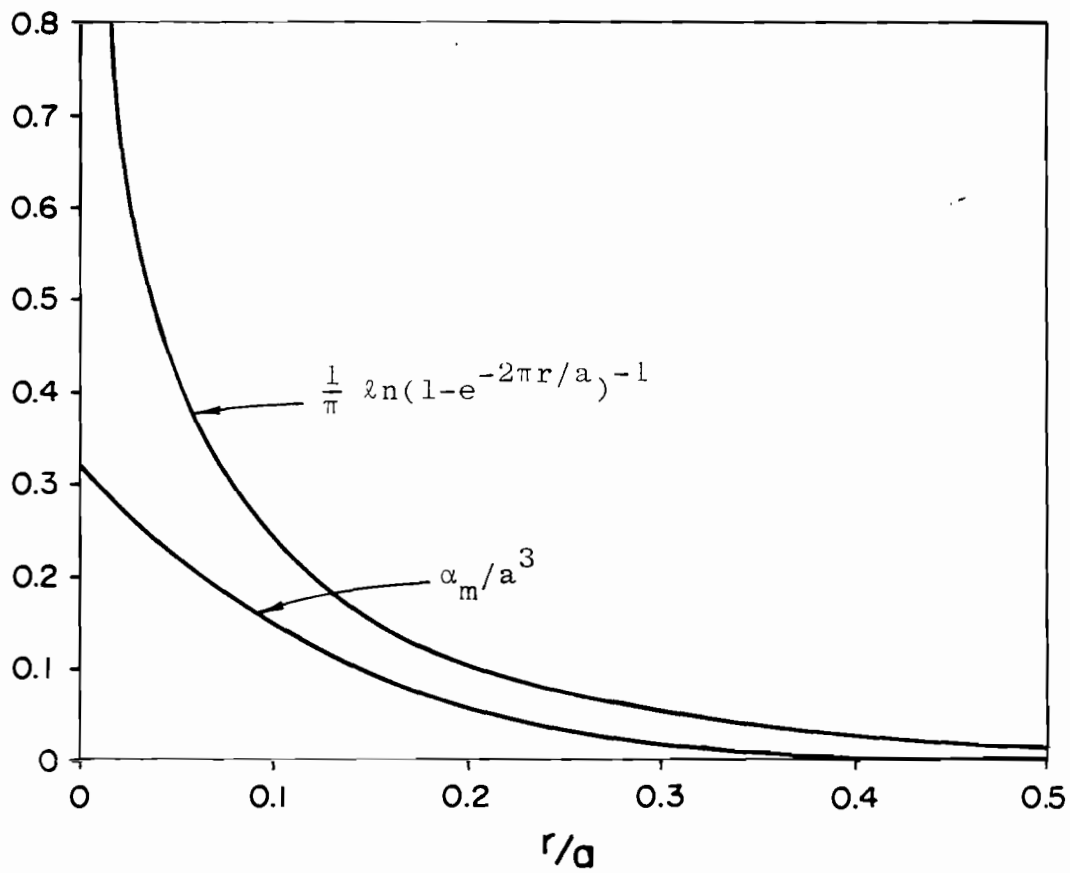
Figure 5.12. Functions $\frac{1}{\pi} \ln(1-e^{-2\pi r/a})^{-1}$ and α_m/a^3 vs. r/a
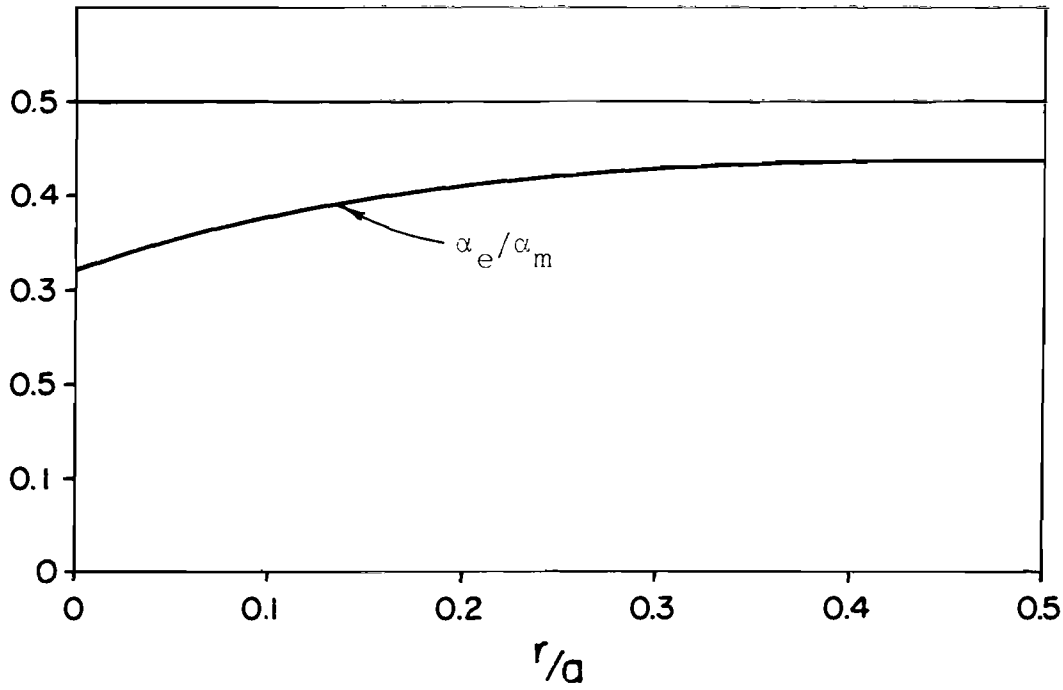
Figure 5.13. α_e/α_m vs. r/a; the constant value 0.5 is also explicitly shown

120

of the effect of a dielectric environment on the wire mesh that including these line dipole moments would decrease the coefficient of the "$\sin^2\theta$" term and thereby improve the accuracy of our approximate solution for the sheet impedance operator $\overline{\overline{Z}}_s$. This aspect of the problem would seem worthy of further study.

7. NUMERICAL COMPUTATION OF GRID CURRENTS

The equations (5.37) and (5.40) can be solved for the modified current harmonics $\tilde{I}'_{xm}$ and $\tilde{I}'_{yn}$ by means of the procedure outlined in this paragraph. We begin by substituting eq. (5.37) into eq. (5.40), thereby eliminating the variable Δ from further consideration and yielding

$$\sum_{n=-\infty}^{\infty} (U_m \delta_{mn} + \frac{jqa}{2} P_m k_{xn}) \tilde{I}'_{xn} + \sum_{n=-\infty}^{\infty} (V_{mn} - \frac{jqa}{2} P_m k_{yn}) \tilde{I}'_{yn} = R_o \delta_m \qquad (5.95a)$$

$$\sum_{n=-\infty}^{\infty} (X_{nm} - \frac{jqa}{2} Q_m k_{xn}) \tilde{I}'_{xn} + \sum_{n=-\infty}^{\infty} (W_m \delta_{mn} + \frac{jqa}{2} Q_m k_{yn}) I'_{yn} = S_o \delta_m \qquad (5.95b)$$

as the coupled sets of equations for $\tilde{I}'_{xn}$ and $\tilde{I}'_{yn}$. Also,

$$q = [\frac{a}{b} (\frac{1}{2} + \frac{k_{yo}^2 b^2}{24}) + (\frac{1}{2} + \frac{k_{xo}^2 a^2}{24})]^{-1} \qquad (5.96)$$

Now define matrices $\overline{\overline{M}}_{xx}$, $\overline{\overline{M}}_{xy}$, $\overline{\overline{M}}_{yx}$, and $\overline{\overline{M}}_{yy}$ such that

$$(\overline{\overline{M}}_{xx})_{mn} = U_m \delta_{mn} + \frac{jqa}{2} P_m k_{xn} \qquad (5.97a)$$

$$(\overline{\overline{M}}_{xy})_{mn} = V_{mn} - \frac{jqa}{2} P_m k_{yn} \qquad (5.97b)$$

$$(\overline{\overline{M}}_{yx})_{mn} = X_{nm} - \frac{jqa}{2} Q_m k_{xn} \qquad (5.97c)$$

$$(\overline{\overline{M}}_{yy})_{mn} = W_m \delta_{mn} + \frac{jqa}{2} Q_m k_{yn} \qquad (5.97d)$$

and let $\tilde{\tilde{I}}'_x$ and $\tilde{\tilde{I}}'_y$ denote the modified space harmonic current vectors. Finally, let $\bar{R}_o$ and $\bar{S}_o$ denote the "driving" vectors; these each possess only a single nonzero element. Then the coupled equations (5.95) may be written

$$\overline{\overline{M}}_{xx} \cdot \tilde{\tilde{I}}'_x + \overline{\overline{M}}_{xy} \cdot \tilde{\tilde{I}}'_y = \bar{R}_o \qquad (5.98a)$$

$$\overline{\overline{M}}_{yx} \cdot \tilde{\tilde{I}}'_x + \overline{\overline{M}}_{yy} \cdot \tilde{\tilde{I}}'_y = \bar{S}_o \qquad (5.98b)$$

This system is readily solved for $\tilde{\tilde{I}}'_x$ and $\tilde{\tilde{I}}'_y$. We obtain

$$\tilde{\tilde{I}}'_x = \overline{\overline{N}}_{xr} \cdot \overline{\overline{R}}_o - \overline{\overline{N}}_{xs} \cdot \overline{S}_o \tag{5.99a}$$

$$\tilde{\tilde{I}}'_y = \overline{\overline{N}}_{yr} \cdot \overline{R}_o - \overline{\overline{N}}_{ys} \cdot \overline{S}_o \tag{5.99b}$$

where

$$\overline{\overline{N}}_{xr} = (\overline{\overline{M}}_{xy}^{-1} \cdot \overline{\overline{M}}_{xx} - \overline{\overline{M}}_{yy}^{-1} \cdot \overline{\overline{M}}_{yx})^{-1} \cdot \overline{\overline{M}}_{xy}^{-1} \tag{5.100a}$$

$$\overline{\overline{N}}_{xs} = (\overline{\overline{M}}_{xy}^{-1} \cdot \overline{\overline{M}}_{xx} - \overline{\overline{M}}_{yy}^{-1} \cdot \overline{\overline{M}}_{yx})^{-1} \cdot \overline{\overline{M}}_{yy}^{-1} \tag{5.100b}$$

$$\overline{\overline{N}}_{yr} = (\overline{\overline{M}}_{xx}^{-1} \cdot \overline{\overline{M}}_{xy} - \overline{\overline{M}}_{yx}^{-1} \cdot \overline{\overline{M}}_{yy})^{-1} \cdot \overline{\overline{M}}_{xx}^{-1} \tag{5.100c}$$

$$\overline{\overline{N}}_{ys} = (\overline{\overline{M}}_{xx}^{-1} \cdot \overline{\overline{M}}_{xy} - \overline{\overline{M}}_{yx}^{-1} \cdot \overline{\overline{M}}_{yy})^{-1} \cdot \overline{\overline{M}}_{yx}^{-1} \tag{5.100d}$$

and the solution is formally complete. Δ can now be calculated using eq. (5.37).

The calculation of the grid impedance $\overline{\overline{Z}}_g$ defined in eq. (5.52) is straightforward. We readily obtain

$$\overline{\overline{Z}}_g = \begin{bmatrix} \dfrac{1}{b} (\overline{\overline{N}}_{xr})_{oo} & -\dfrac{1}{b} (\overline{\overline{N}}_{xs})_{oo} \\[2ex] \dfrac{1}{a} (\overline{\overline{N}}_{yr})_{oo} & -\dfrac{1}{a} (\overline{\overline{N}}_{ys})_{oo} \end{bmatrix}^{-1} \tag{5.101}$$

Now using eq. (5.53), we may calculate the equivalent sheet impedance $\overline{\overline{Z}}_s$.

The efficient numerical evaluation of the matrix elements defined in eq. (5.97) has already been discussed (cf. eqs. (5.42) and (5.43)).

We have calculated the eigenvalues of the equivalent sheet impedance operator $\overline{\overline{Z}}_s$ as a function of N, the number of modified space harmonics included in $\tilde{\tilde{I}}'_x$ and $\tilde{\tilde{I}}'_y$ (note that N = 1,3,5,...), for the case d/a = 1,

$b/a = 1$, $r/a = 0.01$, $\varepsilon_r = 4.5$, $\sigma_w = \infty$, $\theta = 60°$, where $\phi = 0°$ and $45°$ and $k_o a = 1.0$ and 0.1. The results of these computations are shown in Figs. 5.14–5.17, in which values of X_s' and X_s'' ($Z_s{}^{',''} = jX_s{}^{',''}$) are plotted vs. N. The rapid convergence of X_s' and X_s'' with increasing N is evident (note, however, that in the $\phi = 45°$ cases this is not at all surprising, since there is no discontinuity in the junction currents when $\phi = 45°$, $135°$, $225°$, or $315°$, by symmetry). The use of the N=1 case to derive an analytical approximation for $\overline{\overline{Z}}_s$ when $k_o a \ll 1$ is justified by the rapidity of convergence apparent in Figs. 5.16 and 5.17 for $k_o a = 0.1^\dagger$.

[†]Note that for typical mesh dimensions the maximum value of $k_o a$ occurring in the EMP frequency range is of order 10^{-3}.
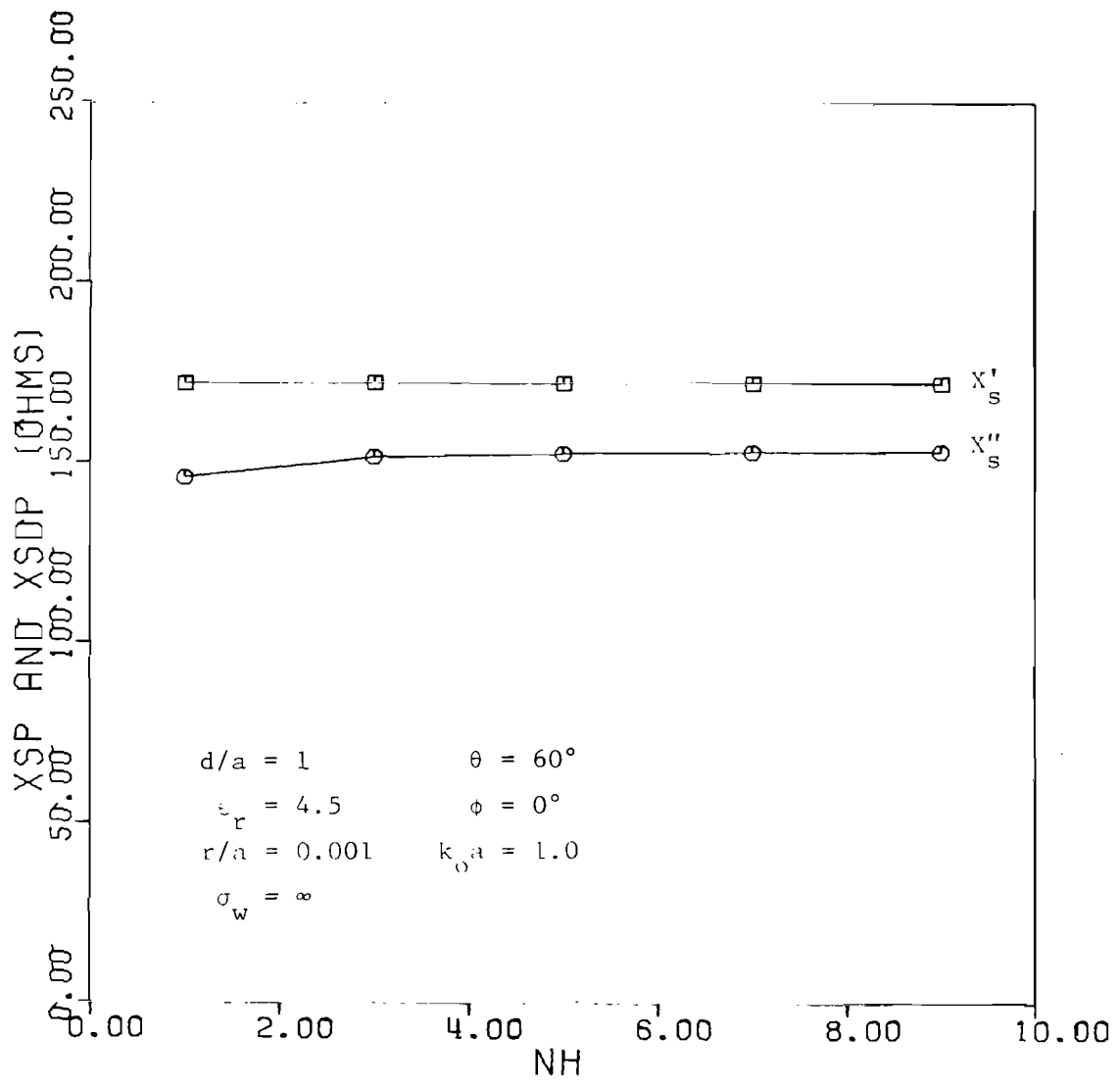
Figure 5.14. X_s' and X_s'' ($Z_s', '' = jX_s', ''$) vs. N; d/a = 1, ε_r = 4.5, r/a = 0.01, σ_w = ∞, θ = 60°, φ = 0°, $k_o a$ = 1.0

Figure 5.15. X_s' and X_s'' ($Z_s'{}'{}'' = jX_s'{}'{}''$) vs. N; d/a = 1, ε_r = 4.5, r/a = 0.01, σ_w = ∞, θ = 60°, φ = 45°, k_oa = 1.0
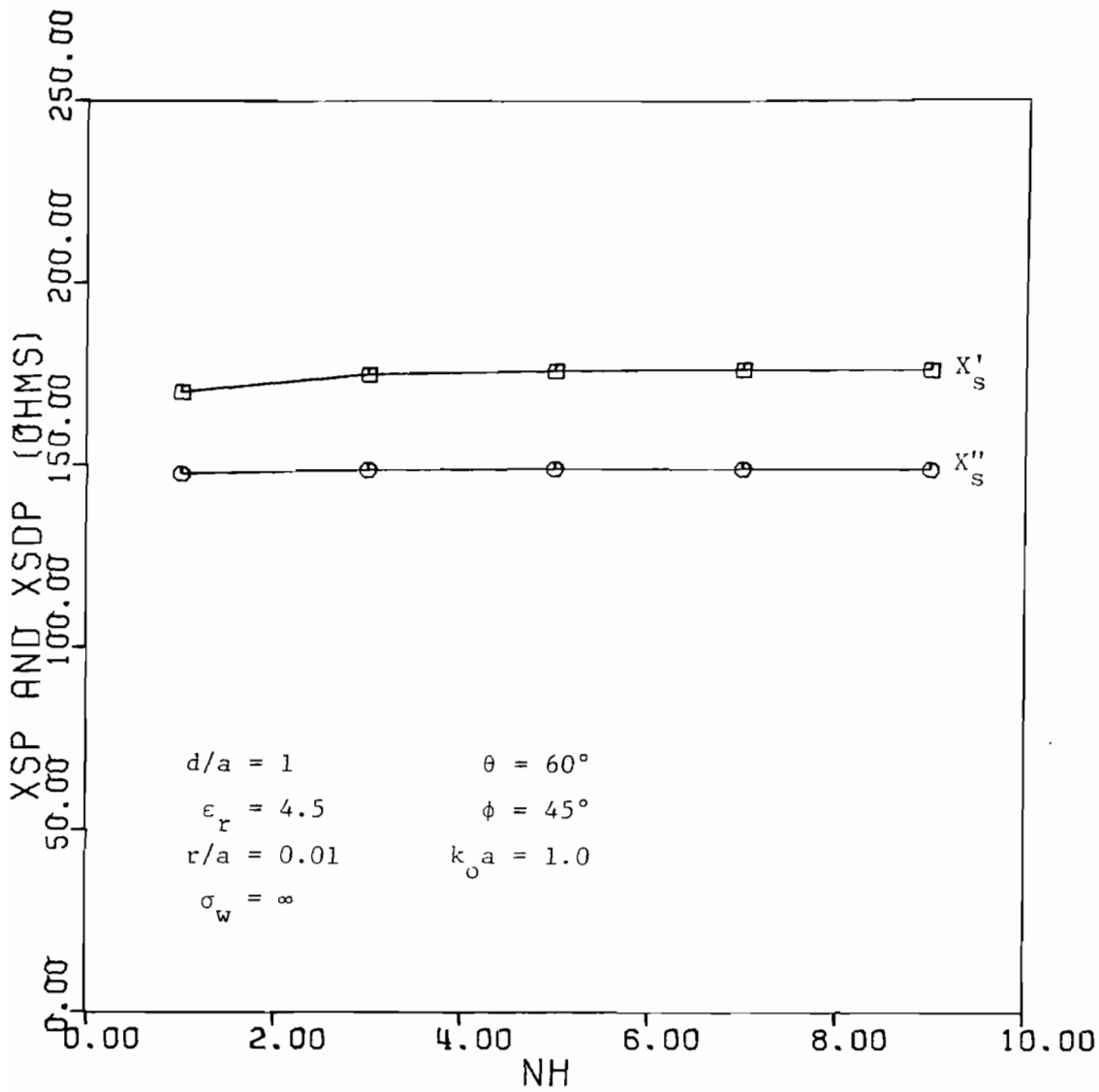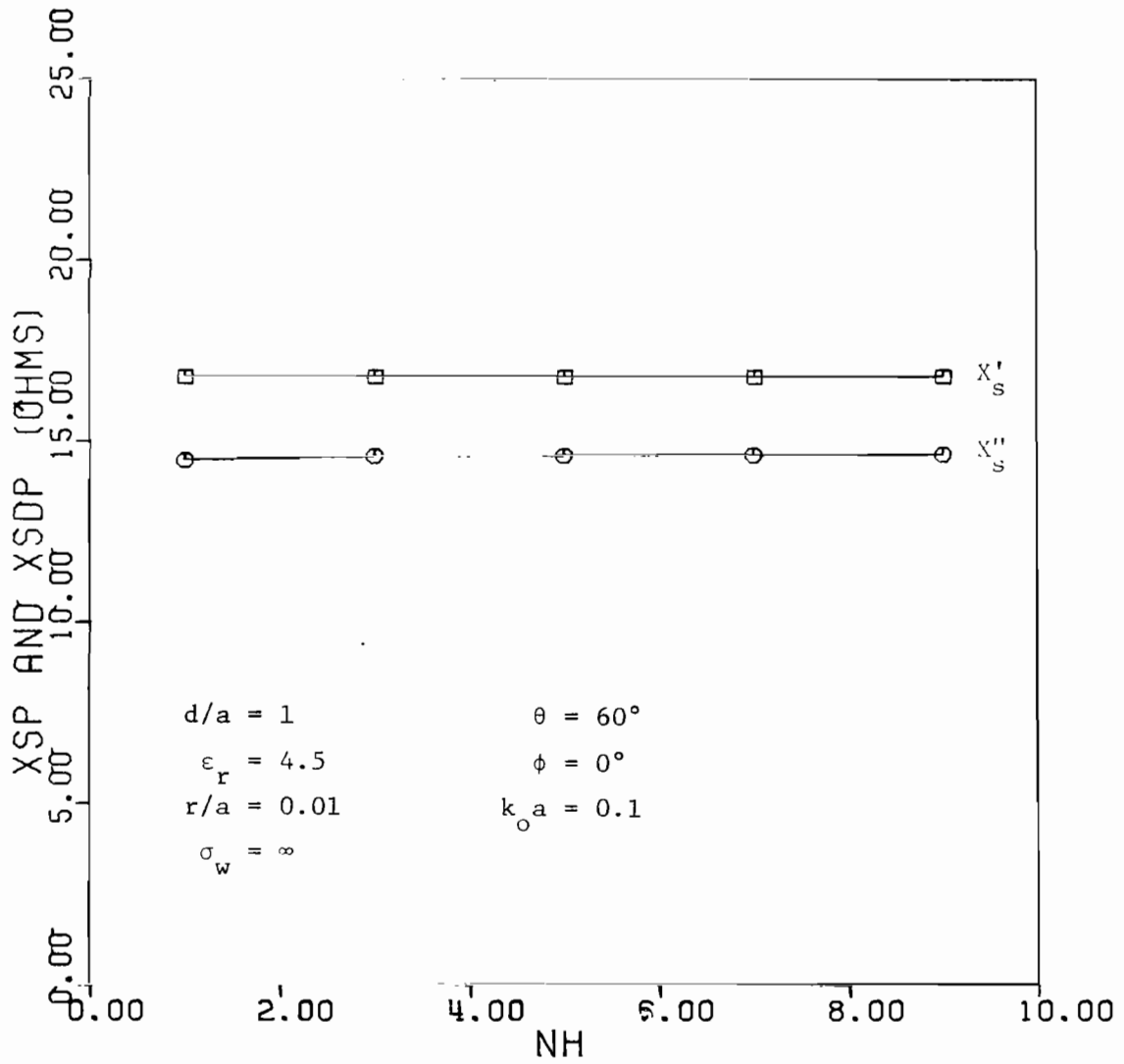
Figure 5.16. X'_s and X''_s ($Z'_s,'' = jX'_s,''$) vs. N; $d/a = 1$, $\varepsilon_r = 4.5$, $r/a = 0.01$, $\sigma_w = \infty$, $\theta = 60°$, $\phi = 0°$, $k_o a = 0.1$
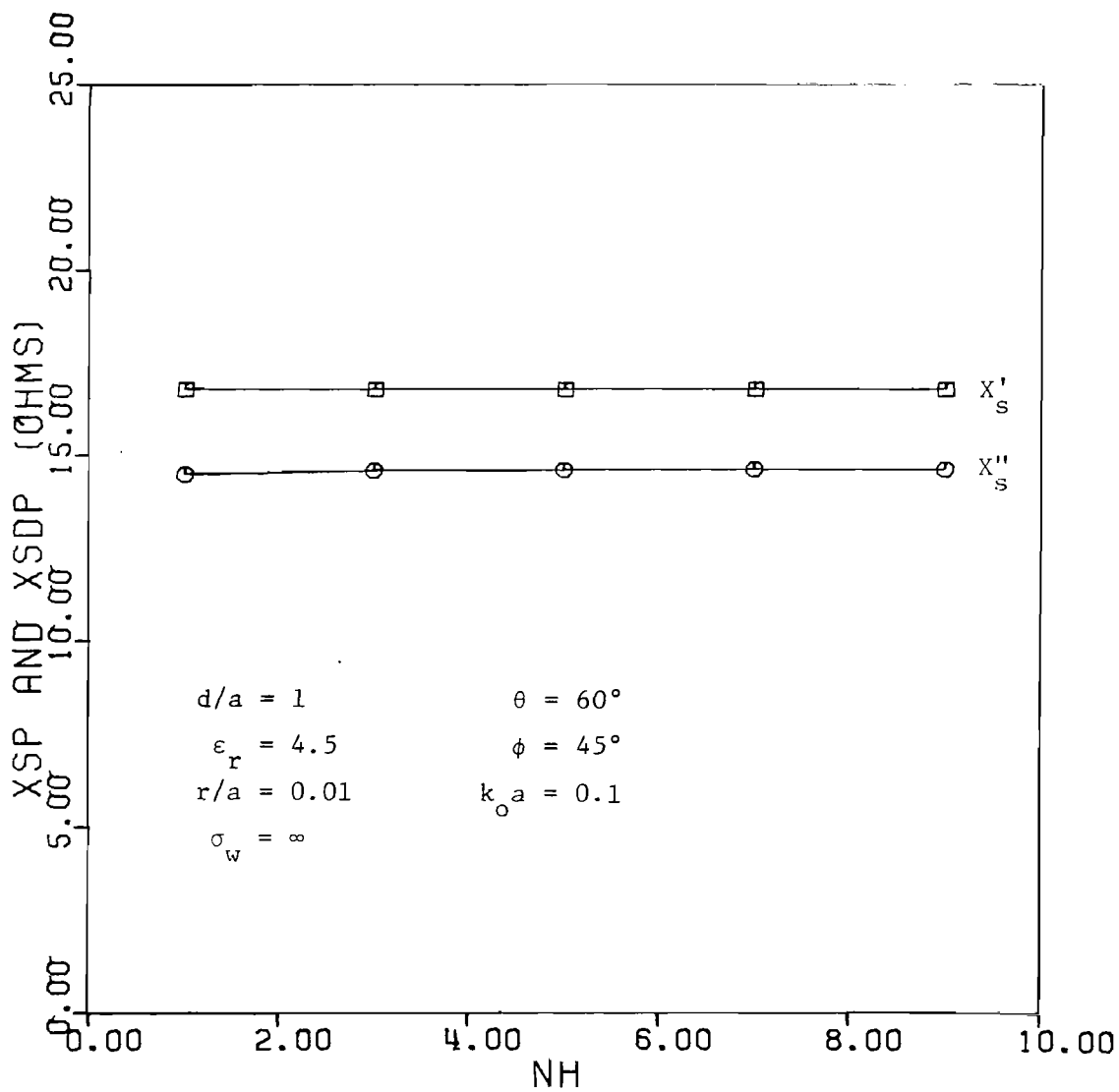
Figure 5.17. X_s' and X_s'' ($Z_s',''=jX_s',''$) vs. N; d/a = 1, ε_r = 4.5, r/a = 0.01, σ_w = ∞, θ = 60°, ϕ = 45°, $k_o a$ = 0.1

CYLINDRICAL WIRE-MESH COMPOSITE SHIELDS

1. INTRODUCTION

In this section we shall consider the interaction of a plane electromagnetic wave with an infinitely long cylindrical shell of wire-mesh composite. As in Section IV, we shall consider only the cases in which the propagation vector of the incident wave has no component along the cylinder axis.

In the next paragraph, the problem is formulated in the frequency domain using the equivalent sheet impedance developed in the previous section to describe the screen in the surface of the composite shell. Some representative frequency-domain results are presented. In paragraph 3, we briefly consider the transient behavior of the internal magnetic field when the circumference of the cylinder is small in comparison to the wavelength over the frequency range of interest and the temporal behavior of the incident wave is that of the standard EMP signal.

2. FORMULATION OF THE PROBLEM

The geometry of the problem is shown in Fig. 6.1. An infinitely long cylindrical shell of wire-mesh composite of inner and outer radii a and b respectively is illuminated by a plane electromagnetic wave. The medium inside and outside the shell is free space and the shell thickness $d = b - a$ is small in comparison to the mean radius $\sqrt{ab}$. The side of the wire-mesh composite in which the grid is embedded is the outer surface of the cylinder. For simplicity we shall again consider only the case in which the incident wave's propagation vector has no axial component, and we shall investigate the two possible wave polarizations separately. The total fields may then be obtained by superposition.
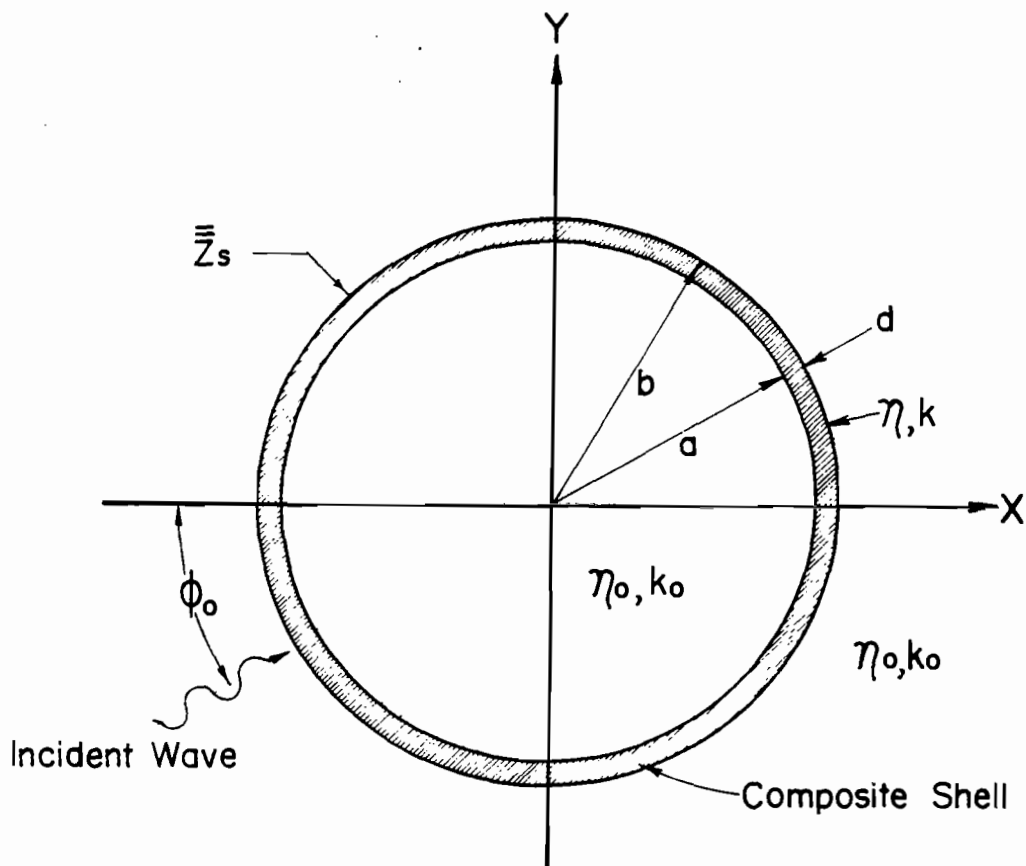
Figure 6.1.   Plane wave penetration of, and scattering by, a cylindrical
              shell of boron-epoxy composite with a bonded wire-mesh screen
              in the outer surface: geometry of the problem

The shell itself is modeled as an equivalent sheet impedance, based on the results obtained for the planar case in the previous section. We shall denote the mean shell radius by ρ_o. Z''_s, which, as will be recalled, depends upon the transverse propagation constant, will be denoted $Z''_{s,n}$ for each angular eigenfunction in the field expansion, and

$$k_{to}^2 = k_{ton}^2 = \frac{n^2}{\rho_o^2} \qquad (6.1)$$

Consider first the case in which the incident electromagnetic wave is polarized TM with respect to z. In this case, the field components are

$$E_z = -j\omega\mu_o\Psi \qquad (6.2a)$$

$$H_\phi = -\frac{\partial\Psi}{\partial\rho} \qquad (6.2b)$$

$$H_\rho = \frac{1}{\rho}\frac{\partial\Psi}{\partial\phi} \qquad (6.2c)$$

where

$$0 \le \rho \le \rho_o: \quad \Psi = \frac{-E_o}{j\omega\mu_o}\sum_{n=-\infty}^{\infty} A_n J_n(k_o\rho)e^{jn(\phi-\phi')} \qquad (6.3a)$$

$$\rho \ge \rho_o: \quad \Psi = \frac{-E_o}{j\omega\mu_o}\sum_{n=-\infty}^{\infty} [J_n(k_o\rho) + B_n H_n^{(2)}(k_o\rho)]e^{jn(\phi-\phi')} \qquad (6.3b)$$

A_n and B_n are to be determined, E_o is the electric field amplitude of the incident wave, and $\phi' = \phi_o + \pi/2$, where ϕ_o is the angle of incidence as shown in Fig. 6.1. The appropriate Z_s for this polarization is Z'_s.

Now the boundary conditions at $\rho=\rho_o$ are applied. We have

$$E_z(\rho = \rho_o-) = E_z(\rho = \rho_o+) = E_z(\rho = \rho_o) \qquad (6.4a)$$

$$H_\phi(\rho = \rho_o+) - H_\phi(\rho = \rho_o-) = (Z'_s)^{-1} E_z(\rho = \rho_o) \qquad (6.4b)$$

131

from which expressions for A_n and B_n are readily obtained. We find

$$A_n = \left[1 + \pi k_o \rho_o \frac{\eta_o (Z_s')^{-1}}{2} J_n(k_o \rho_o) H_n^{(2)}(k_o \rho_o) \right]^{-1} \tag{6.5a}$$

$$B_n = -\pi k_o \rho_o \frac{\eta_o (Z_s')^{-1}}{2} J_n^2(k_o \rho_o) A_n \tag{6.5b}$$

When the incident wave is polarized TE with respect to z, the field components are

$$H_z = j\omega\varepsilon_o \Phi \tag{6.6a}$$

$$E_\phi = -\frac{\partial \Phi}{\partial \rho} \tag{6.6b}$$

$$E_\rho = \frac{1}{\rho} \frac{\partial \Phi}{\partial \phi} \tag{6.6c}$$

where

$$0 \le \rho \le \rho_o: \quad \Phi = \frac{E_o}{jk_o} \sum_{n=-\infty}^{\infty} A_n' J_n(k_o \rho) e^{jn(\phi-\phi')} \tag{6.7a}$$

$$\rho > \rho_o: \quad \Phi = \frac{E_o}{jk_o} \sum_{n=-\infty}^{\infty} [J_n(k_o \rho) + B_n' H_n^{(2)}(k_o \rho)] e^{jn(\phi-\phi')} \tag{6.7b}$$

A_n' and B_n' are to be determined. At $\rho = \rho_o$, the boundary conditions to be applied are

$$E_\phi(\rho = \rho_o-) = E_\phi(\rho = \rho_o+) = E_\phi(\rho = \rho_o) \tag{6.8a}$$

$$H_z(\rho = \rho_o+) - H_z(\rho = \rho_o-) = -(Z_s'')^{-1} E_\phi(\rho = \rho_o) \tag{6.8b}$$

in which

$$(Z_s'')^{-1} E_\phi(\rho_o) \equiv \sum_{n=-\infty}^{\infty} (Z_{s,n}'')^{-1} E_{\phi n}(\rho_o) \tag{6.9}$$

We find for A_n' and B_n'

$$A_n' = \left[1 + \pi k_o \rho_o \frac{\eta_o (Z_{s,n}'')^{-1}}{2} J_n'(k_o \rho_o) H_n^{(2)'}(k_o \rho_o) \right]^{-1} \tag{6.10a}$$

132

$$B_n' = -\pi k_o \rho_o \frac{\eta_o (Z_{s,n}'')^{-1}}{2} [J_n'(k_o\rho_o)]^2 A_n' . \qquad (6.10b)$$

The energy shielding ratios r_w and r_w' are given in terms of A_n and A_n' in eqs. (4.12) and (4.20). To obtain expressions for r_w and r_w' appropriate for the screened composite cylindrical shell, A_n and A_n' given in eqs. (6.5a) and (6.10a) are substituted into eqs. (4.12) and (4.20) respectively. When $k_o a \ll 1$, approximate expressions for r_w and r_w' are

$$r_w \Big|_{k_o a \ll 1} \simeq \frac{1}{2} \left\{ \left| 1 - jk_o\rho_o \, \eta_o (Z_s')^{-1} \, \ell n \, k_o\rho_o \right|^{-2} \right.$$

$$\left. + \left| 1 + jk_o\rho_o \, \frac{\eta_o (Z_s')^{-1}}{2} \right|^{-2} \right\} \qquad (6.11a)$$

$$r_w' \Big|_{k_o a \ll 1} \simeq \frac{1}{2} \left\{ \left| 1 + jk_o\rho_o \, \frac{\eta_o (Z_{s,0}'')^{-1}}{2} \right|^{-2} \right.$$

$$\left. + \left| 1 - j\eta_o \, \frac{(Z_{s,1}'')^{-1}}{2k_o\rho_o} \right|^{-2} \right\} \qquad (6.11b)$$

Curves of r_w and r_w' as functions of frequency are given for various values of screen parameters and a cylinder radius $\rho_o = 1$ m in Figs. 6.2 and 6.3. (a_m, rather than a, denotes the mesh size in this section). As in the related curves for the graphite shell, we note that unless $\sigma_w = \infty$; $r_w \to 1$ and $r_w' \to 0.5$ as $f \to 0$. The reason for this behavior, as before, is that r_w' contains only a contribution from the internal magnetic field, while both the internal electric and magnetic fields contribute to r_w. Also, we have not included curves for r_w' in the case $\epsilon_r = 1$; over the frequency range shown, they are indistinguishable from the curves for the case $\epsilon_r = 4.5$.

Comparison of Figs. 6.2 and 6.3 with Figs. 4.2-4.7 reveals
that for cylindrical geometries the screened boron-epoxy composite shells
with σ_w = 1.1 × 10^6 mho m^{-1} are comparable to graphite composite shells
in shielding effectiveness, while those with σ_w = 3.72 × 10^7 mho m^{-1} are
decidedly superior. The reason for this is that the principal break
frequency, below which the shielding is relatively poor, is approximately
$1/(\pi\mu_o\rho_o(\pi r^2 \sigma_w/a))$; and $\pi r^2 \sigma_w/a$, which is the equivalent conductivity-
thickness product for the mesh is comparable to $\sigma_g d$ for graphite shells
when σ_w = 1.1 × 10^6 mho m^{-1}, but is significantly larger than $\sigma_g d$ when
σ_w = 3.72 × 10^7 mho m^{-1}.

Not shown in the r_w and r'_w curves is the higher-frequency effect of
the screen inductance. This is apparent in the time-domain internal field
response, which is discussed in the next paragraph.

3.   TIME-DOMAIN SHIELDING

The ratio of the internal magnetic field to the incident magnetic
field in the frequency domain is readily shown to be given when $k_o\rho_o$ << 1
by

$$\frac{H_{int}}{H_{inc}} = [1 + jk_o\rho_o \frac{\eta_o}{2} (Z'_s)^{-1}]^{-1} \qquad (6.12)$$

for either polarization. This result does not involve the relative
permittivity of the composite shell at all, since the case in which
the magnetic field is perpendicular to the cylinder axis corresponds
to perpendicular polarization (and Z'_s does not involve ϵ_r), and the
case in which the magnetic field is parallel to the cylinder axis
utilizes only the n=0 angular eigenfunction in the low-frequency limit
(and $Z''_{s,0}$ does not involve ϵ_r).

134
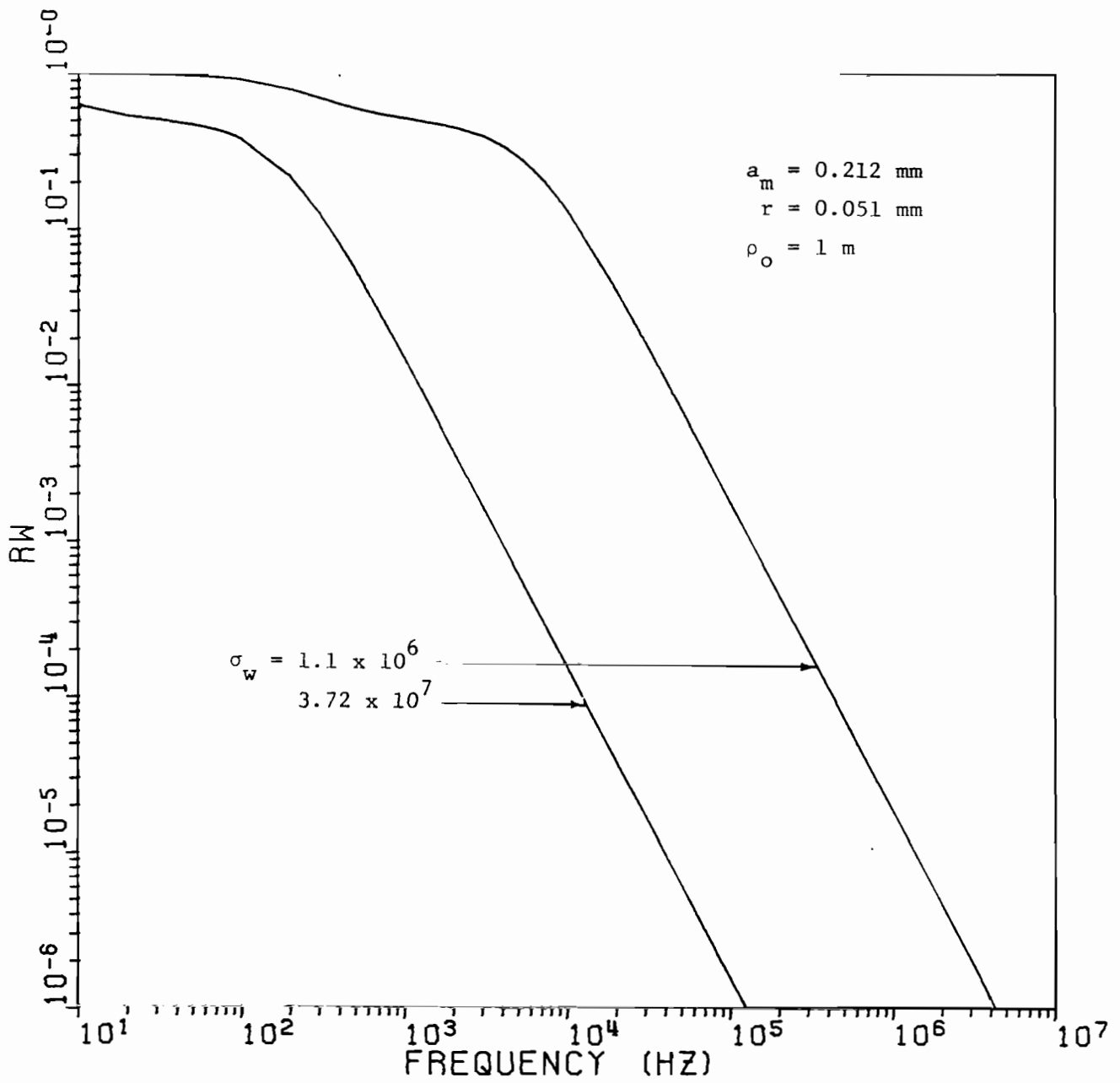
Figure 6.2a. r_w vs. frequency; $a_m = 0.212$ mm, $r = 0.051$ mm, $\rho_o = 1$ m; $\sigma_w = 1.1 \times 10^6$ and 3.72×10^7 mho m^{-1}

135
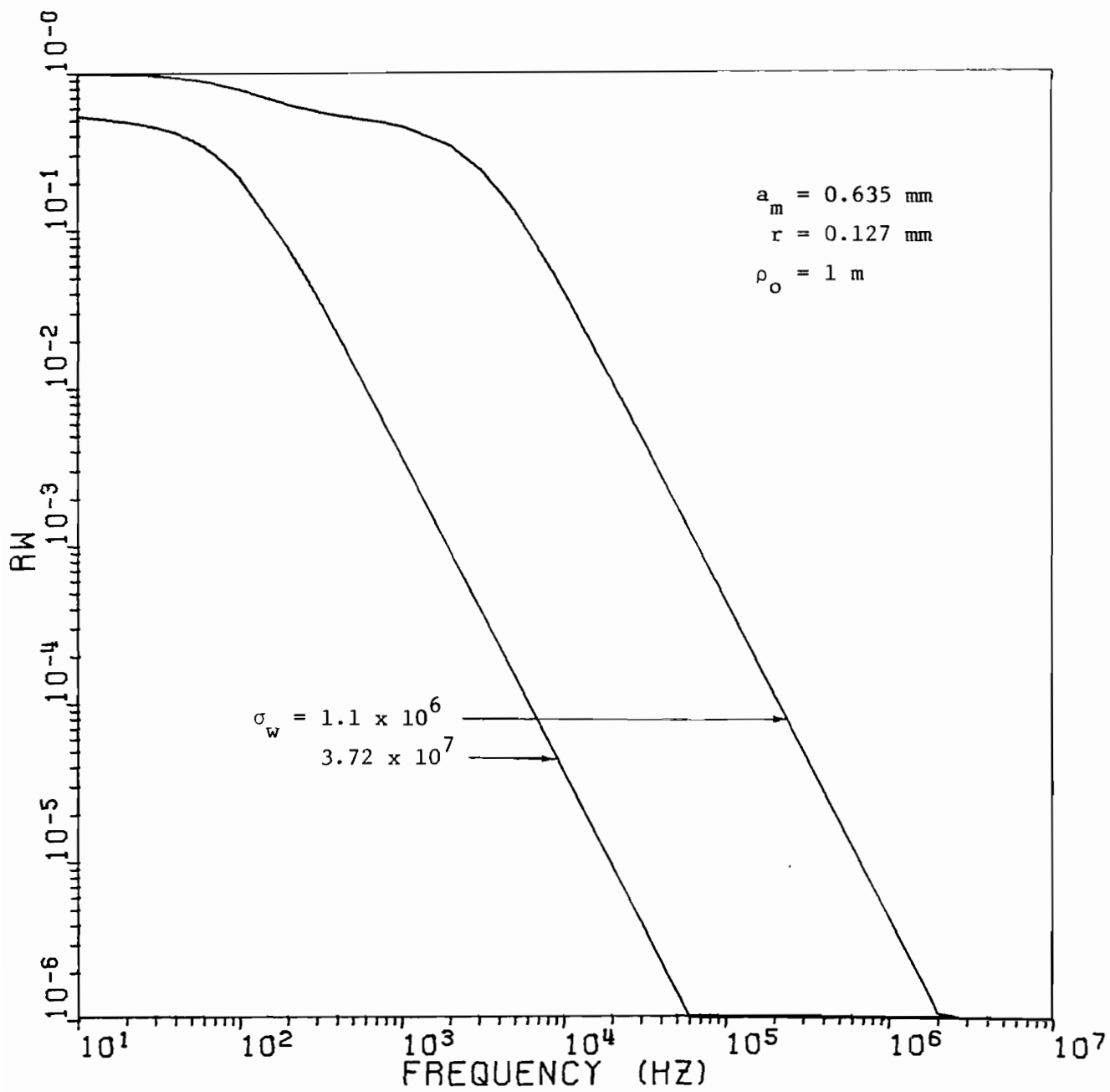
Figure 6.2b. r_w vs. frequency; a_m = 0.635 mm, r = 0.127 mm, ρ = 1 m; σ_w = 1.1 x 10^6 and 3.72 x 10^7 mho m^{-1}

136
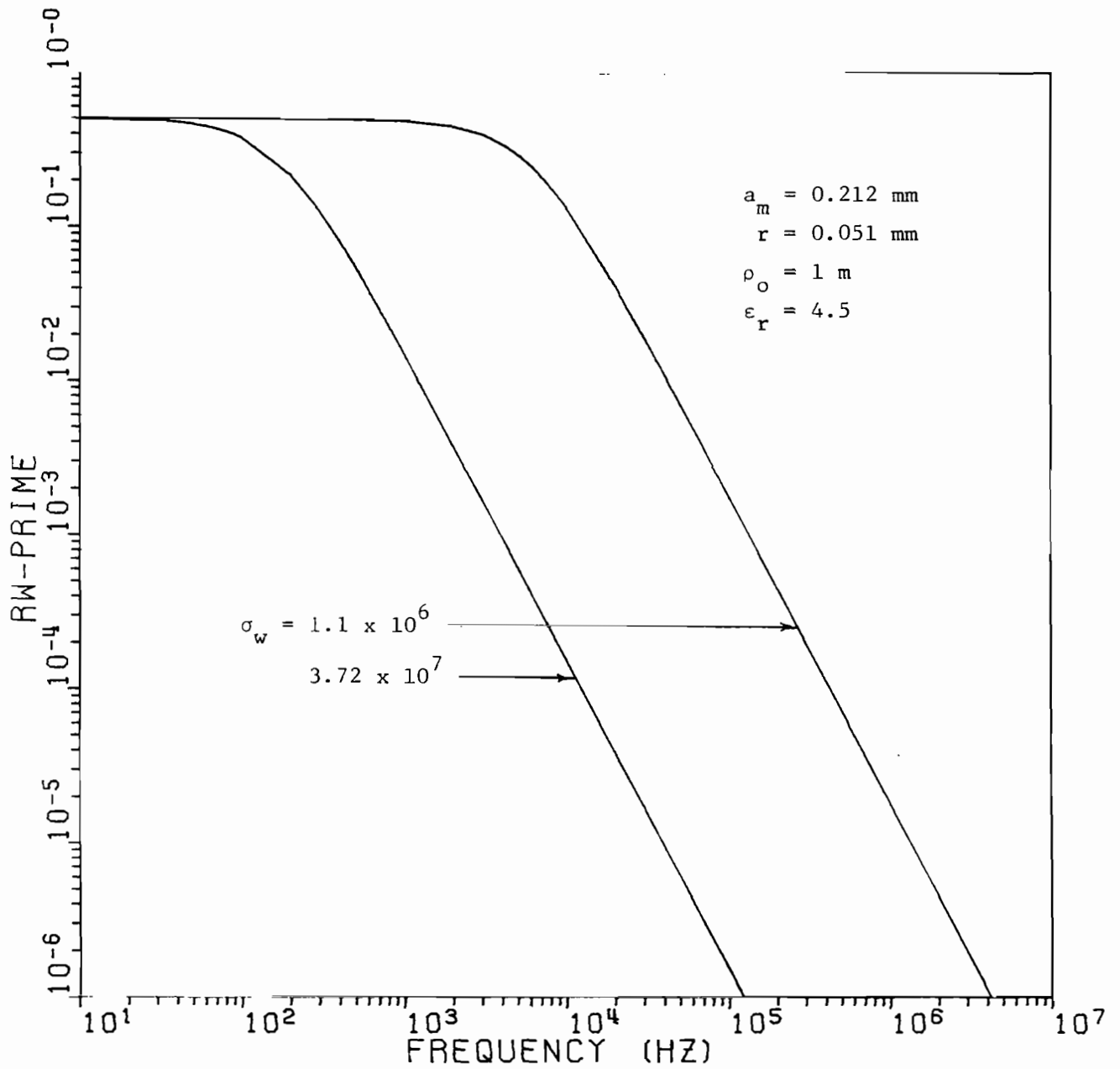
Figure 6.3a. r'_w vs. frequency; a_m = 0.212 mm, r = 0.051 mm, ρ_o = 1 m; σ_w = 1.1 x 10^6 and 3.72 x 10^7 mho m^{-1}; ϵ_r = 4.5

137
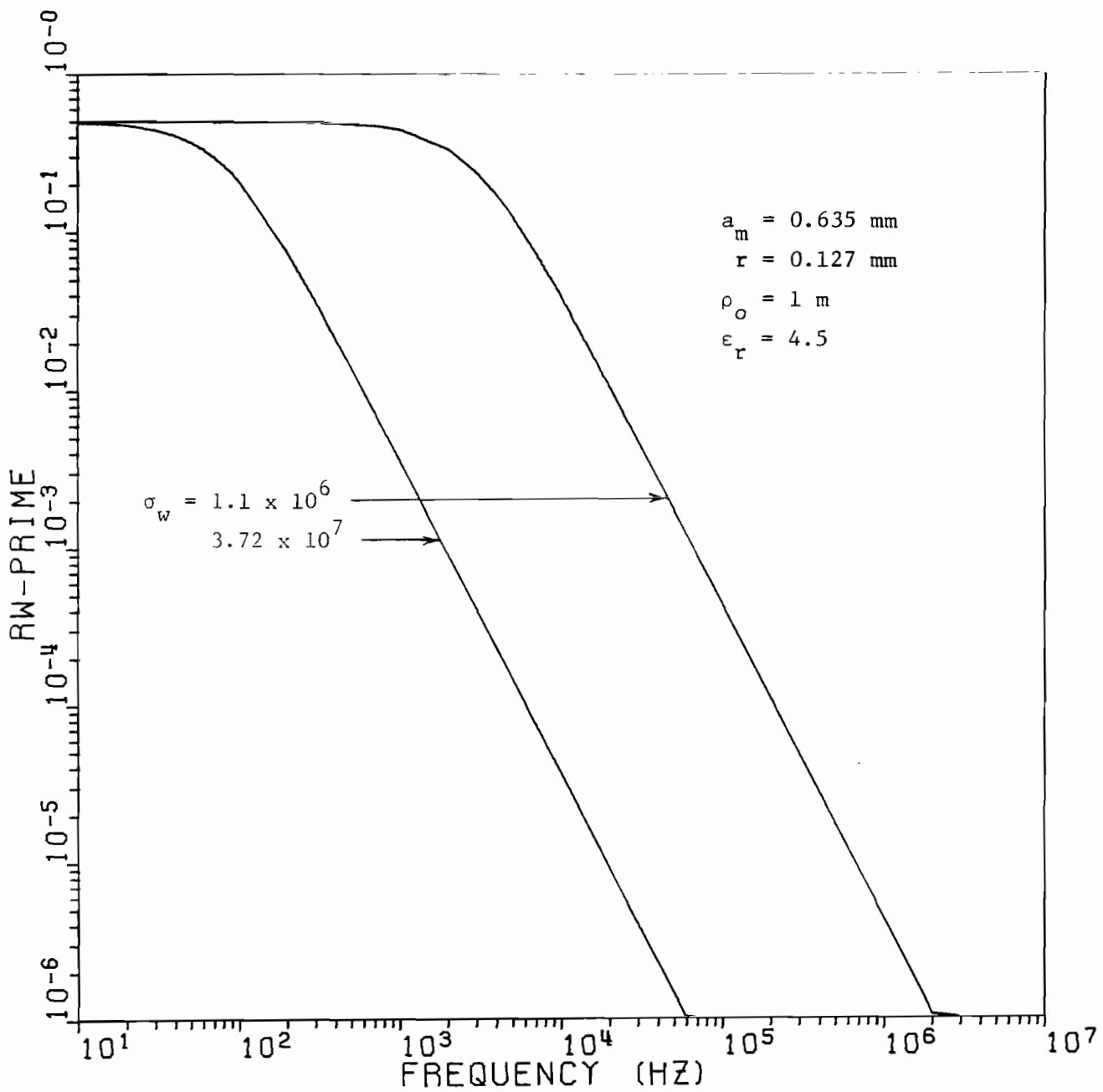
Figure 6.3b. r_w' vs. frequency; a_m = 0.635 mm, r = 0.127 mm, ρ_o = 1 m; σ_w = 1.1 x 10^6 and 3.72 x 10^7 mho m^{-1}; ε_r = 4.5.

When the screen wires are perfectly conducting, the result in eq. (6.12) reduces to

$$\frac{H_{int}}{H_{inc}} = \left\{ 1 + \frac{\pi\rho_o}{a_m} \ell n^{-1}(1 - e^{-2\pi r/a_m})^{-1} \right\}^{-1}$$

$$\simeq \frac{a_m}{\pi\rho_o} \ell n(1 - e^{-2\pi r/a_m})^{-1} \qquad (6.13)$$

which is a constant, independent of frequency. Thus the time dependence of the internal magnetic field is identical to that of the incident field, except for a constant attenuation. This behavior is attributable to the combined "differentiating" effect of the perfect screen and the "integrating" effect of the cylindrical geometry.

Another simple result of some interest is obtained if we assume that $Z_w = R_w$ over the frequency range of interest, where $R_w = (\pi r^2 \sigma_w)^{-1}$ is the resistance per unit length of the screen wires. In this case, we find that when $(a_m/\pi\rho_o)\ell n(1-e^{-2\pi r/a_m})^{-1} \ll 1$,

$$\frac{H_{int}}{H_{inc}} \simeq \frac{a_m L}{\pi\rho_o} \frac{j\omega + 2\pi R_w/\mu_o L}{j\omega + 2R_w a_m/\mu_o \rho_o} \qquad (6.14)$$

in which L denotes $\ell n(1-e^{-2\pi r/a_m})^{-1}$. The impulse response of the internal magnetic field is therefore approximately given by

$$H_{int}(t) \simeq \frac{a_m L}{\pi\rho_o} \delta(t) + \frac{2R_w a_m}{\mu_o \rho_o} e^{-(2R_w a_m/\mu_o \rho_o)t} \qquad (6.15)$$

so that the internal field response to a standard EMP waveform is dominated at late times by the slowly decaying exponential function in the second term in (6.15). More specifically, under standard EMP excitation, the internal magnetic field is given by

$$\eta_o H_{int}(t) \simeq \frac{a_m L}{\pi \rho_o} A[e^{-\alpha t} - e^{-\beta t}] + A\left(\frac{2R_w a_m}{\mu_o \rho_o}\right)[\frac{1}{\beta} e^{-\beta t} - \frac{1}{\alpha} e^{-\alpha t}]$$

$$+ A(\frac{1}{\alpha} - \frac{1}{\beta}) \left(\frac{2R_w a_m}{\mu_o \rho_o}\right) e^{-(2R_w a_m/\mu_o \rho_o)t} \tag{6.16}$$

in which we have made use of the fact that $(\beta$ and $\alpha) >> 2R_w a_m/\mu_o \rho_o$ in typical cases. Representative curves of $\eta_o H_{int}(t)$ vs. t are shown in Figs. 6.4 and 6.5 for various values of screen parameters and a cylinder radius, $\rho_o = 1$ m.

The curves in Figs. 6.4 and 6.5 show very clearly the enhancement in shielding effectiveness with increasing wire conductivity. In the curves of Fig. 6.4, for example, the peak value of the internal field drops from about 0.09 to about 0.005 when σ_w is increased from 1.1×10^6 to 3.72×10^7 mho m^{-1}. One will also note the long "tails" of the internal field waveforms due to the term in the expression in (6.16) depending on t as $\exp(-2R_w a_m t/\mu_o \rho_o)$.

Comparing the lower-conductivity curves in the two figures, one notes immediately that the 0.635/0.127 mesh is a better shield than the 0.212/0.051 mesh; this is a consequence of the larger equivalent conductivity-thickness product of the former configuration. It is also apparent that the "integrating" effect of the cylindrical geometry has delayed the onset of the peak signal, in comparison with the planar case (cf. Figs. 5.9 and 5.10). Thus the wire conductivity (or, more precisely, the equivalent conductivity-thickness product) controls the behavior of the internal waveform. In the higher-conductivity cases the inductive reactance of the screen becomes more important: one will notice the peak in the
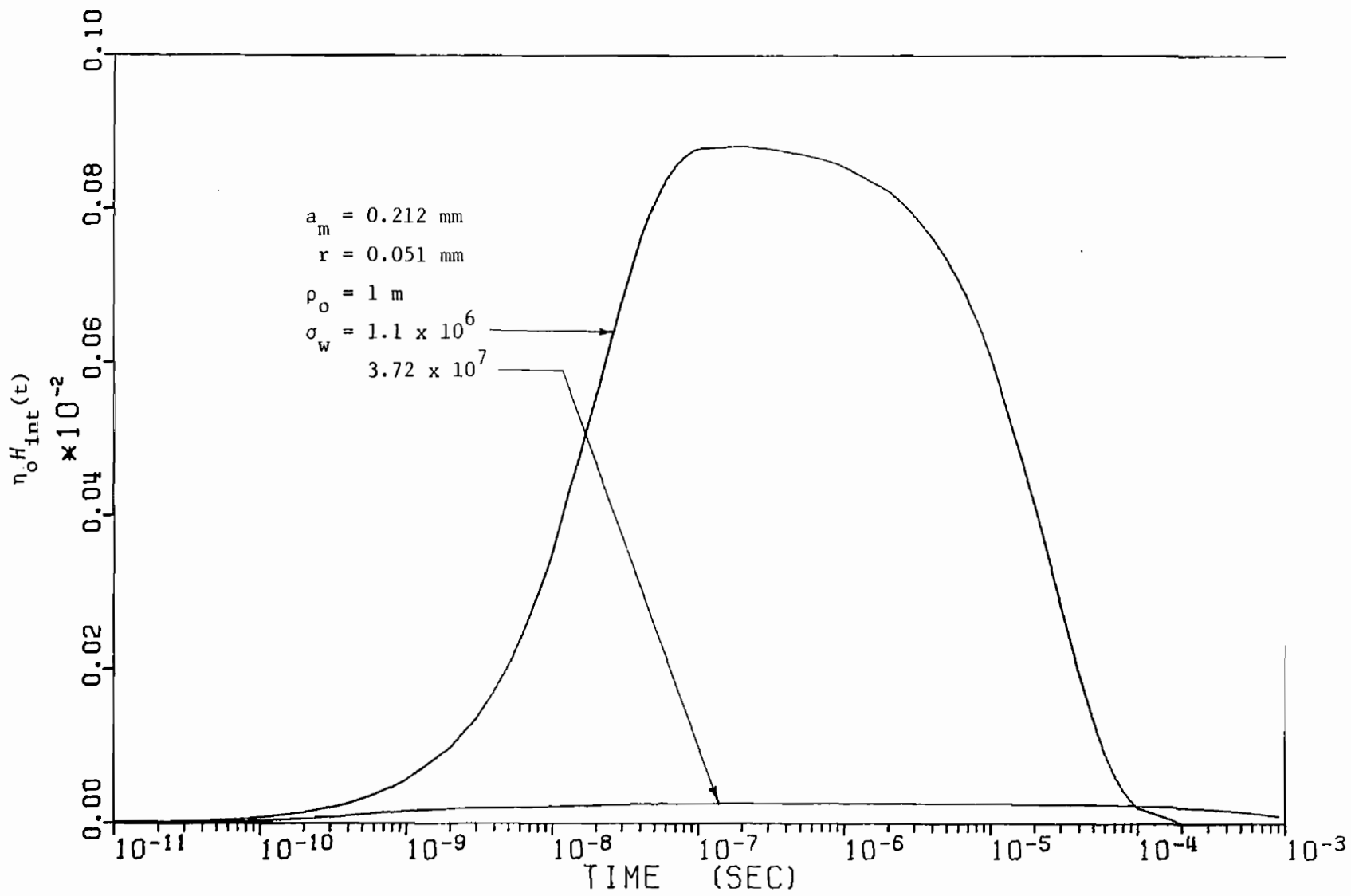
Figure 6.4. $\eta_o H_{int}(t)$ vs. time; $a_m = 0.212$ mm, $\mathbf{r} = 0.051$ mm, $\rho_o = 1$ m; $\sigma_w = 1.1 \times 10^6$, 3.72×10^7 mho m^{-1}

141
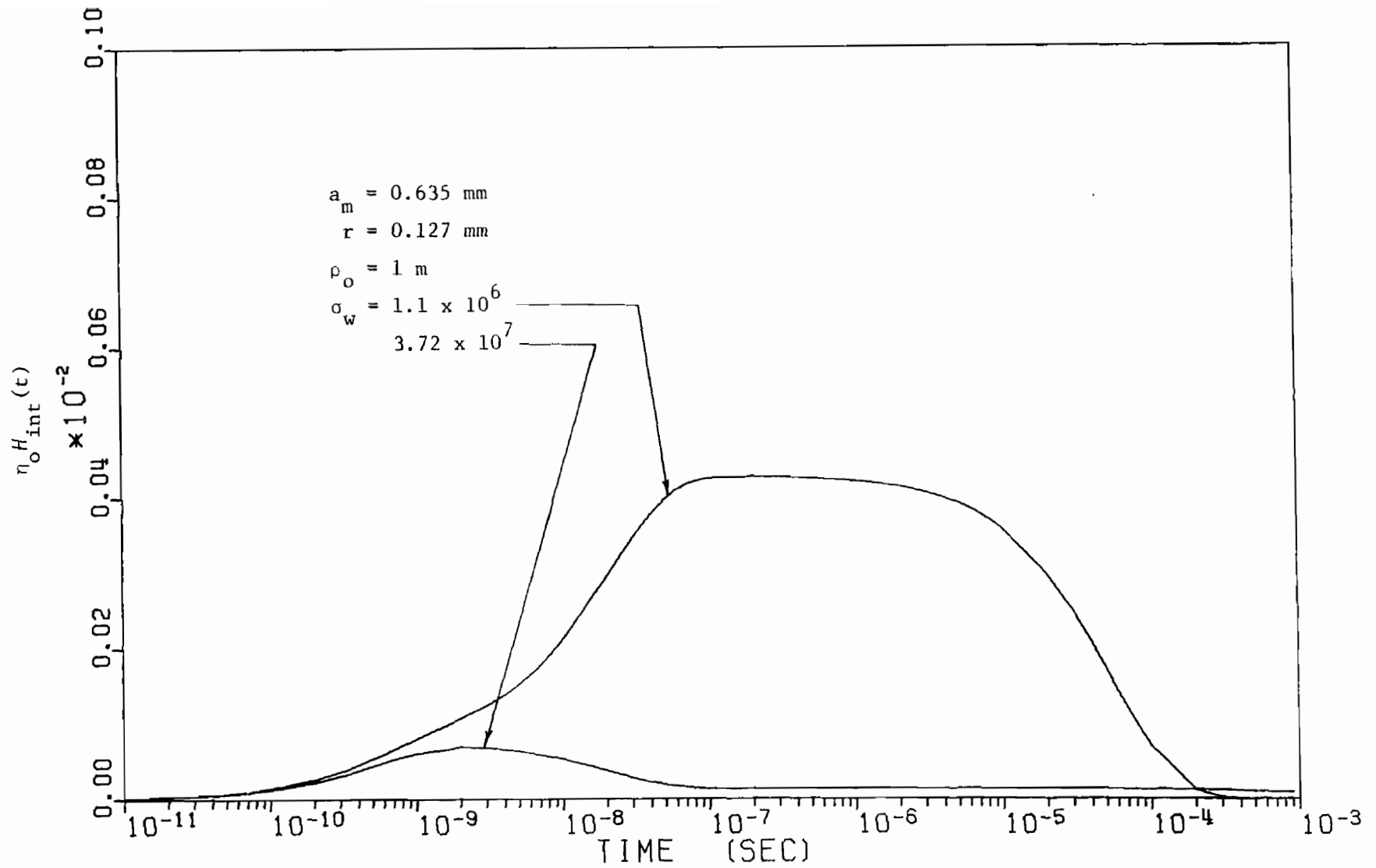
Figure 6.5. $\eta_o H_{int}(t)$ vs. time; $a_m = 0.635$ mm, $r = 0.127$ mm, $\rho_o = 1$ m; $\sigma_w = 1.1 \times 10^6$, 3.72×10^7 mho m^{-1}

In the figure:

$a_m = 0.635$ mm

$r = 0.127$ mm

$\rho_o = 1$ m

$\sigma_w = 1.1 \times 10^6$

3.72×10^7

Vertical axis: $\eta_o H_{int}(t) \times 10^{-2}$

Horizontal axis: TIME (SEC)

response for the 0.635/0.127 mesh near $t = 2 \times 10^{-9}$ sec. This peak is absent in the response of the 0.212/0.051 mesh because of its lower inductive reactance.

Finally, if one compares the responses in Figs. 6.4 and 6.5 with those in Fig. 4.8 for the graphite composite cylindrical shells' internal field, one notes that the peak internal field for the thickest graphite composite shell is about the same as that for the "worst-case" screened boron-epoxy composite shell; furthermore, the "best-case" screened boron-epoxy shell response is lower than that of the thickest graphite shell by a factor of roughly 20. One could conclude from these results that a fine mesh screen made of highly conducting (Al or Cu) wire would be a much better shield for cylindrical geometries and EMP waveforms than even a thick graphite laminate.

SECTION VII

CONCLUDING REMARKS

1. SUMMARY AND DISCUSSION

In this Note we have considered both the frequency-domain and time-domain shielding provided by graphite-epoxy and screened boron-epoxy composite laminates in planar or cylindrical geometries, with respect to EMP signals and spectra. Graphite-epoxy composites have been modeled as isotropic, homogeneous conducting materials and boron-epoxy composites as isotropic, homogeneous dielectrics. The screen used in screened boron-epoxy panels has been modeled under the assumptions that the wire junctions are bonded and that the thin-wire approximation applies. These assumptions may, in fact, not be well-satisfied in practice (the wire junctions may be imperfect due to oxidation at the junction points of overlapping wires and the condition that the wire radius is small in comparison to the mesh period is not generally well met); however, they provide a reasonable starting point for analysis and yield conservative estimates of the mesh shielding effectiveness, since the thin-wire approximation tends to underestimate the mesh current.

We have developed a boundary connection supermatrix formalism which is a generalization of the transmission matrix of network theory. Such a formalism will be useful in dealing with shielding problems involving bodies of non-separable shape as long as the local radii of curvature are small in comparison to the shield thickness. The boundary connection supermatrix possesses many intersecting properties which have not been touched on here but which will be the subject of a forthcoming Interaction Note. The principal utilities of the boundary connection supermatrix are its generality (in that general multilayer shields with sheet

144

immittances between layers are easily described) and the fact that its use effectively reduces the number of regions which must be considered in a shielding calculation by at least one.

The transmission of electromagnetic plane waves through planar graphite composite laminates is straightforward to analyze, and some useful approximate formulas for the transmission coefficients of such a structure have been given. The transmitted time-domain field behaves in a manner easily understood on the basis of the low-pass filter characteristic of conducting materials. We have calculated some time-domain curves for typical cases and have found, for example, that the peak value of the electric field transmitted through a 2 mm thick graphite composite panel is approximately 10^{-4} of the peak value of the incident field.

Penetration of electromagnetic fields into the interior of cylindrical shells of graphite composite has been considered. Over the frequency range which has been of principal interest to us, and for cylinder radii on the order of 2 m or less, resonance effects are of little importance. Consequently, low-frequency approximations are useful. We have suggested a new frequency-domain measure of the shielding effectiveness of closed surfaces in terms of the time-average electromagnetic energy stored in the interior of the region, and have given simple formulas for this quantity for cylindrical bodies. We have also presented representative curves to illustrate the dependence of this shielding parameter on frequency for several typical graphite-composite cylinders, and have pointed out that the principal "break frequency" below which the shielding is poor is given approximately by $1/\pi \mu_o \sigma_g d \rho_o$. The time-domain internal magnetic field resulting from an incident EMP signal has been calculated for some

145

representative cases. Its time dependence can be understood on the basis of the "low-pass" character of both the composite shell material and the cylindrical geometry itself.

The principal difficulty in treating screened boron-epoxy composite laminates lies in finding an appropriate sheet-immittance description for the screen. We have developed such a description appropriate for the case where the mesh dimensions are electrically small, and which takes the presence of the composite panel into account. Our result constitutes an extension of the classic work of Kontorovich. Using this method of characterizing the mesh we have addressed the problems of plane-wave transmission through a planar screened boron-epoxy composite layer and penetration into the interior of a cylindrical shell of screened composite material. We have found that the composite layer itself, except for its effect on the sheet impedance of the screen, is relatively unimportant insofar as the shielding behavior of the screened laminate is concerned. Thus one needs to consider only the sheet impedance, properly modified to take into account the presence of the composite layer, in the analysis of shielding problems.

The principal difference between graphite and screened boron-epoxy composites from a signal-transmission standpoint is that the graphite composite tends to act as a low-pass or integrating filter, while the screened boron-epoxy composite behaves as a high-pass or differentiating filter. Thus the time-domain field transmitted through a planar layer of screened composite contains a contribution proportional to the derivative of the input waveform, as a result of the inductive component of the screen impedance. For standard EMP incident signals, this leads to an early-time

146

response dominated by this derivative term, while the later-time response is influenced most strongly by the wire conductivity in the mesh.

The cylindrical screened-composite shell is of particular interest from an analytical standpoint because the integrating effect of the cylindrical geometry tends to cancel the differentiating effect of the wire-mesh screen. In fact, for an ideal screen with perfectly conducting wires the internal magnetic field waveform is identical, except for a reduction in amplitude, to the incident waveshape. For the screen parameters which have been considered in this report, it has been shown that the energy shielding ratio principal break frequency tends to be lower than that of a comparable graphite composite shell, especially when the screen wires are highly conductive. Thus the screened boron-epoxy composite shell can be a much better shield than a graphite composite shell as a consequence of its larger equivalent conductivity-thickness product. However, we have also noted that the equivalent conductivity-thickness product alone is not a completely valid descriptor of screened composite panels; it is only useful at low frequencies, or, equivalently, at late times. At early times the mesh size is the critical parameter, since it determines the inductance of the sheet. In fact, we have presented numerical data which indicate that overall, a screen with a smaller equivalent conductivity-thickness product can be a better shield than another with a larger product, at least with respect to the incident-field waveforms considered here. This result suggests the possibility that one might even design a screen, whose wires have a given conductivity and which possesses a given amount of metal per unit area, for optimum shielding performance against a given incident waveshape.

147

2. CONCLUSION

It is clear that while advanced composite laminates are not yet as effective as, say, aluminum panels in shielding against unwanted penetration of electromagnetic fields, they are nonetheless good enough to be used as aircraft or missile skins without placing an unreasonable burden on the internal shielding (conduit, cable braids, etc.). This fact, coupled with the strength and weight advantages of advanced composites, guarantees the increased future use of these materials, and points up the importance of continued study both of their intrinsic electrical properties and of the fundamental electromagnetic boundary-value problems which involve them.

Some suggested problems for future study include the following:

(a) Integral-equation formulation of scattering problems involving hollow composite shells, using the boundary connection supermatrix[†].

(b) Singularity Expansion Method (SEM) solutions of transient scattering/penetration problems involving hollow composite shells of separable or non-separable shape

(c) Study of effects of imperfect panel-to-panel joints and joints between metallic and composite panels

(d) Field penetration through apertures in composite panels

(e) Continued study of bonded and unbonded wire meshes, including the effects of linear and nonlinear junction impedance and dielectric environments

(f) Canonical problems involving the propagation of surface waves on wire meshes, including interactions with nearby conductors; composite waveguides.

These are only a few of the many problems which come to mind. Advanced composites provide solutions to many problems because of their great strength and light weight; but to the electromagnetic theorist and the

---

[†]Currently under study by the author.

148

engineer concerned with electromagnetic shielding, they are a source of many future challenges. It is sincerely hoped that this report will contribute to an improved understanding of the electromagnetic shielding behavior of these materials and excite the interest of other investigators who will continue to study them.

REFERENCES

[1] "A Technology Plan for Electromagnetic Characteristics of Advanced Composites," RADC-TR-76-206, July 1976.

[2] L. Allen, W. F. Walker, and K. R. Siarkiewicz, "An Investigation of the Electromagnetic Properties of Advanced Composite Materials," IEEE 1976 International Symposium on Electromagnetic Compatibility Record, pp. 174-179.

[3] K. F. Casey, "EMP Penetration through Advanced Composite Skin Panels," Interaction Notes, Note 315, December 1976.

[4] M. I. Kontorovich, "Averaged Boundary Conditions at the Surface of a Grating with Square Mesh," Radio Engineering and Electronic Physics, Vol. 8, pp. 1446-1454, 1963.

[5] T.-K. Wu and L. L. Tsai, "Time Domain Shielding Properties of Conducting Cylindrical Shells," IEEE Transactions on Electromagnetic Compatibility, Vol. EMC-17, pp. 191-193, August 1975.

[6] G. L. Ragan, Microwave Transmission Circuits: Dover Publications, New York, 1965, Ch. 9.

[7] R. F. Harrington and J. R. Mautz, "An Impedance Sheet Approximation for Thin Dielectric Shells," IEEE Transactions on Antennas and Propagation, Vol. AP-23, pp. 531-534, July 1975.

[8] J. R. Wait, "Propagation of Electromagnetic Waves along a Thin Plasma Sheet," Canadian Journal of Physics, Vol. 28, pp. 1586-1594, December 1960.

[9] D. Schieber, "Shielding Performance of Metallic Cylinders," IEEE Transactions on Electromagnetic Compatibility, Vol. EMC-15, pp. 12-15, February 1973.

[10] D. Schieber, "Correction to 'Shielding Performance of Metallic Cylinders'," IEEE Transactions on Electromagnetic Compatibility, Vol. EMC-15, p. 88, May 1973.

[11] C. W. Harrison, Jr., "Comments on 'Shielding Performance of Metallic Cylinders'," IEEE Transactions on Electromagnetic Compatibility, Vol. EMC-15, p. 150, August 1973, and Author's Reply, same issue.

[12] J. R. Wait, "Comments on 'Shielding Performance of Metallic Cylinders' and Comments by C. W. Harrison, Jr. and Reply by D. Schieber," IEEE Transactions on Electromagnetic Compatibility, Vol. EMC-16, p. 52, February 1974.

[13] T.-K. Wu and L. L. Tsai, "Shielding Properties of Thick Conducting Cylindrical Shells," IEEE Transactions on Electromagnetic Compatibility, Vol. EMC-16, pp. 201-204, November 1974.

[14] T.-K. Wu and L. L. Tsai, "Shielding Properties of Thick Conducting Cylindrical Shells with an Obliquely Incident Plane Wave," IEEE Transactions on Electromagnetic Compatibility, Vol. EMC-17, pp. 189-191, August 1975.

[15] R. W. Latham and K. S. H. Lee, "Theory of Inductive Shielding," Canadian Journal of Physics, Vol. 46, pp. 1745-1752, 1968.

[16] M. I. Kontorovich, V. Yu. Petrun'kin, N. A. Yesepkina, and M. I. Astrakhan, "The Coefficient of Reflection of a Plane Electromagnetic Wave from a Plane Wire Mesh," Radio Engineering and Electronic Physics, Vol. 7, pp. 222-231, February 1962.

[17] M. I. Astrakhan, "Averaged Boundary Conditions on the Surface of a Lattice with Rectangular Cells," Radio Engineering and Electronic Physics, Vol. 9, pp. 1239-1241, August 1964.

[18] M. I. Astrakhan, "Reflecting and Screening Properties of Plane Wire Grids," Telecommunications and Radio Engineering, Vol. 23, pp. 76-83, January 1968.

[19] D. A. Hill and J. R. Wait, "Electromagnetic Scattering of an Arbitrary Plane Wave by a Wire Mesh with Bonded Junctions," Sensor and Simulation Notes, Note 231, Section II, 10 June 1977.

[20] R. W. Latham, "Small Holes in Cable Shields," Interaction Notes, Note IN 118, September 1972.